

**On the interaction between proteins and nanoparticles:
Coiled coil peptides organize nanoparticles
and vice versa**



Dissertation zur Erlangung des akademischen Grades des
Doktors der Naturwissenschaften (Dr. rer. nat.)

eingereicht im Fachbereich Biologie, Chemie, Pharmazie
der Freien Universität Berlin

vorgelegt von

Diplom-Chemikerin SARA C. WAGNER
aus Berlin, Deutschland

Januar, 2010

1. Gutachterin: Prof. Dr. Beate Koksch
2. Gutachterin: Prof. Dr. Sabine Schlecht

Disputation am 19.01.2010

ERKLÄRUNG

Hiermit erkläre ich, dass ich die hier vorliegende Arbeit ohne die unzulässige Hilfe Dritter und ohne die Verwendung anderer als der angegebenen Hilfsmittel angefertigt habe. Die aus anderen Quellen direkt oder indirekt übernommenen Daten und Konzepte sind unter Angabe der Quelle gekennzeichnet.

Die vorliegende Arbeit wurde in keinem früheren Promotionsverfahren angenommen oder als ungenügend beurteilt.

Berlin, Januar 2010

Sara C. Wagner

Die Dissertation wurde in englischer Sprache verfasst. Aus dieser Dissertation gingen folgende Veröffentlichungen hervor:

- Sara C. Wagner, Meike Roskamp, Manjula Pallerla, Raheleh Rezaei Araghi, Sabine Schlecht, Beate Kokschi, Nanoparticle induced folding and fibril formation of coiled coil based model peptides, submitted.
- Sara C. Wagner, Meike Roskamp, Helmut Cölfen, Christoph Böttcher, Sabine Schlecht, Beate Kokschi, Switchable electrostatic interactions between gold nanoparticles and coiled coil peptides direct colloid assembly, *Org. Biomol. Chem.* **2009**, 7, 46-51.
- Kevin Pagel*, Sara C. Wagner*, Raheleh Rezaei Araghi, Hans von Berlepsch, Christoph Böttcher, Beate Kokschi, Intramolecular charge interactions as a tool to control the coiled-coil-to-amyloid transformation, *Chem. Eur. J.* **2008**, 14, 11442-11451 (* Joint first authors).

DANKSAGUNG

Mein herzlicher Dank gilt Frau Prof. Dr. Beate Koksch für die Überlassung und Betreuung dieses sehr interessanten und hoch aktuellen Promotionsthemas. Dabei habe ich insbesondere die gewährte Freiheit zur Umsetzung geschätzt. Auch für die Finanzierung und weitere Förderung meiner Arbeit durch die Teilnahme an internationalen Konferenzen möchte ich mich bedanken.

Auch Frau Prof. Dr. Sabine Schlecht und Diplom-Chemikerin Meike Roskamp bin ich zu großem Dank für die sehr fachkundige und erfolgreiche Kooperation verpflichtet. Sowohl die sehr fachkundige Herstellung und Charakterisierung der Nanopartikel als auch die kompetente Diskussionsbereitschaft haben erheblich zum Gelingen dieser Promotionsarbeit beigetragen. Außerdem möchte ich mich bei Frau Schlecht ganz besonders für die Übernahme der Begutachtung der Arbeit innerhalb eines sehr knappen Zeitraumes bedanken.

Weiterhin gilt mein Dank Herrn PD Dr. Christoph Böttcher für die sehr kompetente und ausführliche Einarbeitung in die Elektronenmikroskopie, die mir eine selbstständige Anwendung dieser Methode auf diverse Fragestellungen in meiner Doktorarbeit ermöglichte. Fachkompetente Diskussionen mit Herrn Dr. Christoph Böttcher und Herrn Dr. Hans von Berlepsch sind von unersetzlichem Wert für das Gelingen dieser Arbeit gewesen.

Herrn Prof. Dr. Rainer Haag danke ich für die Erlaubnis zur Benutzung des isothermalen Titrationskalorimeters. Bei M.Sc. Mohiuddin Abdul Quadir möchte ich mich für die engagierte experimentelle Einführung in die Isothermale Titrationskalorimetrie bedanken.

Frau Antje Völkel und Herrn Dr. Helmuth Coelfen danke ich für die Kooperation zur Durchführung und Auswertung der Ultrazentrifugationsexperimente.

Bei meinen Kollegen in der Arbeitsgruppe Koksch möchte ich mich für die freundschaftliche und hilfsbereite Zusammenarbeit bedanken. Insbesondere M.Sc. Raheleh Araghi Rezaei und Dr. Kevin Pagel danke ich für die Mitwirkung bei der Entwicklung pH-sensitiver Modellpeptide.

Ich danke auch der Deutschen Forschungsgemeinschaft, dem Fonds der Chemischen Industrie und der FU Berlin für die Finanzierung meiner Promotionstätigkeit und der Teilnahme an internationalen Konferenzen.

Zu guter letzt möchte ich mich bei meiner Familie und meinem Freund Michael für den privaten Rückhalt und nötigen Freizeitausgleich danken.

REFERAT

Nanotechnologie ist ein sehr junger und schnell wachsender Forschungsbereich, der neue und sehr viel versprechende Lösungen für verschiedene Wissenschaftsbereiche wie die Materialchemie oder Medizin verspricht. Die Verknüpfung mit dem Bereich der Biotechnologie stellt einen sehr eleganten Ansatz dar, die ohnehin einzigartigen optischen, elektronischen sowie magnetischen Eigenschaften von Nanopartikeln um die vielfältigen und evolutionär selektierten Eigenschaften der Biomoleküle wie z. B. hoch-spezifische Erkennungseigenschaften oder enzymatische Kontrolle zu erweitern. Mehrere Studien haben erfolgreich gezeigt, dass Proteine eine Aggregation von Nanopartikeln induzieren können, die gegebenenfalls in Abhängigkeit von Umgebungsbedingungen wie pH-Wert oder Gegenwart von Metallionen schaltbar ist. In keiner der bisherigen Veröffentlichungen konnte ein direkter Zusammenhang zwischen der Symmetrie des Proteinfaltungsmotifs und der Geometrie der peptid-induzierten Nanopartikelarchitektur gezeigt werden. Dennoch ist eine hochgeordnete Anordnung der Nanopartikel ein entscheidendes Kriterium für materialwissenschaftliche Anwendungen.

Im ersten Teil dieser Arbeit wird die Anwendbarkeit des α -helikalen coiled coil Faltungsmotif für die Organisation von Nanopartikeln untersucht. Das Peptiddesign wurde um zusätzliche Elemente erweitert, um elektrostatisch anziehende Wechselwirkungen mit anionischen Goldnanopartikeln eingehen zu können. Das hier entwickelte coiled coil-basierte Peptiddesign konnte erfolgreich dazu genutzt werden, eine Aggregation der Nanopartikel zu induzieren. Diese Strukturierung konnte zudem mittels pH-Wert reversibel geschaltet werden. Ein direkter Einfluss des Oligomerisierungsgrads der coiled coil-Struktur auf die Strukturierung der Nanopartikel konnte allerdings nicht nachgewiesen werden.

Der zweite Teil dieser Arbeit beschäftigte sich mit dem umgekehrten Sachverhalt, nämlich dem Einfluss des Nanopartikels auf die Proteinstruktur. Publikationen zu nanopartikel-induzierten Proteinmissfaltungen führen zu wachsenden Bedenken insbesondere hinsichtlich medizinischer Anwendungen von Nanoobjekten. Im Rahmen dieser Dissertation wurde dieses Phänomen erstmals mit Hilfe von Modellpeptiden untersucht. Insbesondere die Rolle der Primärstruktur sollte anhand eines coiled coil-basierten Modellsystems geklärt werden. Es konnte gezeigt werden, dass vorrangig die Bindungsstöchiometrie die Anreicherung des Peptids auf der Nanopartikeloberfläche bestimmt und damit dramatisch die Konzentrationsgrenze für die Amyloidbildung herabsetzt. Dennoch sind β -Faltblatt-induzierende Faktoren in der Peptidsequenz für eine Missfaltung und Aggregation in Gegenwart von Nanopartikeln erforderlich.

ABSTRACT

Nanotechnology is a very young and rapidly growing field that offers novel and very promising solutions to different scientific areas such as materials science and medicine. Its combination with biotechnology is a sophisticated way to complement the unique optical, electronic, and magnetic properties of nanoparticles with the manifold and evolutionarily selected features of biomolecules, i.e. highly specific recognition interactions, structural diversity, sensitivity towards environmental conditions, or enzymatic control. Several studies have already shown the applicability of proteins for the assembly of nanoparticles that may be tuned by environmental conditions such as the pH or the presence of metal ions in some cases. Nevertheless, to the best of our knowledge, none of these approaches successfully devolved the symmetry of protein folding motif to the geometry of the nanoparticle architecture in solution. At the same time, a highly ordered nanoparticle arrangement is an essential requirement in materials science.

In the first part of this thesis, the suitability of the α -helical coiled coil folding motif for the organization of nanoparticles was investigated. The general coiled coil design was modified such that the peptides were able to undergo electrostatically attractive interactions with anionic nanoparticles. The design of coiled coil peptides developed here induced an assembly of nanoparticles whereupon pH conditions were feasible to direct this structuring in a reversible and repeatable manner. These results also confirmed that the direct impact of the protein folding on the geometry of nanoparticle arrangement is quite challenging and hardly achievable in solution.

The second part focused on the reversed effect, namely on the impact of nanoparticle on the protein structure. In recent years, the observation of nanoparticle-induced misfolding of proteins has provoked growing concerns about the medical applications of nanoparticles. The system of coiled coil peptides and nanoparticles applied here made the first steps towards systematic studies on the role of the peptide sequence in this phenomenon. It turned out that the enrichment of peptide on the surface of nanoparticle dramatically lowered the concentration limit for the self-assembly of peptide. Especially the binding stoichiometry decides on the extent of this increase in peptide density, as was shown here. Nevertheless, this system of peptide and nanoparticle still required the presence of β -sheet inducing elements within the primary structure to observe β -sheet and fibril formation in the presence of nanoparticle.

LIST OF ABBREVIATIONS

A β	amyloid β
Abz	anthranilic acid
Ad12	adenovirus 12
AuNps	gold nanoparticles
BSA	bovine serum albumin
CD	circular dichroism
C _p	peptide concentration
CR	Congo red
CSQ	calsequestrin
DLS	dynamic light scattering
DNA	deoxyribonucleic acid
DNP	dinitrophenol
EDX	energy dispersive X-ray (spectrometer)
ELISA	enzyme-linked immunosorbent assay
ESI	electrospray ionization
FFT	Fast Fourier Transform
FL	fluorescence intensity
Fmoc	9-Fluorenylmethoxycarbonyl
FRET	fluorescence resonance energy transfer
GdnHCl	guanidine hydrochloride
Glu	glutamine
His	histidine
HPLC	high pressure liquid chromatography
IgE	immunoglobulin E
IgG	immunoglobulin G
ITC	isothermal titration calorimetry
LC	liquid chromatography
Leu	leucine
Lys	lysine
MALDI	matrix assisted laser desorption/ionization
MMP	matrix metalloproteinase
MS	mass spectrometry
MUA	mercapto undecanoic acid
NTA	nitrilotriacetic acid
PEG	polyethylene glycol

pI	isoelectric point
PMMA	polymethylmethacrylate
PTA	phosphotungstic acid
SAXS	small angle X-ray scattering
SH2	Src Homology 2
TEM	transmission electron microscopy
TFA	trifluoroacetic acid
ThT	thioflavin-T
TMAH	tetramethylammonium hydroxide
T_M	midpoint temperature
TOF	time of flight
Tris	tris(hydroxymethyl)aminomethane
UAc	uranyl acetate
UV	ultra-violet
Vis	visible

TABLE OF CONTENTS

1	Introduction	1
2	Inorganic nanoparticles and their modification with biomolecules	4
3	Design of Biomolecule-directed nanoparticle assembly	7
4	Examples of protein-mediated assembly of nanoparticles.....	9
4.1	Organization of nanoparticles by protein-recognition motifs.....	9
4.2	Enzymatic control of protein-based nanoparticle systems	13
4.3	Organization of nanoparticles by the coiled coil folding motif.....	17
5	Protein folding and misfolding.....	21
5.1	Coiled coil based model peptides to study amyloid-formation	25
5.2	Impact of nanoparticles on protein folding and misfolding	32
5.2.1	Conformational changes upon adsorption to nanoparticles	33
5.2.2	Surface-crowding effect leads to nanoparticle-induced fibril formation	34
6	Scientific Goals	37
7	Applied analytical methods	39
7.1	Surface Plasmon resonance	39
7.2	Circular dichroism (CD) spectroscopy	40
7.3	Transmission electron microscopy	42
7.4	Thioflavin T binding assay	45
7.5	Isothermal titration calorimetry	46
8	Results: Coiled coil peptides for organization of nanoparticles.....	49
8.1	Concept.....	49
8.1.1	Design of nanoparticles.....	49
8.1.2	Peptide design for organization of nanoparticles.....	50
8.1.3	Analytical techniques.....	52
8.2	Publication.....	54
8.3	Modifications of the peptide design (unpublished results).....	55
8.4	Critical discussion of the protein-directed geometry of nanoparticle architectures (unpublished results).....	59
9	Results: Coiled coil model peptides to study protein misfolding	63
9.1	Concept.....	63
9.1.1	Peptide design.....	63
9.1.2	Analytical techniques.....	65
9.2	Publication.....	66
10	Results: Nanoparticle-induced peptide folding and fibril formation	67
10.1	Design of nanoparticles.....	67

10.2	Peptide design.....	68
10.3	Analytical techniques.....	70
10.4	Manuscript.....	71
10.5	Further modifications in VW19 (unpublished results).....	108
11	Summary and Conclusions	110
12	Outlook	113
13	Literature	115

1 Introduction

Already in 1961, the tremendous potential of nanotechnology was realized by the Nobel physicist Richard Feynman, who made the famous comment “There is plenty of room at the bottom”.¹ Although the term “nanotechnology” was not directly used, he also said: “What I want to talk about is the problem of manipulating and controlling things on a small scale... What I have demonstrated is that there is room - that you can decrease the size of things in a practical way... I will not discuss how we are going to do it, but only what is possible in principle... We are not doing it simply because we haven’t yet gotten around it.”¹ Four decades later, scientists have learnt how to manipulate atoms, molecules, and clusters on surfaces and that new fundamental physics governs the properties of nanoobjects. Thereby, the rapid progress in this field can be very well illustrated by the progressing miniaturization of electronic devices which, in principle, is enabled by the development of new conducting materials as well as by new methods to structure materials on a small scale. By conventional top-down processes (miniaturization processes) such as lithography, structural dimensions of computer microprocessors are limited to a size of some 200 nm (Figure 1.1). For that

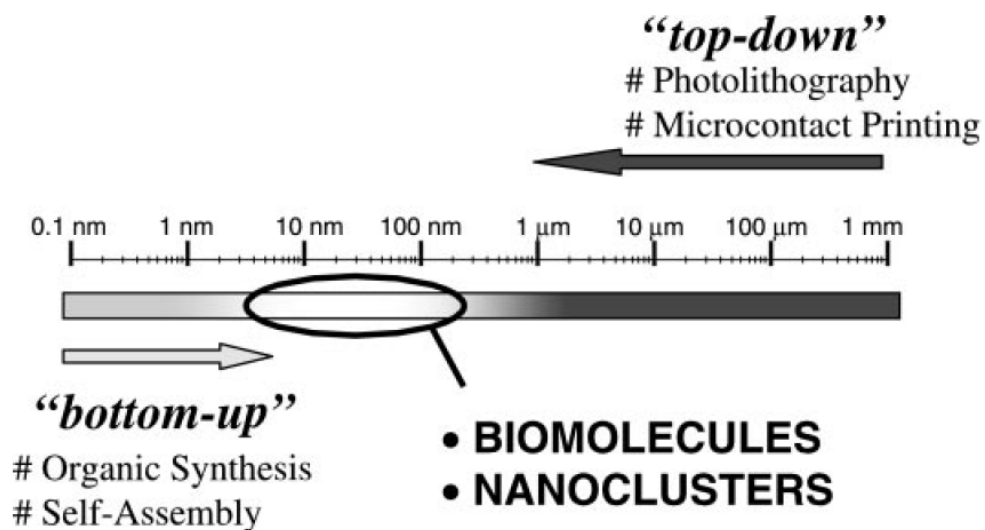


Figure 1.1. The engineering of small-scale devices currently displays a gap. Whereas conventional top-down processes hardly allow the production of structures smaller than about 200-100 nm, the limits of regular bottom-up processes are in the range of about 2-5 nm. Because of their structural dimensions, two different components seemed to be applicable for addressing that gap: 1) biomolecules such as proteins and DNA, and 2) colloidal inorganic nanoparticles (according to C. M. Niemeyer).²

reason, scientists spend a lot of effort on the development of bottom-up strategies (enlargement strategies), which concern the self-assembly of macromolecular and colloidal building blocks to create larger, functional devices.

In order to bridge the gap between the submicrometer dimensions that are reachable by classical top-down engineering and the dimensions achievable by classical bottom-up approaches including chemical synthesis and supramolecular self-assembly, the organization of inorganic nanoparticles has become of particular interest. For the preparation of inorganic nanoparticles, a variety of materials like metals, metal oxides, and semiconductor materials, such as CdS and CdSe can be used. The strong interest in nanoparticles can be explained by their newly-discovered size-dependent optical, electronic, and catalytic properties, while their size can be controlled from one to about several hundred nanometers, with a fairly narrow size distribution. The arrangement of nanoparticles within 2D or 3D architectures on surfaces is often associated with new collective properties like, for instance, coupled-plasmon absorbance, interparticle energy transfer, and electron transfer or conductivity.³

Both biotechnology and materials science meet at the same length scale. Biomolecular components size dimensions are typically in the range of about 5 to 200 nm, similar to those of nanoparticles. A combination of both bio- and nanotechnologies leads to a biomolecule-mediated organization of nanoparticles. Biomaterials are important future building blocks for nanoparticle architectures because of the following fundamental features:

- Biomaterials display specific and strong complementary recognition interactions, for instance, antigen-antibody, nucleic acid-DNA, and hormone-receptor interactions. The functionalization of nanoparticles with biomolecules could lead to biomolecule-nanoparticle recognition interactions which may induce self-assembly.
- Various biomolecules possess several binding sites, for example, antibodies exhibit two Fab (antigen-binding fragment) sites and proteins like streptavidin or concanavalin A display four binding domains. This allows a multidirectional growth of nanoparticle structures, while the symmetry of protein folding motif or other biomolecules may influence the geometry of nanoparticle structures.
- By means of genetic methods, proteins may be modified with specific anchoring groups for aligned binding to nanoparticles or the site-specific linkage of the biomaterial to surfaces. Consequently, the directional growth of nanoparticle structures may be influenced. Also other biomolecules, i.e., double-stranded DNA

may be synthetically modified such that they act as templates for the assembly of nanoparticles by intercalation, electrostatic binding to phosphate groups, or association to functionalities tethered to the DNA.

- Since enzymes can be used to change the properties of biomolecules, they are a very interesting tool to control the shape and structure of biomolecule-nanoparticle hybrid systems.
- The structural diversity of biomolecules represents a promising approach to invent tunable and/or switchable materials depending on environmental conditions such as pH or the presence of metal ions.

Currently, the combination of nanoparticles and biomolecules is a very young and rapidly growing research field located at the crossroads of materials science, nanosciences, and molecular biotechnology. Such hybrid materials do not only lead to the invention of nanoelectronic devices, but also allow promising applications in other fields such as biosensors or biomedical applications. To mention one of the numerous examples in nanomedicine, nanoparticles are applied as targeted biomarkers and drug-delivery agents to tumor cells and medical treatment of cancers.⁴ Although several areas of medical care are already benefiting from the advantages that nanotechnology offers, relatively little is known about the possible risks of this new technology. For that reason, it is of utmost importance to examine carefully and with responsibility possible side effects to human beings and the environment, summarized by the area of nanotoxicology.

While dealing with basic studies on the interaction between peptides and nanoparticles, this thesis can be divided into two parts. The first part focuses on the application of nanoparticles in materials science. For that reason, the suitability of the α -helical coiled coil folding motif for the tunable structuring of functionalized gold nanoparticles was studied. The second part of this thesis deals with possible biological side-effects related to the medical treatment with nanoparticles. Systematic studies were carried out on the potential of nanoparticles to induce aggregation of peptide similar to that observed in neurodegenerative diseases.

2 Inorganic nanoparticles and their modification with biomolecules

Due to their very interesting optical, electronic, and catalytic properties, nanoparticles that consist of metals (for instance Au, Ag, Pt, and Cu) or semiconductors (for instance PbS, Ag₂S, CdS, CdSe, and TiO₂) have attracted a lot of attention for the generation of larger superstructures. Their remarkable features allow the particles to be addressed by means of external electronic and photonic signals. A variety of synthetic strategies are available to prepare nanoparticles within a narrow size distribution.⁵ The reduction of metal sources in the presence of capping ligands results in the formation of clusters of metal atoms coated with a stabilizing reagent. Moreover, it has been shown that reducing reagents such as an amine-borane complex with a weaker reducing ability allows a controlled growth of nanoparticles and yield a narrower size distribution of nanoparticles compared to commonly used reducing agents such as NaBH₄ or LiBH₄.⁶ The entity of nanoparticles can be summarized by the term nanotechnology [from the Latin *nanus*, Greek *nanos* dwarf]. Generally, nanotechnology is referring to dimensions of 0.1-100 nm, as well as the manipulation of single atoms and molecules. In 2000, the US National Nanotechnology Initiative gave a more specific definition: "Nanotechnology is concerned with materials and systems whose structures and components exhibit novel and significantly improved physical, chemical and biological properties, phenomena and processes due to their nanoscale size." In general, nanotechnology includes the following key physical and chemical issues:

- The occurrence of novel physical properties characteristic of the nanoscale,
- analysis at the atomic and molecular scale at predefined positions,
- control of matter at the atomic scale, and
- the generation of complex functional systems with qualitatively novel properties.

Depending on their functionality, nanoparticles are able to assemble into 2D and 3D nanoparticle architectures. At the same time, this aggregation may be accompanied by the occurrence of new collective properties, such as coupled Plasmon absorbance, interparticle energy transfer or conductivity.

The combination of bio- and nanotechnology to hybrid materials implies the application of biomolecules such as proteins and DNA as functional groups for the assembly of nanoparticles. Several reasons support the concept of utilizing biomolecules as building blocks of nanoparticle structures:

- The diversity of biomolecules offers a variety of different building blocks of predesigned size, shape, and functionality.
- Chemical and biological methods are available to modify and synthesize biomolecules.
- Enzymes may be used as biological tools for manipulation of the biomaterials including reactions such as hydrolysis of peptide bonds, ligation or scission of DNA.
- The structural diversity of biomolecules may be used to invent tunable and/or switchable nanomaterials depending on environmental conditions such as pH or the presence of metal ions.

Due to their easy synthetic accessibility and high chemical stability, nucleic acids have preferentially been used in the early stages of research on the functionalization of nanoparticles to provide highly specific binding sites.⁷ Nevertheless, the growing use of proteins has been employed in order to combine the special properties of nanoparticles not only with the binding properties of proteins, but also to introduce additional intrinsic features such as optic, catalytic, mechanic, or switching capabilities.

Despite the variety of synthetic methods for the preparation of inorganic nanoparticles, the coupling and functionalization with biological compounds is limited to only a small number of chemical methods.⁸ Typically, nanoparticles are synthesized by wet-chemical methods in the presence of stabilizing agents (often citrate, phosphanes, or thiols) which bind to the atoms exposed at the surface of the nanoparticles. This capping provides a stabilization of the metal core and prevents uncontrolled growth or aggregation of nanoparticle. If the capping layer consists of a labile layer such as citrate, biomolecules can be linked directly with the metal particle by exchange reactions with stronger binding ligands (Figure 2.1a). This method is frequently used to immobilize cysteine-containing proteins on colloidal gold. Thereby, chemical means or genetic engineering allows the site-directed modification of proteins with thiol functions. If the nanoparticles are stabilized by non-proteogenic charged ligands like citrate or mercaptoundecanoic acid, the biomolecules can be immobilized through noncovalent interactions such electrostatically attractive interactions (Figure 2.1b). Apart from that, a ligand containing carboxy, amine, or maleimide groups can be used to covalently attach proteins to the nanoparticles by means of carbodiimide-mediated esterification and amidation, or reaction with thiol groups (Figure 2.1c).

These examples demonstrate that chemical strategies have already been explored for the physical linkage of inorganic and biological materials. Nevertheless, coupling methods, especially considering covalent attachment of protein, often require extreme conditions which may lead to the degradation and inactivation of sensitive biological compounds. For that reason, the development of alternative methods is becoming of great interest for the development of hybrid materials.

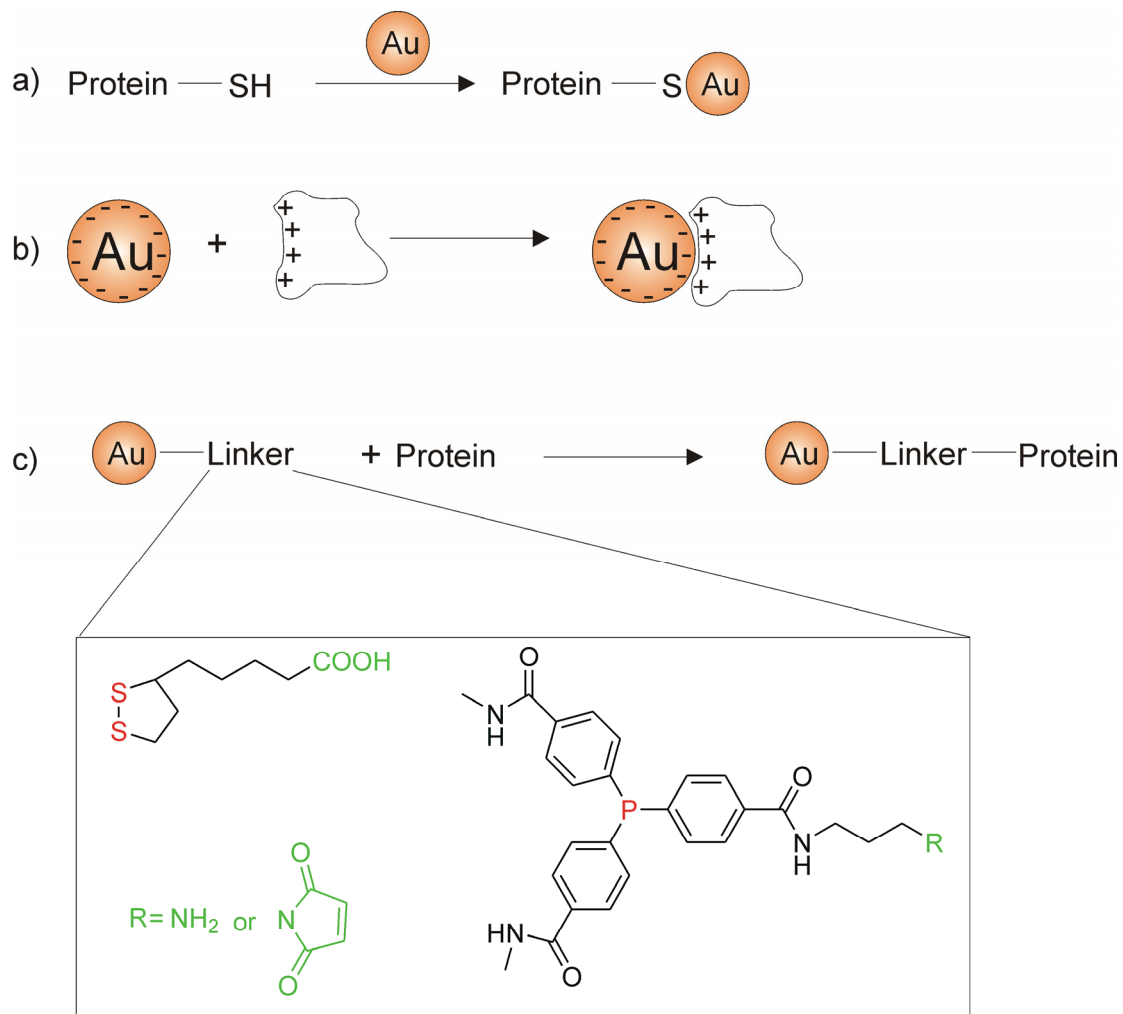


Figure 2.1. Schematic representation of methods to immobilize proteins on inorganic nanoparticles. Red: Positions coordinating to gold nanoparticles; green: functionalities for coupling of proteins.

3 Design of Biomolecule-directed nanoparticle assembly

In theory, the application of biomolecules to the organization of nanoparticles can be divided into the following concepts:

1. **Organization without linker.** According to Figure 3.1a), the functionalization of nanoparticles with biomolecules allows the direct use of biomolecule-based recognition systems for the assembly of one or more species of nanoparticles. For instance, the strong interaction between neutravidin and biotin can be used to achieve an aggregation of particles.⁹⁻¹⁰
2. **Organization with linker.** Here, an additional interaction partner can be applied to cross-link functional groups on the surface of nanoparticle (Figure 3.1b). Based on its design, this linker molecule may mediate the assembly of either one or more kinds of nanoparticles. One example for this concept is provided by a system of gold and silver nanoparticles, each kind coated with different antibodies that can be cross-linked by a molecule containing both antigens.¹¹ However, the general concept of a linker-based organization of nanoparticles also allows an application of biomolecules that do not have to be necessarily introduced as functional groups on the surface of nanoparticles. Provided that the nanoparticles are coated with organic molecules, biomolecules such as proteins may serve as multivalent templates to induce an organization of nanoparticles. Thereby, interaction forces such as electrostatic interactions or hydrogen bonding may be used to bind non-covalently the protein or peptide to the nanoparticle. Furthermore, the symmetry of the protein folding motif may be used to influence the symmetry of the nanoparticle network.
3. **Organization with direct recognition of metal surfaces.** Suitable de novo generated protein linker units may also directly recognize distinct surfaces of semiconductor materials and allow a linking of nanoparticles without previous chemical functionalization (Figure 3.1c). Hence, Bencher and co-workers used phage-display techniques to select 12 amino acid peptides with a binding specificity for semiconductor materials depending on crystal composition as well as crystal face.¹² Nevertheless, the basis for this selectivity is not completely understood and is matter of current investigations.

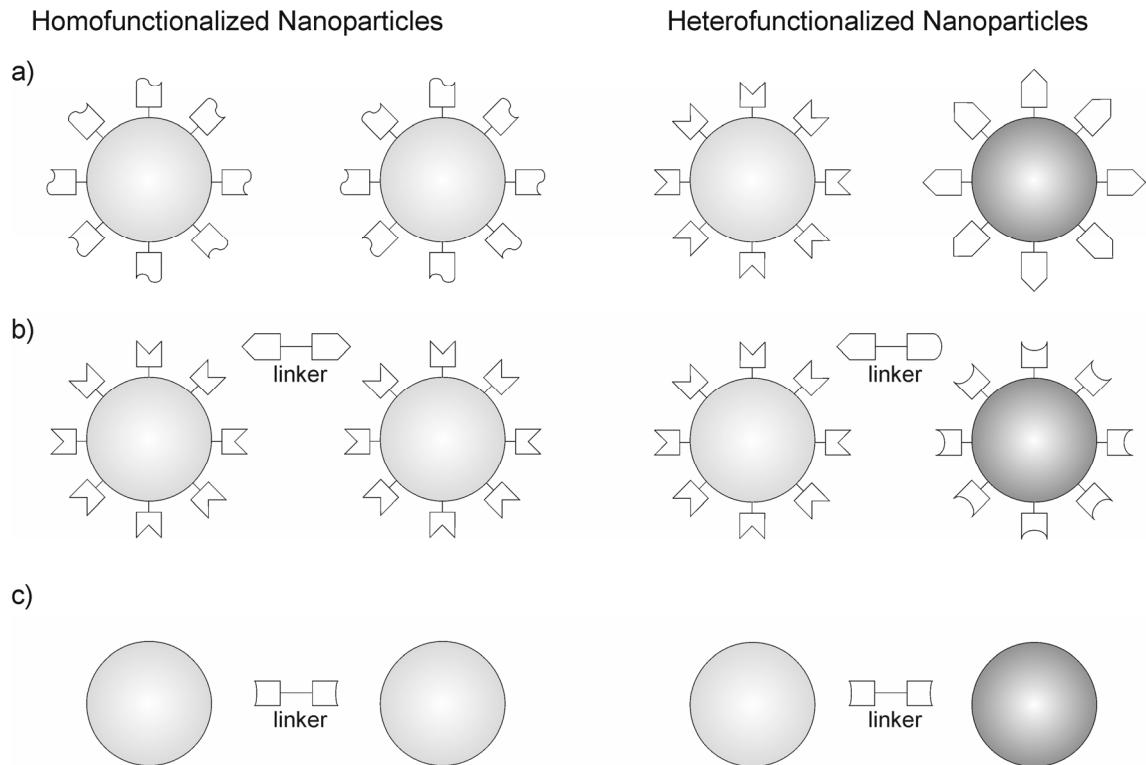


Figure 3.1. Solution-phase chemical coupling with biomolecular recognition elements. a) One or two sets of nanoparticles carry functional groups which are complementary to each other. b) The particle-attached recognition groups are not complementary to each other, but can be bridged by means of bispecific linker molecules. c) A bivalent linker directly recognizes the surfaces of one or two sets of nanoparticle.

These three design strategies allow the application of a variety of biomolecule recognition motifs and biomolecular templates for the assembly of nanoparticles. These coupling approaches have been experimentally realized by using protein-based recognition systems, which will be explained in more detail in the next chapter.

4 Examples of protein-mediated assembly of nanoparticles

Because of the very high and rapidly growing number of reported studies on nanobiomaterials, the following examples represent only a selection with the aim to show the manifoldness of design approaches as well as possible applications of peptide-nanoparticle systems. More detailed and extensive summaries on nanobiomaterials also including the application of nucleic acids can be found elsewhere.^{8,13}

Since the application of the α -helical coiled coil folding motif for the assembly of nanoparticles is an essential topic of this thesis, the application of this structure will be discussed in an extra chapter in order to demonstrate the potential of this structure for nanoparticle structuring as well as to point out the novelty of the results achieved in this thesis.

4.1 Organization of nanoparticles by protein-recognition motifs

One very attractive protein-recognition system for the organization of nanoparticles is the interaction between biotin and the biotin-binding protein streptavidin due to its extraordinarily high binding constant that makes it the strongest ligand-receptor binding interaction presently known.¹³ Another advantage of this system is the extremely high chemical and thermal stability of the streptavidin protein. Similar to the scheme in Figure 3.1, a homogenous functionalization of gold nanoparticles with thiol derivatives

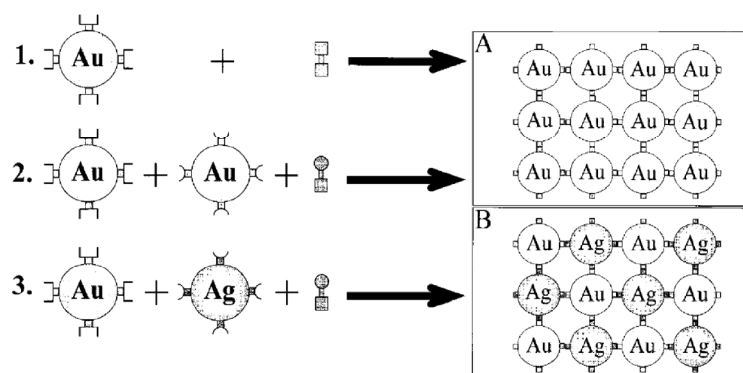


Figure 4.1. Schematic representation showing possible concepts for the directed self-assembly of metallic (1, 2) and bimetallic (3) nanoparticles using antibody-antigen cross-linking (according to Shenton et al.).¹⁶

of biotin yields a cross-linkage upon binding to streptavidin as a molecular linker.¹⁴ On the other hand, a more complex architecture was derived by a pre-incubation of streptavidin with biotin disulfide derivatives yielding a complex which was then treated with gold nanoparticles.¹⁵ Both design concepts generate a spontaneous aggregation of nanoparticles.

The biomolecule-mediated assembly by means of antigen-antibody interactions allows not only the construction of bionanomaterials, but also provides the route towards medical applications, such as immunoassay procedures. In one of the simplest approaches, anti-dinitrophenol (DNP) IgE antibodies were adsorbed onto gold nanoparticles and then cross-linked with a synthetic antigen containing two hapten DNP groups (Figure 4.1).¹⁶ By means of a more sophisticated design, the antigen-antibody recognition system can also be used to assemble differently functionalized nanoparticles. This system even allows the formation of bimetallic nanoparticle aggregates, as observed for anti-DNP IgE functionalized gold nanoparticles and anti-biotin IgG functionalized silver nanoparticles in the presence of DNP-biotin bivalent antigens.¹⁶

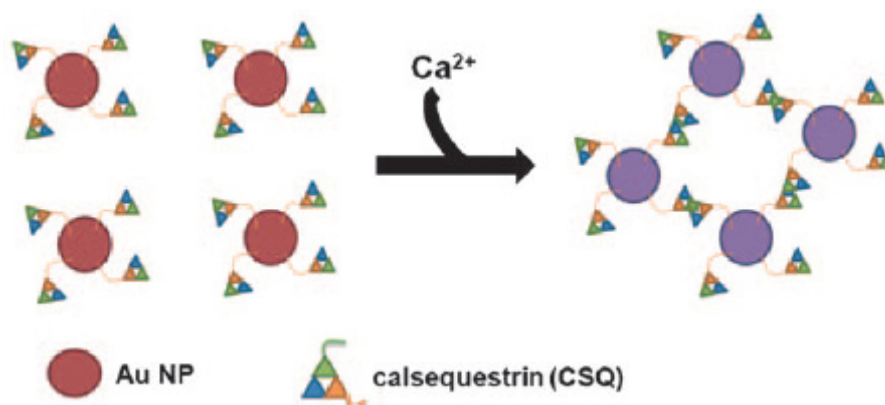


Figure 4.2. Schematic representation of the calcium ion sensor: the aggregation of calsequestrin functionalized gold nanoparticles caused by binding of Ca^{2+} ions results in a color change (according to Kim et al.).¹⁷

One example for an organization of nanoparticles without a linker has been reported by Kim et al. using calsequestrin (CSQ) functionalized gold nanoparticles (Figure 4.2).¹⁷ Calsequestrin itself is a calcium-binding protein of the sarcoplasmic reticulum. Despite its very low binding affinity, calsequestrin possesses a very high binding capacity for Ca^{2+} ions due to 40-50 binding sites per molecule. Upon binding Ca^{2+} ions, CSQ undergoes a conformational change from an unfolded into a more compact monomeric protein structure followed by oligomerization. Kim et al. successfully showed that the calcium-sensitivity of calsequestrin is transferable to the whole nanoparticle system

whose extent of aggregation strongly depends on the calcium concentration. The combination of protein and nanoparticle selected here leads to the development of novel and highly sensitive detection systems which allows the visualization of changes in blood calcium levels, and may be useful in the detection of several diseases associated with hypercalcemia or malignant tumors.

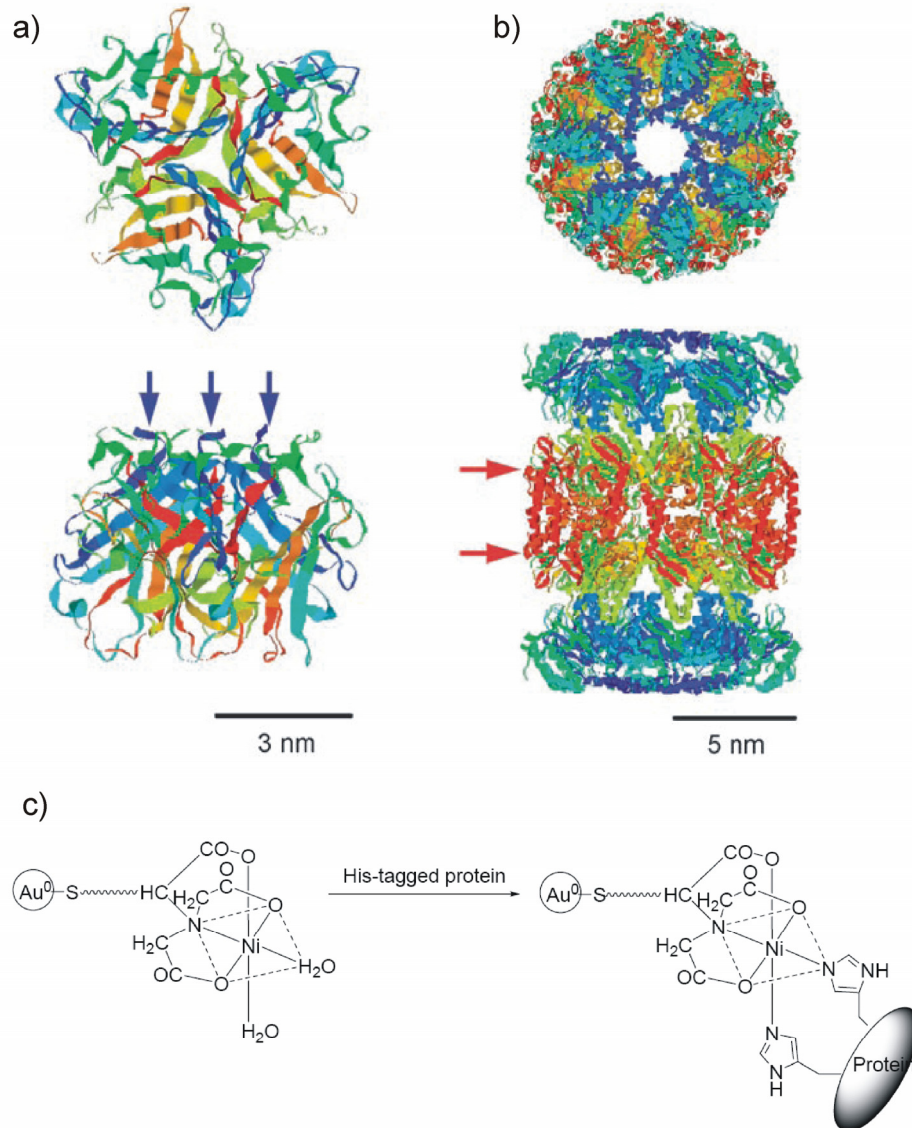


Figure 4.3. 3D structures of (a) Ad12 knob and (b) 20S proteasome proteins showing the binding motif to gold nanoparticles. The arrows indicate the attachment of the 6xHis tag to each subunit. c) Binding of Ni-NTA gold nanoparticles to 6xHis-tagged proteins (according to Hu et al.).¹⁸

One of the very few studies on a highly-ordered organization of nanoparticles in solution has been published by Hu et al.¹⁸ The authors applied two proteins of different

symmetries, namely the Ad12 knob and 20S proteasome protein, to the binding of nanoparticle and investigated the morphology of nanoparticle structures by electron microscopy. Moreover, a direct attachment of protein to gold nanoparticles was used by the highly specific interaction of the (1S)-N-[5-[(4-Mercaptobutanoyl)amino]-1-carboxy-pentyl]iminodiacetic acid (NTA-Lys-SH) ligand shell of the nanoparticle with 6xhistidine tags attached to the proteins. Their studies revealed that only in the case of the 20S proteasome protein, an ordered structure of nanoparticles was obtained. Moreover, the ordered arrangement was tetragonal which does not agree with the D7 symmetry of the original protein folding. However, this discrepancy seems to be very likely a consequence of sterical restriction that allows an arrangement of not more than four nanoparticles around one protein molecule.

In addition to naturally occurring protein folding motifs, many studies also focus on the application of de novo designed short peptide sequences in order to organize nanoparticles. Synthetic polypeptides are attractive components in hybrid designs since they are chemically and physically robust, functionally and structurally versatile, and can be produced at moderate cost and effort by well-established methods. For instance, Si et al. applied a tripeptide sequence containing glutamic acid to the modification of gold nanoparticles in order to derive an assembly of nanoparticles at low pH values due to the hydrogen-bonding between protonated glutamate residues.¹⁹ In another study, the same authors were able to show that their modification of nanoparticles not only creates sensitivity to pH but also to the presence of metal ions such as Hg²⁺ ions.²⁰

Recapitulating, the above-mentioned examples show that protein-recognition motifs can be successfully applied to induce the assembly of nanoparticles if necessary in dependence on environmental conditions such as pH or the presence of metal ions. At the same time, a highly-ordered arrangement of nanoparticles based on the symmetry of the protein folding seems to be quite challenging. For that reason, these examples provide a more promising route towards novel detecting systems than for applications in materials science. An emerging area of such nanoparticle-based detection systems is in regard to enzymes, which will be discussed in more detail in the next part.

4.2 Enzymatic control of protein-based nanoparticle systems

In medicine, the analytical detection of enzymes is a very important tool for screening noxious toxins and pathologies where they are present and for applying very effective and selective therapy. For instance, the analytical detection of proteases has been reached by the application of fluorogenic substrates including an internally quenched fluorophore.²¹²² Upon enzymatic cleavage, an increase in fluorescence intensity can be measured. While this kind of assay was used for widespread applications because of its usefulness and practicability, the exact quenching mechanism has to be resolved for every substrate. For that reason, recent studies worked on nanoparticle-based assays including enzymatically-controlled elements for aggregation. This approach allows the detection of enzyme in the simplest case by eye because of a color change, but may also require analytical techniques like UV/Vis spectroscopy or MR imaging. The use of nanoparticle-based assays allows a detection level comparable to that of other techniques like FRET- or ELISA assays. In addition to the analytical detection, enzymatically-responsive hybrid materials based on nanoparticles are also of growing interest for drug delivery.

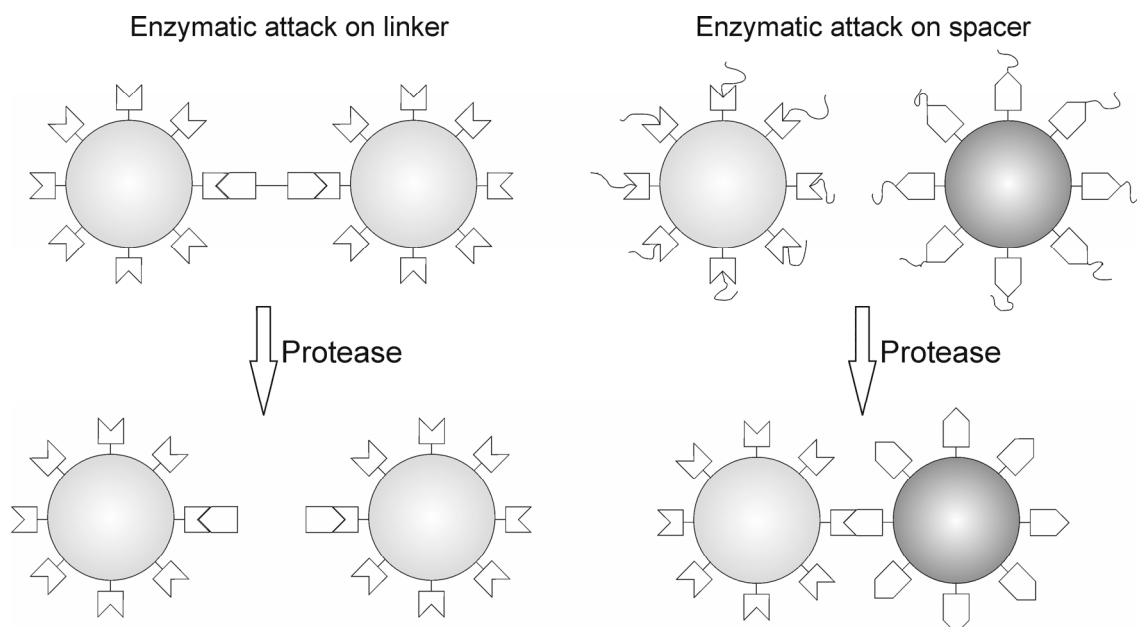


Figure 4.4. Scheme of two different approaches to control the nanoparticle assembly by means of proteases.

The enzymatically-controlled aggregation of nanoparticles can be reached by several concepts. Figure 4.4 shows two different approaches how to use enzymes to control

the aggregation of nanoparticles. A comparably simple approach is based on a multivalent peptide that carries a recognition domain for a specific protease and, without cleavage, interacts with more than one nanoparticle leading to aggregation in the absence of enzyme. Cleavage of this linker-peptide in the presence of protease interrupts the connection between nanoparticles and their aggregation (Figure 4.4a).

One of the earliest studies by Weissleder et al. followed this concept on enzymatically-controlled aggregation of nanoparticles.²³ Here, the peptide carries a biotinylated residue on each terminal in order to induce aggregation of avidin-coated magnetic nanoparticles. Moreover, they designed several derivatives of the peptide, each one carrying a recognition domain for a specific protease such as trypsin, renin and MMP-2. Both latter proteases play an important role in blood pressure regulation and tumor angiogenesis, respectively. An incubation of the particles with the untreated peptides resulted into a colloidal assembly. In contrast, when preincubating the peptide with the corresponding enzyme and then exposing it to avidin-coated magnetic nanoparticles, the presence of protease can finally be measured by changed magnetic properties like the T2 relaxivity due to the prohibited aggregation.

A quite similar system was published by Guarise et al. containing gold nanoparticles that were cross-linked by a peptide carrying a cysteine residue at the N- and C-terminus.²⁴ Moreover, these cysteine residues were acylated to avoid any reaction and possible inactivation of the enzyme, while the acylation of the cysteine did not affect the interaction with the gold colloids. As indicated by a color change of the solution from pink to violet-blue, the peptide alone induces an aggregation of nanoparticles. Since the peptide contained recognition elements for thrombin, a serine protease, a pre-treatment of the peptide with this enzyme prohibited an aggregation of gold nanoparticles which could be measured by absorption spectroscopy. By incubation with other enzymes like chymotrypsin and plasmin, they showed that this system is highly specific for thrombin.

Molly M. Stevens applied a peptide containing cysteine at the C-terminus to the interaction with gold nanoparticles.²⁵ However, in contrast to the studies of Guarise, the aggregation of gold nanoparticles was driven by π -stacking interactions between the Fmoc-groups which were N-terminally attached to the peptidic ligand (Figure 4.5). An introduction of a suitable recognition domain made the system sensitive to the presence of thermolysin.

While the above-mentioned examples deal with the enzymatically-prohibited aggregation of nanoparticle, a detection of enzyme can also be achieved by a more sophisticated design of an enzymatically-induced aggregation of nanoparticles (Figure 4.4). In this case, two kinds of nanoparticles have to be synthesized, each one is

coated with only one component of a biomolecular recognition motif. Without further modification, both species of nanoparticles spontaneously assemble into aggregates. This system can be made to indicate the presence of enzymes by introducing huge spacer molecules which are bound to one or both ligands via a peptidic recognition sequence specific for a certain enzyme.

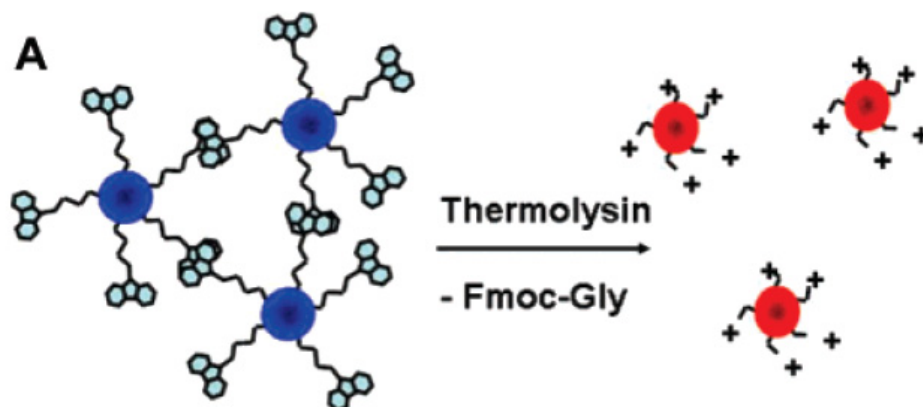


Figure 4.5. Schematic representation of the protease-triggered nanoparticle dispersion approach.²⁵

This approach was realized by Bhatia and colleagues who worked on the enzymatically-directed aggregation of superparamagnetic Fe_3O_4 .^{9,10} The nanoparticles were modified with either biotin or neutravidin. Neutravidin is a deglycosylated derivative of avidin, a protein which occurs in hen's egg and binds biotin. As spacer molecules, linear PEG chains were attached by a proteolytic substrate sequence to at least one kind of nanoparticles. With regard to the linker sequence, Bhatia et al. introduced sensitivity towards the MMP-2 protease alone⁹, or in combination with the MMP-7 protease¹⁰, while both enzymes are expressed at very high levels in carcinogenic cells. In both examples, they successfully showed that these nanoparticle-derived substrates are specifically recognized by these metalloproteinases and that the enzymatic cleavage of the proteinogenic substrate and the removal of the PEG spacers successfully induce a self-assembly of the two sets of nanoparticles. By including MRI measurements in their studies, their results document an external targeting of exclusively malignant cells by magnetic fields, which presents a very novel and promising route for cancer therapy.

Further studies of the group of Bhatia demonstrated that a system of protein and nanoparticle not only allows sensitivity towards proteases but may also enable the detection of further enzymes such as the tyrosine kinase or phosphatase.²⁶ The new design did not include any spacers into the peptide sequence. Here, the corresponding sets of nanoparticles were equipped with either a tyrosine containing peptide or the Src

Homology (SH2) domain, respectively. In the case of phosphorylation of the tyrosine residue, both kinds of nanoparticles undergo an assembly, which can be reversed upon the addition of the phosphatase.

In light of the above-mentioned examples, the application of enzymes turned out to be a valuable tool for controlling the assembly of nanoparticles. Nevertheless, this does not only imply the modification of nanoparticle architectures by means of enzymes, but leads also to an emerging area of medical research with very promising solutions of nanoparticles for cancer therapy among others.

4.3 Organization of nanoparticles by the coiled coil folding motif

In this thesis, a coiled coil based linker peptide was used to achieve an organization of nanoparticles. Due to its defined folding, a coiled coil peptide extends the features of a simple linker by additional elements such as a more complex symmetry available for a higher-ordered nanoparticle arrangement or elements to direct this arrangement in dependence on environmental conditions.

In general, the α -helical coiled coil structure consists of two to seven α -helices wound around one another to form a left-handed coil.²⁷ Thereby, the super-coiled α -helices go through 3.5 residues for each complete turn of the helix, instead of 3.6 residues in the case of a regular α -helix. As a result, one complete turn can be described by means of the so-called heptad repeat commonly denoted as (a-b-c-d-e-f-g)_n. Figure 4.6 shows a

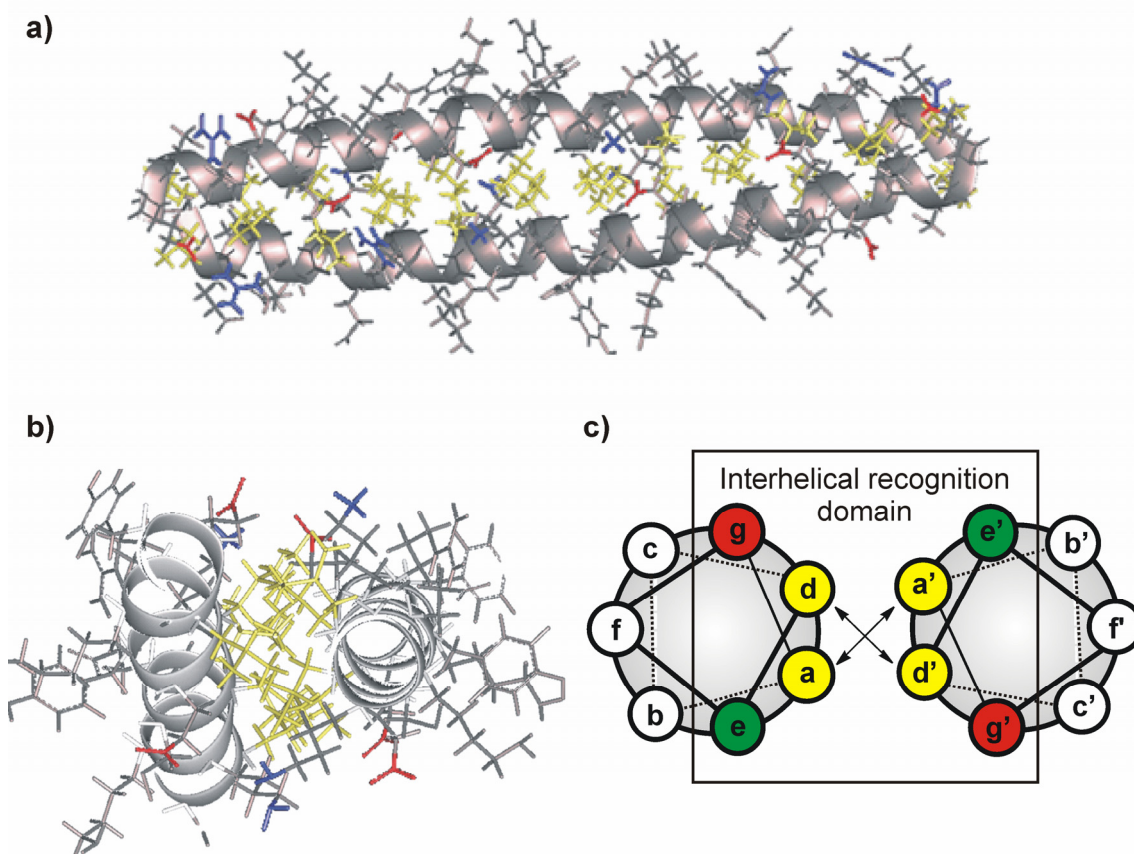


Figure 4.6. a) Spatial view, b) view perpendicular to the helix axis of a molecular modelling structure of an antiparallel, 41 residue coiled coil peptide. c) Helical wheel presentation of a parallel dimeric coiled coil peptide. Yellow: hydrophobic residues at positions a and d; red/green: complementarily charged residues at positions e and g; white: solvent exposed residues at positions b, c, and f.

molecular modelling structure as well as the helical wheel diagram of a dimeric parallel coiled coil peptide. Due to the simplicity and regularity of the coiled coil structure, the occupation of the positions a to g follows relatively simple design rules.²⁸⁻³¹ Since the thermodynamic stability of this quaternary structure is mainly driven by the formation of a hydrophobic core between the helices, positions a and d often contain hydrophobic amino acids such as leucine, valine, and isoleucine. Moreover, the helices may also interact by salt bridges, thus preferring oppositely charged residues (most commonly glutamate, lysine, and arginine) in position e and g. At the same time, the occupation of these positions may be used to specify a homo- or heterooligomerization as well as to determine a parallel or antiparallel alignment of α -helices. For instance, a placement of exclusively glutamate in positions e and g favors a binding of a second coiled coil peptide with complementarily charged residues in positions e' and g'. The remaining positions b, c, and f are not directly involved in the recognition domain of the helices, but often contain polar residues since they are solvent-exposed. Apart from that, these positions can be also used to influence the stability of the helix itself or to present an interaction domain with further molecules such as nanoparticles.

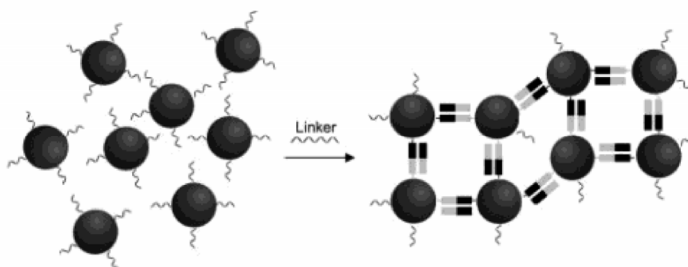


Figure 4.7. A concept for assembling nanoparticles using coiled coil derived linkers (according to Ryadnov et al.).³³

The α -helical coiled coil structure is very attractive for the assembly of nanoparticles due to the following reasons. First, the design principles of coiled coils have been intensively studied and are well-understood and allow the de novo design of α -helical peptides. For that reason, the flexibility in design serves as a very good foundation for the rational development of nanoparticle systems with controlled spacing and architecture. For instance, the oligomerization state of coiled coil peptides may be used to influence the geometry of nanoparticle architecture. Second, the formation of coiled coil structure implies an oligomerization of different peptide strands which, in return, may be used to assemble different nanoparticles. As a third very important point, an appropriate modification of the coiled coil design may enable the destabilization of the folding motif and/or oligomerization at certain conditions, which can be used to direct

the arrangement of nanoparticles in dependence on environmental conditions such as pH or the presence of metal ions.

In one of the simplest approaches, a heterofunctionalization of two different kinds of nanoparticles, each one coated with one of the two complementary coiled coil peptides, yield nanomaterials with novel spectroscopic properties.³² Moreover, Ryadnov et al. skillfully applied the coiled coil folding in order to generate a “belt and braces” system for the organization of gold nanoparticles (Figure 4.7).³³ Two different kinds of nanoparticles, each functionalized with one of the two half-sized peptides (“the braces”) were co-assembled by a linking coiled coil sequence (“the belt”). One of the first approaches on coiled coil systems used the pH dependent stability of coiled coil structure in order to allow a pH-dependent assembly of gold nanoparticles.³⁴ Stevens et al. described a peptide design in which equally charged glutamate residues in position e and g yield repulsion at pH 7, but upon protonation enable an oligomerization of α -helices and aggregation of nanoparticles at acidic conditions.

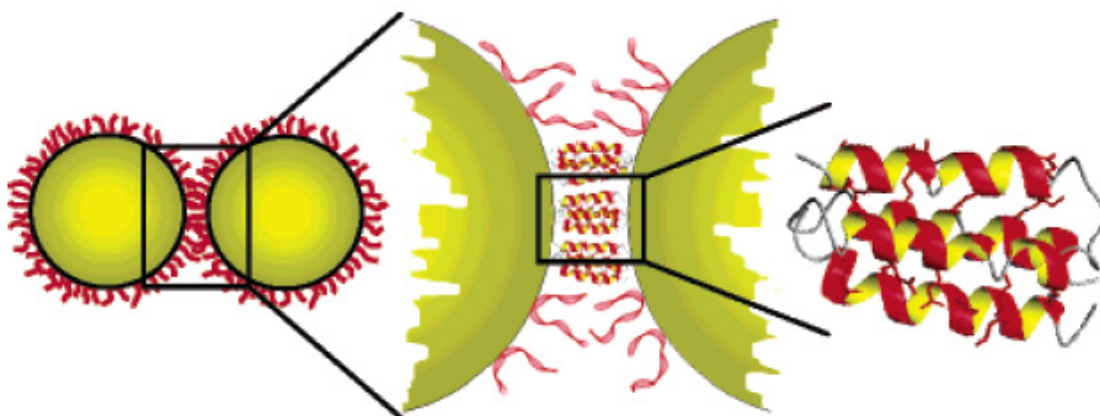


Figure 4.8. Schematic representation of the interaction between two nanoparticles modified with complementary helix-loop-helix peptides (according to Aili et al.).³⁶

The group of Liedberg has extensively studied the application of de novo designed helix-loop-helix peptides for the induced aggregation of nanoparticles. The design principles of helix-loop-helix motif is based on the design features of coiled coil peptides, and can be described as two α -helical peptide strands covalently linked by a loop sequence. Depending on the applied peptide design, the homo- or hetero-dimerization of helix-loop-helix peptides resulting into a molten globule-like four-helix bundle enables the assembly of gold nanoparticles provided that the peptides were covalently attached by a cysteine moiety (Figure 4.8).³⁵⁻³⁶ Similar to Stevens et al., an arrangement of equally charged residues within the interhelical recognition domain also allows the control of nanoparticle-assembly by pH.³⁶ Based on the complexation of

metal ions such as Zn^{2+} ions by glutamate or aspartate residues, the zinc ion concentration may be also used to direct the assembly of nanoparticles by mediating dimerization of the helix-loop-helix peptides.³⁷

Altogether, the α -helical coiled coil motif is a very attractive building block for the construction of bionanomaterials, due to its well-studied and flexible design principles. This protein folding motif enables an assembly of nanoparticles and even allows a switchable assembly dependent on environmental conditions such as pH or the presence of metal ions providing access to novel detection systems. Nevertheless, use of these concepts including a covalent attachment of coiled coil peptide, did not obtain a defined geometry of nanoparticle assemblies, an essential requirement of the application of these systems to materials science. For that reason, the question remains whether the coiled coil folding motif can be applied to the organization of nanoparticles such that highly-ordered structures can be achieved. However, a general design concept for a protein-based nanoparticle organization also implies that, in the presence of nanoparticles, the protein structure is predictable and does not undergo undesirable folding transformations. Such alterations may not only prevent applications in materials science but also play a crucial role for medical applications of nanoparticles.

5 Protein folding and misfolding

As can be calculated by theoretical methods, a tremendously high number of possible conformations can be conceivably adopted by one protein. For that reason, the mechanism of proteins to fold correctly into their native state is a very interesting issue and attracted the attention of many research areas such as bioinformatics or physics. In most cases, the native state of protein corresponds to the structures that are most thermodynamically stable under physiological conditions.³⁸ Now, it has been widely accepted that protein folding does not involve a series of mandatory steps between specific partially folded states, but rather a stochastic search of the many conformations accessible to a polypeptide chain.³⁹ The intrinsic fluctuations of a polypeptide chain enable the contact even between residues that are highly separated in the primary structure. Many studies suggest that the fundamental mechanism of protein folding is based on the formation of a folding nucleus, which involves a relatively small number of residues establishing the native-like fold within local regions of the protein sequence. Once formed, the folding nucleus very likely forces the remaining amino acids into the correctly folded state of protein.³⁹

In the cell, protein synthesis is taking place onto ribosomes by means of translation and is encoded by the genetic information in the cellular DNA. Protein folding is in some cases co-translational, meaning that the protein sequence already starts to fold although the translation process is still on-going.⁴⁰ In other cases, the final state of protein is achieved either in the cytoplasm or in specific compartments, such as mitochondria or the endoplasmic reticulum.⁴¹ In other words, the details of the folding process are determined by its particular environment, whereby an inappropriate interaction with other molecules within the crowded environment of the cell constrains may threaten the correct protein folding. Since a correctly folded state of protein is essential for the functioning of living systems, the cellular environment displays a range of strategies such as molecular chaperones to assist the adoption process and to prevent particularly aggregation. A misfolding of proteins may lead to a pathogenic form followed by malfunctioning of living systems and diseases. Especially proteins secreted to the extracellular environment may escape the protective mechanisms when misfolded. Hence, a growing number of neurodegenerative disorders, including Alzheimer's and Parkinson's disease are associated with a folding transformation of a native state of protein into a malicious β -sheet rich form. This β -sheet rich form undergoes a self-assembly into malicious deposits in tissues, including the brain, heart,

or spleen.⁴²⁻⁴⁴ Per definition, the class of proteins involved in such diseases is summarized by the term amyloid.

Although the about 30 known proteins involved in amyloidosis do not have homologies in their sequences, their aggregated forms share common characteristics. Amyloids show a specific optical behavior such as birefringence when stained with certain dye molecules such as Congo Red.⁴⁵ Amyloid deposits display an unbranched fibrous morphology, as revealed by electron microscopy, as well as a characteristic “cross- β ” X-ray fiber diffraction pattern.⁴⁶ The ability to form amyloidogenic structures is regarded as a generic feature of polypeptide chains, since the core structure of fibrils seems to be stabilized especially by hydrogen bonds involving the polypeptide main chain.⁴⁷ In general, the intrinsic propensity of polypeptide chains to self-assemble into fibrils correlates with their physiochemical properties such as charge, secondary-structure propensities, and hydrophobicity.⁴⁸

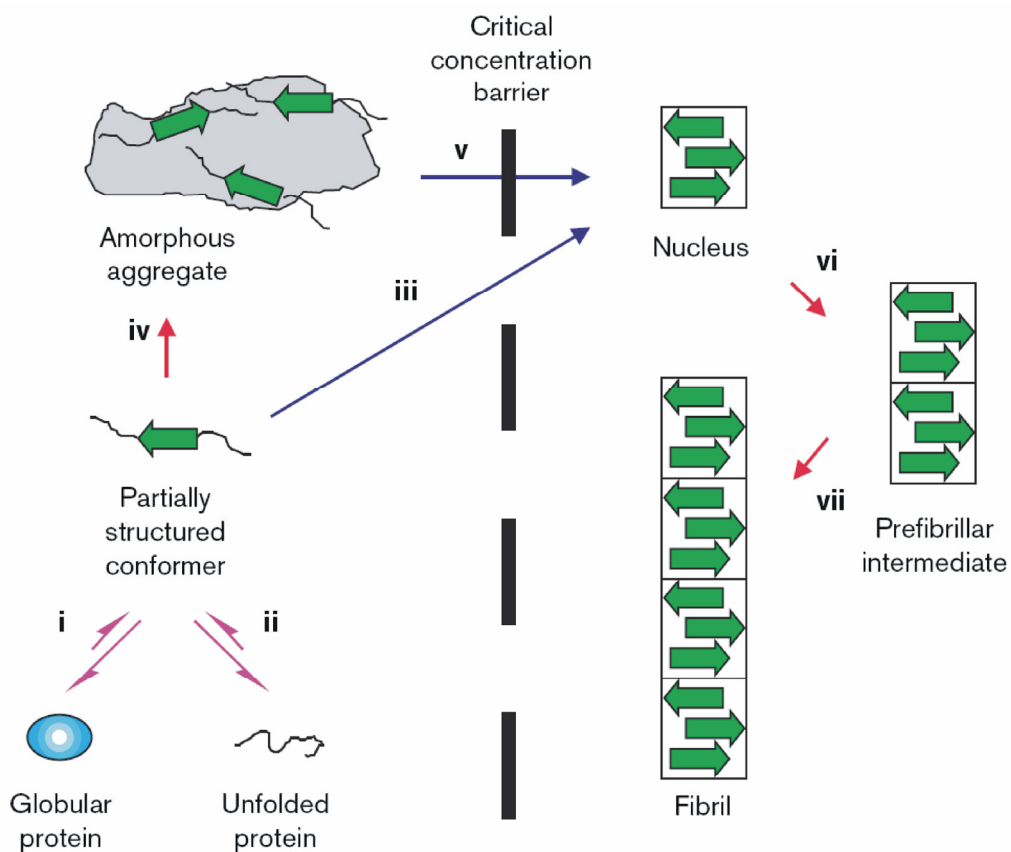


Figure 5.1. Proposed mechanism of amyloid formation by partial folding and unfolding. (i, ii) Formation of partially structured intermediate out of a globular or unfolded state of protein. These intermediates either self-assemble to form the nucleus (iii) or associate forming amorphous aggregates followed by a realignment (iv, v). Extension of the nucleus results in the formation of prefibrillar intermediates (vi) and fibrils (vii) (according to J.-C. Rochet et al.).⁴⁹

The assembly of β -sheet rich structures into fibrils generally occurs via a nucleation-dependent oligomerization, including the formation of an ordered nucleus after a lag phase. Importantly, nuclei are not a fixed unit; once formed, they can either progress to fibrils or disintegrate if not extended in time (a detailed mechanism is shown in Figure 5.1).⁵⁰ For that reason, the nucleus is extended to prefibrillar intermediates and the final fibrillar structure only if above a critical concentration limit. Moreover, some proteins form amyloid structures via a non-nucleation pathway.⁵¹

Most neurodegenerative diseases are reckoned as incurable to date. For that reason, research towards understanding the mechanism of amyloid formation within meaningful biological contexts paves the way for an efficient diagnosis and medical treatment. Environmental factors such as temperature, ionic strength, pH, and oxidation potential are widely accepted to have a triggering impact on the misfolding of proteins. Moreover, a particular composition of membranes is regarded to support fibril formation. However, the low solubility of amyloid forming proteins, their complex structure, and a mostly poor synthetic accessibility make it difficult to do a detailed characterization of their folding behavior by means of the usually applied analytical methods. Therefore, in the recent years, the development of de novo designed model peptides became of huge interest for systematic studies on the general mechanism of amyloid formation at a molecular level.

The design approaches of these model peptides can be divided into different strategies:

- Empirical approaches generally focus on the identification of amyloid-promoting regions of a protein. The model peptides derived from these fragments usually display the same characteristic morphology of fibers as found for the full-length peptide.
- Combinatorial design approaches focus on the elucidation of the sequence features that promote or prevent β -sheet aggregation. For instance, amphiphilicity of peptides generated by a binary pattern of hydrophilic and hydrophobic residues was shown to result into β -sheet formation with subsequent aggregation into β -sheet rich fibrils.⁵² Amphiphilic β -strands are not stable in aqueous solution; they require to stabilize the backbone atoms by hydrogen bonding and to bury nonpolar surfaces within the tertiary structure.

- The creation of model peptides by means of rational approaches is based on two aspects: first, to constitute the principles underlying the structural transitions of proteins before the amyloid assembly; and second, to elucidate the factors required for the β -sheet polymerization into amyloidogenic assemblies or amorphous aggregates. At the same time, rational approaches also include de novo design approaches.

A very high number of studies to the design of amyloid-forming model peptides can be found in the literature. Since the aim of this study was not only referring to the development of amyloid-forming model peptides but also to their application to studying nanoparticle-induced misfolding, the next chapter only contains extracted examples of rational design approaches based on the α -helical coiled coil folding motif. A more detailed summary of various model systems can be found elsewhere.⁵³⁻⁵⁶

5.1 Coiled coil based model peptides to study amyloid-formation

In recent years, the α -helical coiled coil folding motif has become a very attractive basic structure for the design of model peptides to study the underlying principles of protein misfolding. This is for several reasons. First of all, the α -helical coiled coil presents a well-defined state of folding that mimics the native state of proteins. Second, the coiled coil structure is an extensively studied folding motif with relatively simple design

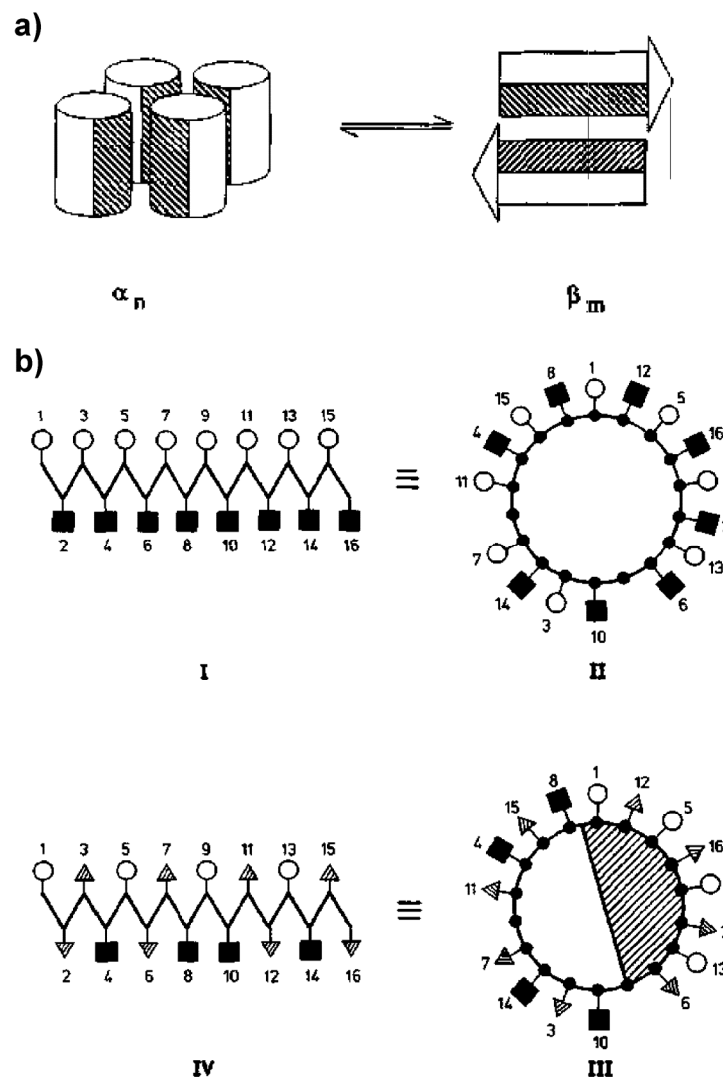


Figure 5.2. a) Schematic representation of the conformational transition between an aggregated α -helical state and a bilayer β -sheet. The conformation transition may be induced by a pH change. b) Design of switch peptides. Left: schematic representation of β -sheet conformation for the starting sequence (I) and the final switch peptide sequence (IV). Right: helical wheel diagram of the starting sequence and the final switch peptide sequence. Circles, squares, and triangles denote hydrophilic, hydrophobic, and neutral amino acids, respectively (according to M. Mutter et al.).⁵⁹

features. These design features may be combined with additional features to allow an adoption of foldings alternative to the α -helical one as well as to introduce elements to direct this transformation by means of environmental conditions. In order to combine the coiled coil folding with increased β -sheet propensity, one widely used design approach modifies the arrangement of hydrophobic residues in i , $i+3$, and $i+4$ positions of the coiled coil sequence so that the peptide sequence contains a binary pattern of hydrophilic and hydrophobic residues if the alignment of peptide sequence is extended. Such binary sequences are amphiphilic and prone to fold into β -strands that bury their nonpolar faces by aggregating into extended fibrillar structures.⁵⁷⁻⁵⁸

This design approach was first published by Mutter et al. in 1991.⁵⁹ The starting point of their design was a repetitive pattern of an amphiphilic β -sheet. Based on this sequence, they introduced neutral amino acids (neither hydrophilic nor hydrophobic) with the result that a helical cylinder containing a hydrophobic and a hydrophilic face was generated (Figure 5.2). Such an arrangement of residues increases the propensity for α -helical structures based on the formation of a hydrophobic core upon oligomerization. For that reason, the sophisticated design chosen by Mutter et al. allows a competition between the α -helical and β -sheet structures. An additional introduction of charged residues was further used to generate a pH dependency of these structural preferences. One very remarkable conclusion made by Mutter et al. was that the occurrence of a particular conformation under certain experimental conditions is mainly dominated by factors due to the intermolecular association process rather than by the intrinsic structural propensity of the peptide sequence itself.

The group of S. H. Gellman used the combination of binary pattern and coiled coil sequence to end up with a redox-triggered secondary structure change by means of coiled coil peptides.⁶⁰⁻⁶¹ Based on the general design of coiled coil structures, methionine residues were placed in the hydrophobic core of an 18-residue peptide sequence which enables in the reduced state an oligomerization of α -helices because of the amphiphilic nature of α -helices. Upon oxidation, the increased polarity of methionine residues successfully disturbed the coiled coil formation. As a result, an increased β -sheet propensity was exclusively observed in the oxidized state of protein. Moreover, Kammerer et al. used an almost similar design approach to allow folding transition from an α -helical into a β -sheet structure by means of coiled coil based model peptides.⁶²⁻⁶⁴ In contrast to the group of Gellman, their system did not require an oxidation but elevated temperatures for this folding transition. Their peptide design also allowed the formation of a hydrophobic core and interhelical salt bridges. Moreover, a modification of the coiled coil sequence with alanine and leucine residues generates a binary pattern of hydrophobic and polar residues, resulting into an increased β -sheet

and fibril formation propensity (Figure 5.3). All model peptides showed an initial dimeric⁶⁴ or trimeric⁶²⁻⁶³ α -helical coiled coil structure that, requiring elevated temperatures of 37°C, was converted into β -sheets with subsequent formation of amyloid-like structures. Similar to the results obtained by Gellman, studies on different oxidation states of methionine residues revealed that a distortion of binary pattern by means of oxidized methionine residues is sufficient to prevent an amyloid formation. At the same time, the oxidation of methionine did not interfere with the coiled coil structure.

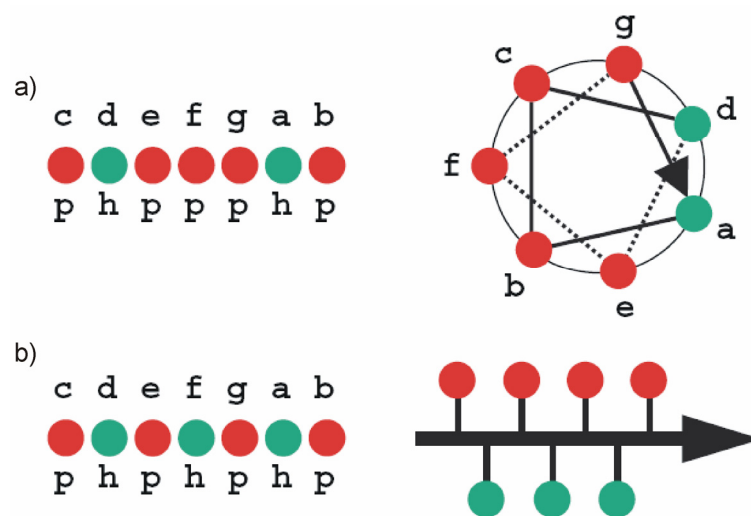


Figure 5.3. Peptide design. a) To allow the adoption of coiled coil structure, polar (p, red spheres) and non-polar (h, green spheres) amino acids are placed at positions a and d of the heptad repeat. b) The two residue periodicity of amphipathic β -strands is obtained by placing polar and non-polar residues in an alternating manner (according to R. A. Kammerer et al.).⁶⁴

All the above-mentioned examples of combining coiled coil design features with the binary patterning approach allow an adoption of β -sheet structure controlled by changing the solvent medium,⁵⁹ redox states of methionine,⁶⁰⁻⁶⁴ and pH⁵⁹. The group of J. D. Hartgerink investigated more deeply the general requirements to the arrangement of non-polar residues in order to induce a β -sheet transformation of coiled coil peptides.⁶⁵ In their studies, they showed that even an arrangement of only a few of hydrophobic residues within a hydrophobic patch at one side of the peptide strand is sufficient for an increase of the β -sheet propensity (Figure 5.4). Obviously, this arrangement may serve as a nucleus for a β -sheet hydrogen-bonded structure. Moreover, they pointed out that position f in the heptad repeat is especially suitable for creating such a hydrophobic patch. Because of the unique position between the

required hydrophobic amino acids in positions a and d three contiguous hydrophobic amino acids cluster on one face of the molecule when it is folded in an extended conformation.

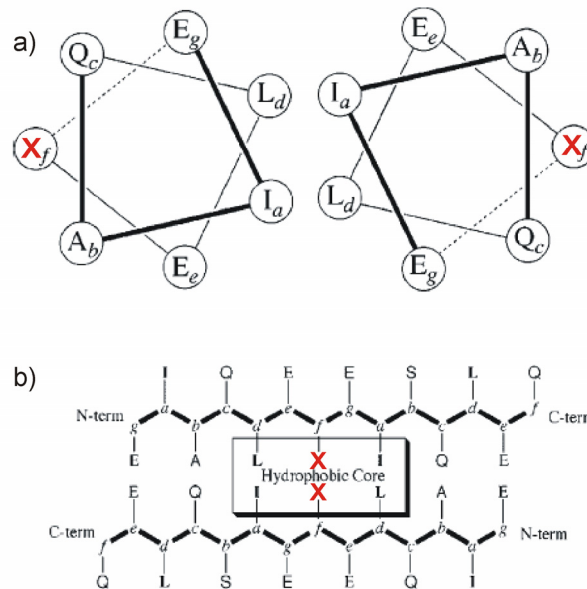


Figure 5.4. Structural arrangement of the model peptide in the coiled-coil or amyloid-like β -sheet packing motifs. The residue X refers to the position selected for systematic substitutions (according to J. D. Hartgerink et al.).⁶⁵

In contrast, D. N. Woolfson and colleagues used a simple coiled coil based system without a binary pattern to induce a transition into β -sheets at elevated temperatures.⁶⁶ Furthermore, they addressed the role of the primary structure to influence the rather extreme α to β transitions. The starting point of their design was a canonical α -helical leucine-zipper peptide, which folds into a stable α -helical structure and did not show any β -sheet tendency even at elevated temperatures. This sequence was then modified in a first step by exchanging three glutamine residues at the f sites for threonine. As threonine possesses a lower α -helix propensity and a higher β -sheet propensity than glutamine, this modification is expected to still allow a coiled coil folding but with decreased stability. Indeed, this peptide sequence folded into a coiled coil at room temperature but underwent a transition into β -structures upon thermal denaturation. Also further modifications by tethering the termini of two peptide strands using a disulfide bond raised the β -propensity of the sequence. All the modifications of a coiled coil sequence selected here showed that straight destabilization of the native

state of protein does not necessarily have to promote folding switches into β -sheets, since elevated temperatures were still required to do so.

A completely different approach based on unnatural modifications has been developed by the group of H. Mihara.⁶⁷ In their design, a two- α -helix part was constructed from a 14-residue peptide whose sequence was based on the classical heptad repeat pattern of the coiled coil design (Figure 5.5). By means of a linker sequence, each end of the sequence was equipped with adamantane groups in order to generate a hydrophobic defect which then drove the peptide into β -sheet structures and fibrillar structures. The necessity of the adamantane groups for this structural transition was further proven by complexation of these groups with cyclodextrine which yielded a stable α -helical conformation of peptide. Furthermore, this model system was used to study the impact of various environmental conditions such as pH, salts and TFE on this folding transition.

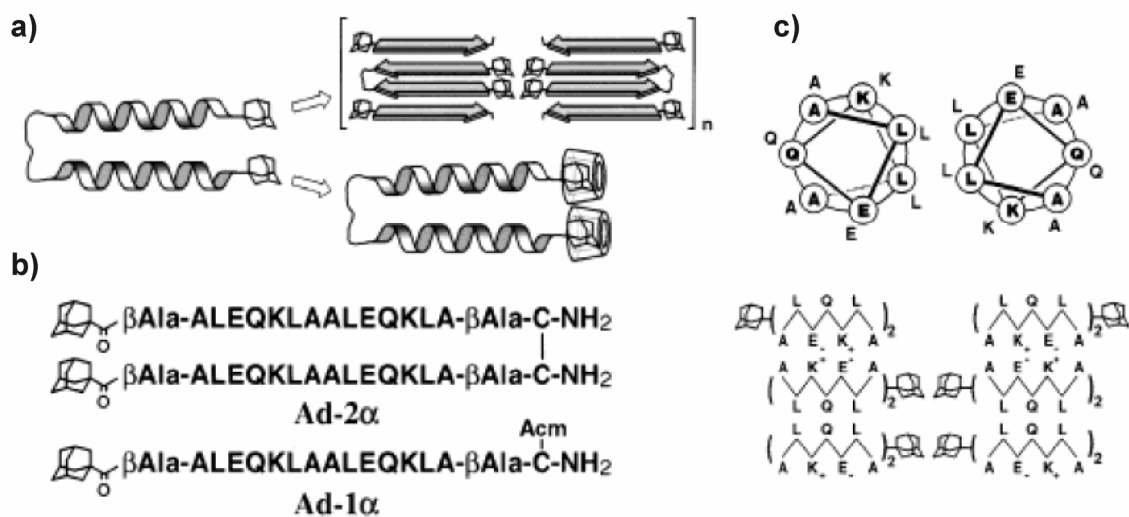
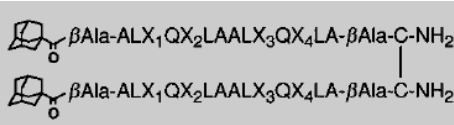


Figure 5.5. Design of the α - β transitional peptide with a hydrophobic defect. a) Schematic representation of transformation of the model peptide into β -sheet and its prevention by β -cyclodextrine. b) Sequence of applied model peptides, with a hydrophobic defect. c) Helical wheel presentation as a coiled-coil form and illustration of associated β -structures of the core of the model peptides (according to Y. Takahashi et al.).⁶⁷

When occupying four positions of the same peptide sequence by either lysine or glutamate, Mihara et al. developed a combinatorial library of peptides with different net charges in order to study the impact of electrostatic interactions on the fibril formation process (Table 5.1).⁶⁸⁻⁶⁹ Since, in general, the intermolecular association of peptide is required for the formation of β -sheet containing fibrils, they expected that neutral peptides assemble into fibrils more easily than negatively or positively charged

peptides. Indeed, mostly neutral peptides were able to form fibrils, although not each of the neutral peptides showed amyloid formation. Moreover, a complementary heterogeneous assembly of differently charged peptides, such as the EKKE/KEEK system, was also achieved. Interestingly, an assembly of the system EEEE/KKKK did not take place which may result from an unstructured initial stage of the peptides. In other words, the α -helix formation in the initial stage may support intermolecular associations that result in the required molecular orientation. Similar investigations showed that this system of charge pairing is also capable of yielding an aggregation of three or four different peptides.⁶⁹

Table 5.1. Primary structure of the design peptides reported by H. Mihara and coworkers.⁶⁸



Peptide	X ₁	X ₂	X ₃	X ₄	Total charge at neutral pH
1.EEEE	E	E	E	E	-8
2.EEEK	E	E	E	K	-4
3.EEKE	E	E	K	E	-4
4.EKEE	E	K	E	E	-4
5.KEEE	K	E	E	E	-4
6.EEKK	E	E	K	K	0
7.EKEK	E	K	E	K	0
8.EKKE	E	K	K	E	0
9.KEEK	K	E	E	K	0
10.KEKE	K	E	K	E	0
11.KKEE	K	K	E	E	0
12.EKKK	E	K	K	K	+4
13.KEKK	K	E	K	K	+4
14.KKEK	K	K	E	K	+4
15.KKKE	K	K	K	E	+4
16.KKKK	K	K	K	K	+8

Recapitulating, a number of studies showed that the α -helical coiled coil folding motif with its calculable design features is a suitable foundation for generating amyloid-forming model peptides. By means of coiled coil based models, the impact of different environmental factors such as pH, oxidative conditions, and solvent medium on the folding transition and assembly process has been systematically studied. Moreover, important knowledge regarding the general mechanism involved in protein misfolding has been gained. For instance, it has been stated in literature that amyloid formation is based on the destabilization of the native state of protein, often including a partial unfolding of protein as an initial step in the transformation process. The above-mentioned studies showed that destabilization of the native state of protein may but

does not have to facilitate the amyloid formation process. Likewise, specific hydrophobic packing interactions in the final state of fibril seem to play an essential role in determining the kinetics of amyloid formation. Therefore, in addition to the general properties of the polypeptide backbone, specific residue placements that favor β -structure may promote amyloid formation. Nevertheless, the model systems presented here are also restricted by some drawbacks. Unnatural modifications as selected by the group of Mihara allow only a very limited comparison to natural systems. Furthermore, many of the above-mentioned systems induced amyloid formation by means of extreme environmental conditions such as acidic pH or elevated temperatures that are far away from physiological conditions. These facts emphasize the importance of the further development of coiled coil based model peptides in order to study amyloid formation preferably at native-like conditions.

5.2 Impact of nanoparticles on protein folding and misfolding

When nanoparticles enter biological fluid, they immediately become coated with biomolecules such as proteins, which may transmit biological effects due to altered protein conformation, exposure of novel epitopes, perturbed function, and/or avidity effects arising from the close spatial repetition of the same protein.⁷⁰ Therefore, the nature of surface is expected to determine which of the many biomolecules will bind to the nanoparticles. Proteins are important biological molecules that are fundamental to the proper function of cells and organisms. For that reason, the impact of nanoparticles on living organisms at the protein level is a critical issue attracting increasing attention. Because of their tremendously high surface-to-volume ratio, nanoparticles have significant adsorption capacities to bind proteins. Moreover, their size allows nanoparticles to enter almost all areas of the human body; they are even able to cross the blood-brain barrier.⁷¹ Consequently, proteins of miscellaneous biological functions and localizations may be concerned by interactions with nanoparticles.

In principle, the impact of nanoparticles on the protein structure can be discussed by means of two main molecular effects.

1. **Conformational changes** may occur when proteins adsorb onto nanoparticle surfaces because the energetic minimum of the binding to the surface may require the proximity of amino acids that may be spatially separated in the native state of protein. As a result, the binding event may result in a destabilization of the native folding of protein and, consequently, may facilitate the transformation into alternative structures.
2. The binding of proteins to nanoparticles may lead to the so-called **surface-crowding effect**. The enrichment of proteins on the surface can stimulate protein aggregation as the reduced free volume favors compact protein states, and the reduced activity of water induces a decreased protein solubility, which favors protein self-assembly reactions.⁷²

5.2.1 Conformational changes upon adsorption to nanoparticles

The general impact of the surfaces of inorganic materials or nanoparticles on protein folding has been shown for naturally occurring proteins as well as for model peptides. Studies on naturally occurring proteins yield diverse effects of nanoparticles. For instance, bovine serum albumin (BSA) showed a decrease in α -helicity when exposed to gold nanoparticles.⁷³ In contrast, lysozyme or β -lactoglobulin was found to undergo unfolding in the presence of silica nanoparticles.⁷³⁻⁷⁴ These and other studies underline that the conformational changes occur due to the intrinsic propensity of the protein combined with features of the nanoparticles, such as surface chemistry and surface curvature. At the same time, the intrinsic propensity of these very complex proteins is hardly predictable.

A more simple relation between the primary structure and the nanoparticle-directed transformation is provided by studies of Rotello et al., whereby the binding of peptide to nanoparticle is based on electrostatic interactions.

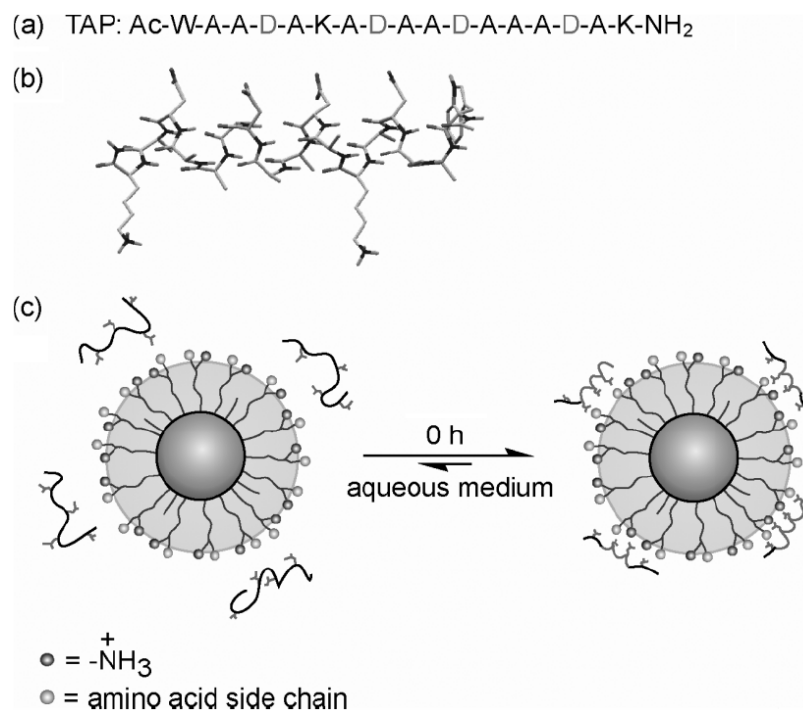


Figure 5.6. (a) Sequence of model peptide. (b) End and side view of the tetraaspartate peptide. (c) Complexation between peptide and functionalized nanoparticles in aqueous medium (according to V. Rotello et al.).⁷⁷

All the Rotello et al. studies were carried out on a 17-residue coiled coil model peptide which contained aspartate residues in alternating i , $i+3$, and $i+4$ positions. This

arrangement of aspartate provides a cofacial presentation of carboxylates suitable for recognition by the colloid surface (Figure 5.6a and b). When exposing this model peptide to trimethylammonium functionalized gold nanoparticles, an electrostatically attractive interaction between peptide and charged surface drives the peptide from an unfolded state into a helical folding.⁷⁵ Further modifications in the ligand shell revealed that just the presentation of positive charge is required for the induction of α -helical conformation, regardless of the chemical structure of the ligand.⁷⁶⁻⁷⁸ In contrast, hydrophobic nanoparticles did not reveal an induction of α -helical folding.⁷⁷⁻⁷⁸ Also studies of other groups applying the same arrangement of charged residues within the peptide's sequence revealed that materials such as hydroxyapatite surfaces⁷⁹ or silica nanoparticles⁸⁰ can stabilize the helical structure of short model peptides upon electrostatic interactions.

5.2.2 Surface-crowding effect leads to nanoparticle-induced fibril formation

One important phenomenon involving protein self-assembly is the class of human neurodegenerative diseases named amyloidosis. With regard to the general impact of surfaces on the misfolding of proteins, studies using membranes have yielded valuable information. In the presence of membranes, the induction of self-assembly is based on the same two main molecular effects as mentioned above for the presence of nanoparticles. For instance, a variety of lipid membranes have been shown to induce electrostatically driven binding of the amyloid β ($A\beta$) peptide; this was followed by accelerated aggregation into toxic species at rates significantly higher than in a membrane-free environment.⁸¹

Several studies showed that the surface-induced pathological self-assembly of proteins occurs not only in the presence of biological membranes but is also relevant for other kinds of materials, such as nanoparticles. Compared to membranes, nanoparticles possess an enormous surface-to-volume ratio so that the influence of the surface-crowding effect becomes even more pronounced. The nanoparticle-induced protein misfolding is a relatively unexplored and novel field. Several studies focused on the aspect of the composition of nanoparticles and their surface characteristics to direct the nanoparticle-induced amyloid formation. Thereby, materials such as TiO_2 nanoparticles,⁸² hydrogenated nanoparticles,⁸³ and gold nanoparticles⁸⁴ among others were found to accelerate the self-assembly process of different proteins such as the $A\beta$

peptide and lysozyme, whereas fluorinated nanoparticles⁸³ seem to prevent fibril formation.

Other studies, however, showed that the impact of nanoparticles on protein misfolding is not only related to the nature of nanoparticle, but also strongly depends on the kind of protein, since the same kind of nanoparticle may lead to opposite effects for different proteins. Hence, Linse et al. found that uncharged copolymer nanoparticles are capable of inducing self-assembly of β_2 -microglobulin, a human protein involved in dialysis-related amyloidosis.⁸⁵ Interestingly, in the case of the A β peptide, it was found that the same kind of nanoparticle can inhibit, and even temporarily, reverse the fibrillation of protein.⁸⁶ At the same time, the authors do not commit whether both proteins bind in a monomeric or oligomeric state to the nanoparticle, an aspect that may be very important for the molecular mechanism involved in nanoparticle-driven misfolding. However, they suggested that the opposite effect for A β might be caused by tight interactions between the nanoparticle surface and the peptide while blocking the binding sites for the addition of new monomers.

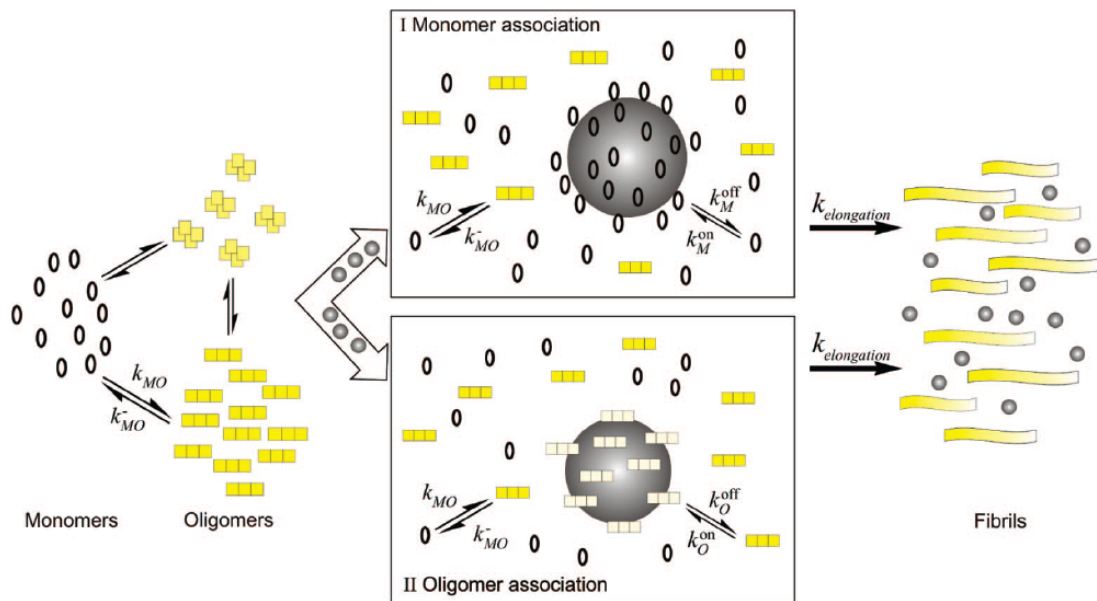


Figure 5.7. Schematic representation of possible interactions between copolymeric nanoparticles and A β . Gray spheres depict nanoparticles, yellow clusters indicate structured and unstructures oligomers (according to Cabaleiro-Lago et al.).⁸⁶

While offering promising solutions for better healthcare, the generation of nanoparticles may be a serious issue with respect to toxicology. Their potentially high reactivity arising from the large surface-to-volume ratio may cause potential risks for all new nanosystems. For that reason, each new nanoparticle system has to be studied carefully with respect to its potential side effects within the human body and its

environment. For instance, medical research is currently looking at applications of nanoparticles for the treatment of neurodegenerative diseases such as Alzheimer's disease.⁸⁷ The above-mentioned studies showed that nanoparticles do not necessarily prevent misfolding of proteins, but may trigger the formation of protein assemblies, depending on the kind of protein as well as on the composition of nanoparticle. To date, the underlying principles including the role of protein sequence to direct this process are not completely understood and have to be elucidated. Therefore, the employment of simple model peptides allows systematic studies with more generalizable trends as the aggregation properties of such peptides can be easily tuned by variations referring to the hydrophobicity, charge, and secondary structure propensities.

6 Scientific Goals

In the last three decades, biotechnology and materials science have developed remarkably into today's powerful disciplines. Since biomolecules and nanomaterials meet at the same length scale, their combination into hybrid materials allows the engineering of new technical devices as well as the development of substances with very promising applications in pharmacy and biomedicine. Several studies have been published about the application of biomolecules including coiled coil peptides for the organization of nanoparticles. Nevertheless, an orderly arrangement of nanoparticles by means of biomolecules seems to be quite challenging and has only been achieved in a few cases. On the other hand, some studies showed that nanoparticles may disturb the native structure and biological function of proteins upon the entry into human body. Therefore, there are growing concerns about the toxicology of such small materials when applied in medical treatment. A profound knowledge about the interaction between nanoparticles and biomolecules is of paramount importance for both, the design of new bionanomaterials as well as for the estimation of possible biological risks of nanoparticles to human health.

In this thesis, a system consisting of gold nanoparticles functionalized with anionic ligands and α -helical coiled coil peptides was systematically investigated in order to shed light on different principles of the interaction between peptides and nanoparticles. The two major objectives of this thesis can be summarized as follows:

1. To apply the α -helical coiled coil folding motif for the organization of nanoparticles based on electrostatic interactions. At the same time, it should be investigated whether the symmetry of the coiled coil structure may be used to generate a highly-ordered architecture of the nanoparticles. Moreover, a tunable and/or switchable structuring of nanoparticles by means of environmental conditions such as pH was intended.
2. To investigate more deeply the phenomenon of nanoparticle-induced misfolding and aggregation of proteins. Although nanoparticles are currently being developed for the medical treatment of Alzheimer's diseases, some proteins show increased amyloid formation tendency in the presence of nanoparticles. This phenomenon strongly depends on the kinds of protein and nanoparticle; the underlying principles have not been resolved to date. For that reason,

preliminary studies concentrated on the design and characterization of coiled coil based model peptides to mimic protein misfolding occurring in neurodegenerative diseases. These model peptides have then been applied to the interaction with anionic nanoparticles to investigate more deeply the crucial role of the peptide sequence in the nanoparticle-induced misfolding process.

Both objectives required the design as well as the analytical characterization of peptides and their combination with nanoparticles. This was done by means of a battery of biophysical techniques which will be explained in more detail in the following chapter.

7 Applied analytical methods

A battery of analytical methods was applied to characterize the conformation and oligomerization state of coiled coiled peptides as well as the ultrastructure of protein and nanoparticle aggregates and their exact binding stoichiometry.

7.1 Surface Plasmon resonance

A very simple method to determine the aggregation state of nanoparticles is using UV/Vis spectroscopy. The application of gold in the core of nanoparticle implies a red color of colloid solution and a detectable absorption maximum in the visible range of light. This optical property of colloidal gold solutions is based on the fact that the electron cloud can oscillate on the particle surface and absorbs electromagnetic radiation at a particular energy termed surface plasmon resonance.⁸⁸⁻⁸⁹ At the same time, plasmon absorbance only occurs for gold nanoparticles bigger than two nanometers. The exact wavelength and intensity of the absorbance maximum depends on the surface functionality, temperature, and the solvent. Nevertheless, this effect can be used to determine the colloidal concentration and particle size in solution provided that the conditions are known.⁹⁰⁻⁹¹ But more importantly, the absorbance maximum is a suitable tool to quantify the assembly of gold nanoparticles. The more particles that are in contact, the longer the range of the Plasmon coupling. Therefore, a distinct red-shift and broadening of the surface-plasmon resonance maximum are associated with a decrease in the interparticle distance for a given dielectric environment (Figure 7.1).

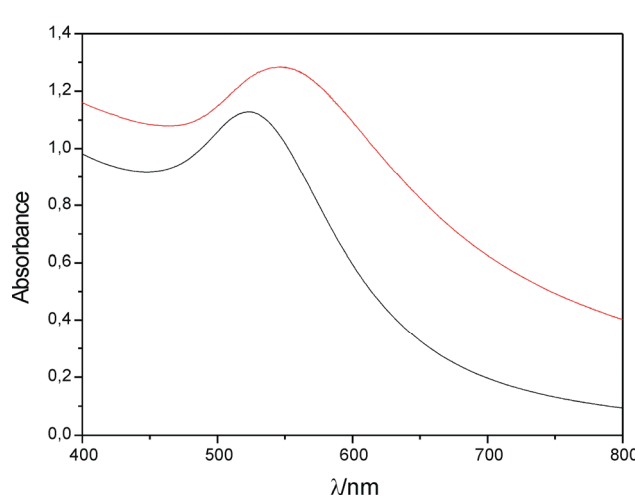


Figure 7.1. The extinction spectra of 6 nm gold nanoparticle in absence (black line) and presence (red line) of a cross-linking interaction partner.

For a better comparison of different conditions such as peptide concentrations, incubation times, and pH values, the presentation of the following measurements simply refers to the position of absorption maxima.

7.2 Circular dichroism spectroscopy

Circular dichroism spectroscopy is a common method for determining the folding of peptides and proteins in solution. The underlying principle is based on the varying wavelength dependent absorbance of left and right circularly polarized light by chromophores in chiral molecules. With the only exception of glycine, all other natural amino acids are enantiomeric and, thus, are measurable in CD spectroscopy. Moreover, within peptides or proteins, all amino acids are linked by peptide bonds, the most ubiquitous chromophore in protein folding. Peptide bonds display two characteristic absorption bands in the far-UV region ($\lambda = 190\text{-}250\text{ nm}$): a $\pi\text{-}\pi^*$ transition at 190 nm and a weaker and broader $n\text{-}\pi^*$ transition at 210 nm.⁹² Since different secondary structures display different dihedral angles of peptide bond, a characteristic CD spectrum occurs in this wavelength range (Figure 7.2).

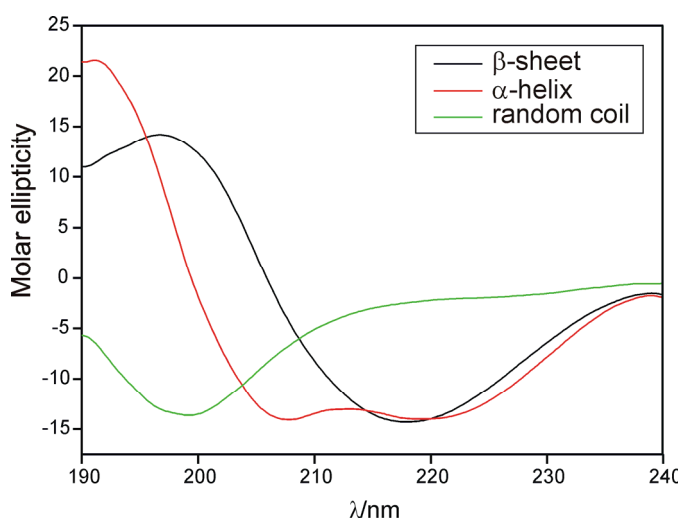


Figure 7.2. Representative far-UV spectra of different secondary structures. β -sheet: positive band at 195-198 nm ($n\text{-}\pi^*$), negative band at 216 nm ($n\text{-}\pi^*$); α -helix: positive band at 192-195 nm ($\pi\text{-}\pi^*$), negative band at 208 nm ($\pi\text{-}\pi^*$) and 222 nm ($n\text{-}\pi^*$); random coil: negative band at 200 nm ($n\text{-}\pi^*$).

A physical explanation of circular dichroism relies on the field vectors of the circularly polarized components. It is assumed that polarized light consists of superimposed left

(E_L) and right (E_R) circularly polarized light. An in-phase combination of both polarized lights with equal amplitude and wavelength yields plane polarized light, as indicated by a simple line (Figure 7.3). If both circularly polarized light waves cross optically active compounds, the difference in absorption coefficients for left and right circularly polarized $\Delta\varepsilon$ light provokes an ellipse instead of a line. Usually, the circular dichroism is reported in degrees of ellipticity $[\theta]$. The relationship between $\Delta\varepsilon$ and $[\theta]$ is as follows:

$$[\theta] = 100 \left(\frac{\ln 10}{4} \right) \left(\frac{180}{\pi} \right) \Delta\varepsilon = 3298.3 \Delta\varepsilon \quad (1)$$

For better comparison of the absolute intensity of proteins of different lengths, CD spectra are usually given in mean residue ellipticity $[\theta]_{mr}$:

$$[\theta]_{mr} = \frac{\theta_{obs}}{10000 \cdot l \cdot c \cdot n}, \quad (2)$$

where θ_{obs} corresponds to the ellipticity measured [millidegrees], l is the optical length of cuvette [cm], c is the concentration of peptide [mole/L], and n is the number of peptide bonds.

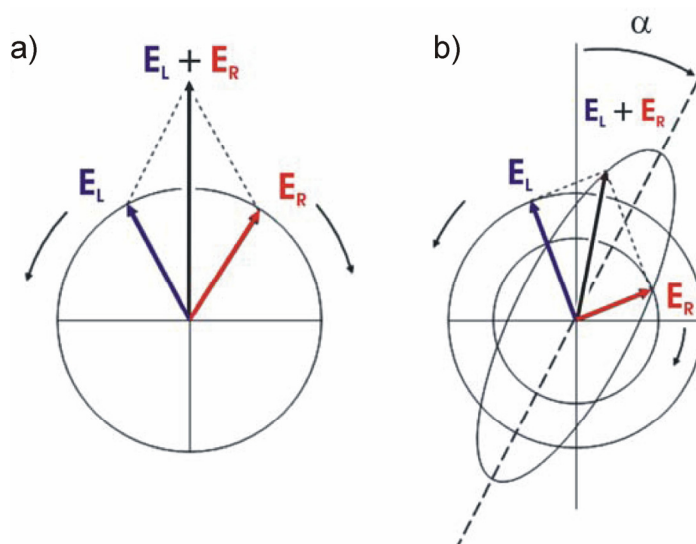


Figure 7.3. Field vectors of left (blue) and right (red) circularly polarized light and their superposition (black), before (a) and after (b) passage through an optically-active sample.

CD spectroscopy always yields averaged information about the secondary structure of proteins and peptides, while the CD spectrum of a complex protein can be deconvoluted into three individual contributions:

$$CD_{protein} = A \cdot X_{\alpha-helix} + B \cdot X_{\beta-sheet} + C \cdot X_{randomcoil} \quad (3)$$

where X represents the relative content of the particular secondary structure element; A, B, and C are the data points of the corresponding basis CD spectra at a certain wavelength. Deconvolution programs were realized quite early after CD was introduced and the standard curves were published in 1969 by Greenfield and Fasman.⁹³ Although these programs are actually based on different conformations of poly-lysine, only little improvement in the accuracy of fits has been achieved by attempting to generate other standard data sets from protein spectra of known structure.⁹⁴ However, the selection of these standard data sets may sometimes impede the exact description of structure of small peptides. Nevertheless, these approximation methods are very reliable for monitoring conformational changes of proteins under different conditions such as time-dependent and denaturation studies among others.

7.3 Transmission electron microscopy

Transmission electron microscopy (TEM) is one of the most powerful techniques for detecting the size and arrangement of gold nanoparticles as well as to visualize fibrillar structures of peptides.

The principle construction of the transmission electron microscopy strongly resembles that of a light microscope, but uses magnetic instead of glass lenses (Figure 7.4). Electrons are emitted in the electron gun by thermionic emission from LaB₆ rods, while a high coherency of electron beam is required. By means of a voltage, usually around 100 kV, a downstream anode accelerates the electron beam which is then focused by a condenser system. A voltage of 100 kV theoretically generates a wavelength of 0.004 nm of the electron beam. When transmitting the sample, the electron beam will be scattered to a certain amount depending on the mass density of the specimen. Consequently, the electron beam carries information about the internal structure of the sample. After being magnified by a three- or four-stage lens system, the electron beam is transferred to the imaging system of the microscope, such as a fluorescent screen or a photographic emulsion.

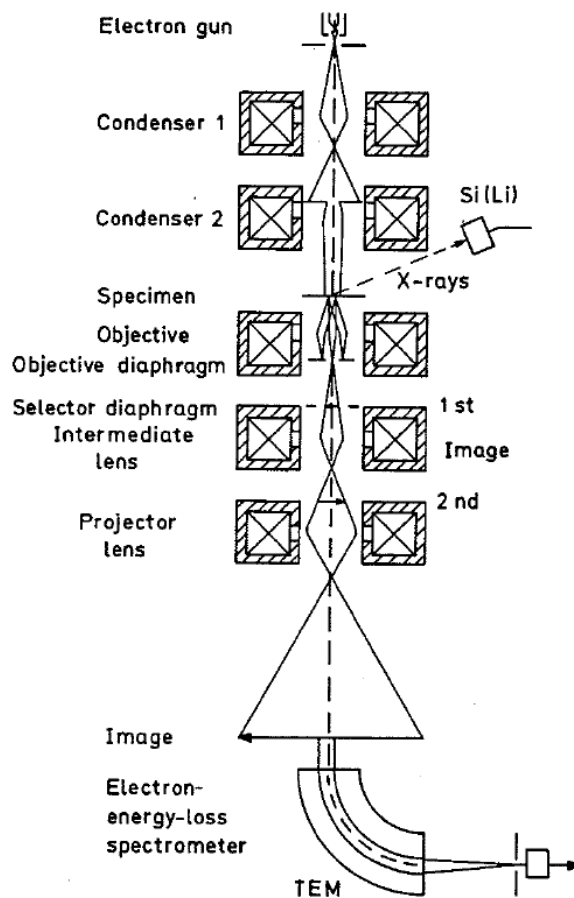


Figure 7.4. Schematic ray path for a transmission electron microscope (according to L. Reimer).⁹⁵

At the same time, the resolution of the microscope strongly depends on the wavelength of the electron beam. For that reason, the microscope is equipped with a very complex vacuum system to ensure a sufficiently high wave length of the electron beam and to minimize any collisions with free gas molecules. Generally, transmission electron microscopes allow a magnification up to 100k fold.

However, the quality of TEM images is not only determined by the resolution, but much more importantly by the contrast of sample, referring to the scattering properties of the sample. The higher the mass density, the higher the scattering properties of electron beam and the contrast of TEM images. Biological samples are usually composed of atoms of low atomic numbers (C, H, N, O, S) and, thus, only display very weak electron scattering. In contrast, heavy metal ions such as gold, uranium, and tungsten possess a much higher mass density and scattering capability. For that reason, coating with heavy metal ions is a widely-used method to visualize biological materials in electron microscopy. In the negative staining preparation, an aqueous solution is deposited on a

carbon coated copper grid and incubated for one minute or shorter to allow an adsorption of sample. After blotting the supernatant fluid with a filter paper, the sample is incubated with a droplet of a staining solution for a further minute and is again blotted dry. In the TEM measurement, the contrast arises from the scattering by means of the staining reagent which is covering the sample such that the superficial structure of the original sample becomes apparent. Despite this simple preparation method, negative staining also contains some drawbacks which have to be taken into consideration. First, several staining solutions have been developed but every staining solution can only be used for a certain pH range.⁹⁶ Second, the blotting procedure implies a drying of the sample. A loss of the hydration shell might go along with the destruction of the native structure of biological molecules. Current studies are working on the addition of trehalose to maintain the shape of biological material during the drying process.⁹⁷

Another method to avoid possible structural changes as well as to gain additional information about the internal structure of sample is the so called “cryo” preparation technique, a quite challenging preparation method which requires a lot of experience. The term “cryo” refers to the frozen state of the sample that ensures an immobilization and, more importantly, a structural conservation of the biological molecule. The challenging step in the cryo-preparation method is the freezing process. A droplet of the sample is deposited on the copper grid and, after an incubation time of about a minute, blotted that only an ultrathin layer of the sample solution remains. Then, the sample is frozen to the temperature of liquid ethane (90 K) by operating a guillotine-like plunging device. Thereby, the cooling rate (100 000 °C/s) is of paramount importance for the quality of sample since only a sufficiently high cooling rate prevents a crystallization of water molecules which, in return, strongly absorbs the electron beam and makes the sample ineligible. Based on results obtained by cryo-TEM, 3D structure modelling of protein structures can be envisaged.

With regard to the nanoparticles measured in this thesis, the gold core gives a very good contrast in transmission electron microscopy without any additional preparation method. In contrast, the visualization of the ligand shell as well as the detection of peptidic structures such as fibrils requires either negative staining reagent or cryo preparation.

7.4 Thioflavin T binding assay

Fluorescence measurements of the dye thioflavin-T (ThT) is commonly used for monitoring the kinetics of amyloid fibril formation.^{98,99} The chemical structure of ThT is shown in Figure 7.5.

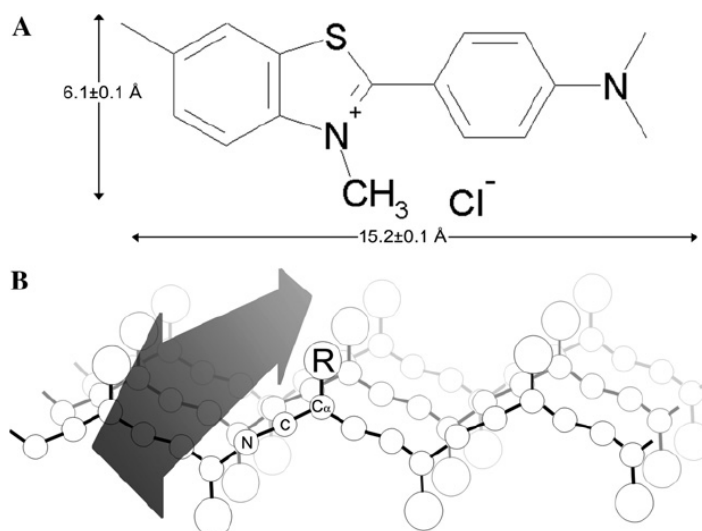


Figure 7.5. a) Chemical structure and dimensions of thioflavin-T. b) Schematic representation of a β -sheet. Especially highlighted are the backbone atoms (N, C, and C_α) and sidechain (R) of one residue. Thioflavin-T is expected to bind with its long axis parallel to the long groove of the β -sheet indicated by an arrow (according to M. R. H. Krebs et al.).¹⁰⁰

Upon binding to β -sheet rich fibrils, the assembly of ThT molecules provoke new optical properties such as a new excitation and emission maximum at 450 and 485 nm, respectively. The measurements of ThT fluorescence at certain time points and the plot of ThT emission against the time allow exclusively a direct monitoring of the fibril formation process; the kinetics of the underlying folding transition cannot be determined by this procedure. In general, the fibril formation process occurs nucleation-dependent and is characterized by the presence of a lag phase as well as a sigmoidal increase in the ThT emission intensity.

The exact mechanism leading to the induced fluorescence of ThT in the presence of amyloids is unknown to date. Nevertheless, more information has been obtained regarding the arrangement of Thioflavin-T on the surface of fibrils. According to Figure 7.5, Krebs et al. suggested an arrangement of the dye in grooves perpendicular to the β -sheet axis.¹⁰⁰ The sterical constraints within these grooves create an environment

unique to amyloidogenic fibrils which may give an explanation for the specificity of this dye for fibrils.

Moreover, it has been shown that ThT is not only specifically binding to amyloids, but may also accelerate the fibril formation process. Thioflavin-T itself forms aggregates that may assist the important nucleation step during the self-assembly process of proteins.¹⁰¹

7.5 Isothermal titration calorimetry

Isothermal titration calorimetry (ITC) is a powerful method to determine the binding stoichiometry of peptide to nanoparticle, provided that no aggregation occurs during the binding assay. It directly measures the change in enthalpy (ΔH) upon titration and has a widespread applicability in studying the interaction between two reactants.¹⁰² An isothermal titration calorimeter comprises two cells; a sample cell, in which the reaction takes place, and a reference cell containing either water or buffer. A typical ITC measurement includes the stepwise injection of one reactant into the reaction cell containing the other reactant. Upon injection of ligand, heat is either generated or taken in (exo- or endothermic processes). These tiny heat effects are detected by semiconductor thermopiles and the instrument applies the thermal power ($\mu\text{cal/s}$) in order to compensate for the ligand induced heat effect and to bring the cells into thermal equilibrium. The heat (q_i) released or uptaken by the injection is proportional to the amount of ligand that binds to the receptor in a particular injection ($v \times \Delta L_i$) and the molar binding energy (ΔH) for the reaction:

$$q_i = v \times \Delta H \times \Delta L_i \quad (4)$$

where v corresponds to the volume of the reaction cell and ΔL_i is the increase in the concentration of bound ligand after the i th injection. The raw data is presented as a series of peaks measured as power ($\mu\text{cal/s}$) versus time (Figure 7.6). Generally, initial injections release large heats, as shown for an exothermic reaction in Figure 7.6, since almost all of the injected ligand molecules bind to the receptor molecule. When the titration proceeds, binding sites become occupied and the magnitude of the heat per injection decreases, until nearly all of the binding sites are saturated. Then, the released heat results only from the dilution heats. The integration of these data and the correction to a per mole basis yield the overall binding isotherm. The shape of this

binding isotherm depends on the association constant as well as the concentration of binding sites and is characterized by the so-called Wiseman c -parameter according to the equation

$$c = n[M]K_a, \quad (5)$$

where $[M]$ is the total concentration of receptors, n is the number of binding sites per receptor, and K_a the association constant.¹⁰³ For c values higher than 10, the shape of curve is clearly sigmoidal, whereas lower c -values lead to a more hyperbolic up to a horizontal function by plotting the released heat of binding against the molar ratio.

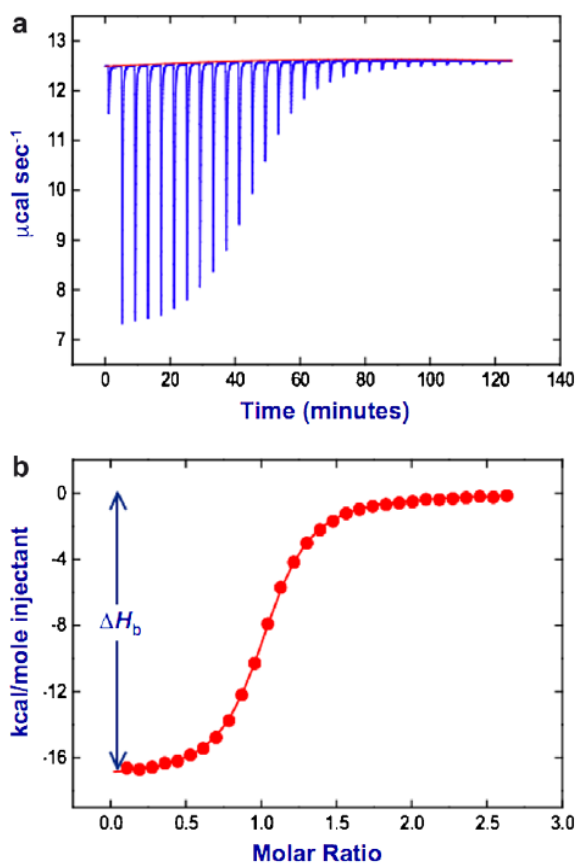


Figure 7.6. Typical titration data; (a) raw data showing difference in power supplied to the two heaters vs. time; (b) integrated heat change per injection with best fitting curve.

By applying a fitting procedure according to an appropriate binding model, thermodynamic parameters such as the molar binding energy ΔH , the binding stoichiometry n , and the association constant K_a can be calculated out of this data.

The ITC data reported in this thesis were fitted by a one-set of binding sites mode, assuming a single set of identical binding sites yielding the change in heat content from injection $i-1$ to i as

$$\Delta Q(i) = Q(i) - Q(i-1) + \frac{dV_i}{V_0} \left[\frac{Q(i) + Q(i-1)}{2} \right]. \quad (6)$$

Each heat of injection is

$$Q = \frac{V_0 [np]_{tot} N \Delta H^0}{2} \left(1 + \frac{[peptide]_{tot}}{N [np]_{tot}} + \frac{1}{K_A N [np]_{tot}} - \sqrt{\left(1 + \frac{[peptide]_{tot}}{N [np]_{tot}} + \frac{1}{K_A N [np]_{tot}} \right)^2 - \frac{4 [peptide]_{tot}}{N [np]_{tot}}} \right) \quad (7)$$

where N is the number of moles of peptides per nanoparticle, ΔH^0 is the enthalpy change upon binding (kcal/mol peptide), V_0 is the cell volume, and K_A is the equilibrium association constant.

In several studies, it has been stated that curve fitting is optimal for c -values in the range of 10-500.¹⁰⁴ However, the optimization of c -values is often limited by the solubility of receptor molecules as well as low binding affinities and the isothermal titration calorimetry at low c -values is the only feasible method to estimate the thermodynamic parameters of interactions between two species.

8 Results: Coiled coil peptides for organization of nanoparticles

8.1 Concept

8.1.1 Design of nanoparticles

The organization of nanoparticles by means of coiled coil peptides was intended to be based on electrostatic interactions. Therefore, these nanoparticles consisted of a gold core coated with mercaptoundecanoic acid as anionic ligand in order to generate a highly charged surface of nanoparticle (Figure 8.1).

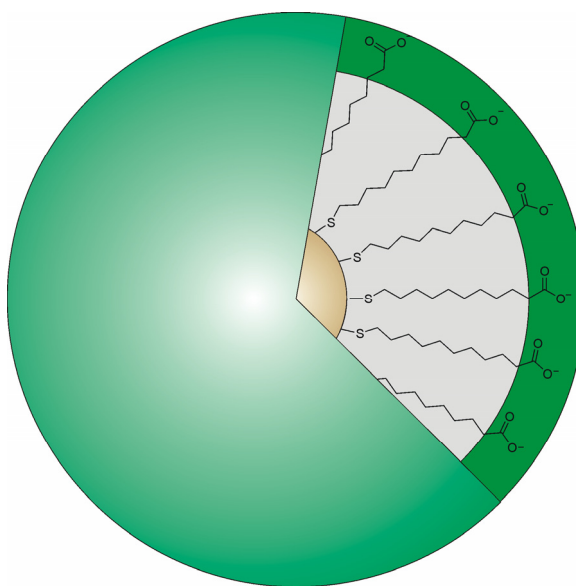


Figure 8.1. Design of MUA functionalized gold nanoparticles, shown for an idealized state of completely extended ligands.

In general, the stability of water-soluble ligand-stabilized nanoparticles depends on the degree of ionization of functional groups at the nanoparticle surface and, therefore, is limited to a particular pH range. The grade of deprotonation of the ligand is determined by the pKa value of MUA that corresponds to a theoretical value of 6.5 as reported in some studies.¹⁰⁵⁻¹⁰⁶ For instance, Simard et al. reported that their MUA-stabilized gold nanoparticles aggregated at pH < 7.¹⁰⁷ In preliminary studies, the stability of these nanoparticles was studied in dependence on pH as well as different kinds and

Since the aim of the present study was to combine the α -helical recognition domain with a further binding site for anionic nanoparticles, the previous work of Toni Vagt presented an essential foundation for the peptide design applied here. Figure 8.2 shows the design of the parent peptide VW05 for electrostatic interactions with anionic nanoparticles. The adoption of an α -helical coiled coil structure was realized by the occupation of positions a and d with hydrophobic leucine residues as well as the juxtaposition of oppositely charged glutamate and lysine residues in positions e and g. The presentation of arginine residues at one face of the peptide helix resulted in a binding site for negatively charged nanoparticles. As reported in literature, the side chains of lysine and arginine possessed theoretical pKa values of 10.5 and 12.5, respectively.¹¹⁰ Because binding studies with MUA-modified gold nanoparticles require pH values of 9 or more, especially arginine with the higher pKa value would be expected to interact with the nanoparticles.

Conceptually, the α -helical coiled coil peptide should be used as a multivalent template to link different nanoparticles and to end up with nanoparticle networks. In materials science, the assembly of nanoparticles in defined geometries is a key feature. Therefore, the question was asked whether the geometry of a coiled coil structure determined by its oligomerization state can be used to direct the arrangement of nanoparticles. In principle, the branching of residues at positions a and d specify the oligomer state selection.¹¹¹ This is a consequence of the different alignments of the α - β bond vector of side-chain according to their positioning in the hydrophobic core. As depicted in Figure 8.3, a dimeric state displays significant differences in the core-packing geometries for positions a and d. At position d, β -branched residues such as isoleucine and valine are precluded, whereas leucine residues are favored. In contrast, the α - β bond vector of position a points out from the helical interface; here, especially β -branched residues (i. e. isoleucine, valine) are preferred since they lead hydrocarbon back into the helical interface. In the design shown in Figure 8.2, the use of only leucine in both positions of the coiled coil peptide design does not specify the oligomer state. According to examples in literature, the occupation of a and d by leucine is expected to specify trimers which has to be further confirmed by analytical techniques such as analytical ultracentrifugation.^{112,113}

Moreover, the aim was to show that a multivalent structural template is required to arrange the nanoparticles into networks and that not every peptide with appropriate charge enables such an organization. As a result, a reference peptide (VW05-ref) was constructed that primarily exists as a monomer in solution and is not able to oligomerize into a coiled coil structure because its primary structure does not follow the classical heptad repeat pattern (Figure 8.2). In particular, the absent arrangement of

leucine in i , $i+3$, and $i+4$ positions prevents the formation of a hydrophobic core. The reference peptide contains the same composition of amino acids and, therefore, possesses the same calculated net charge for an electrostatic interaction with anionic nanoparticles.

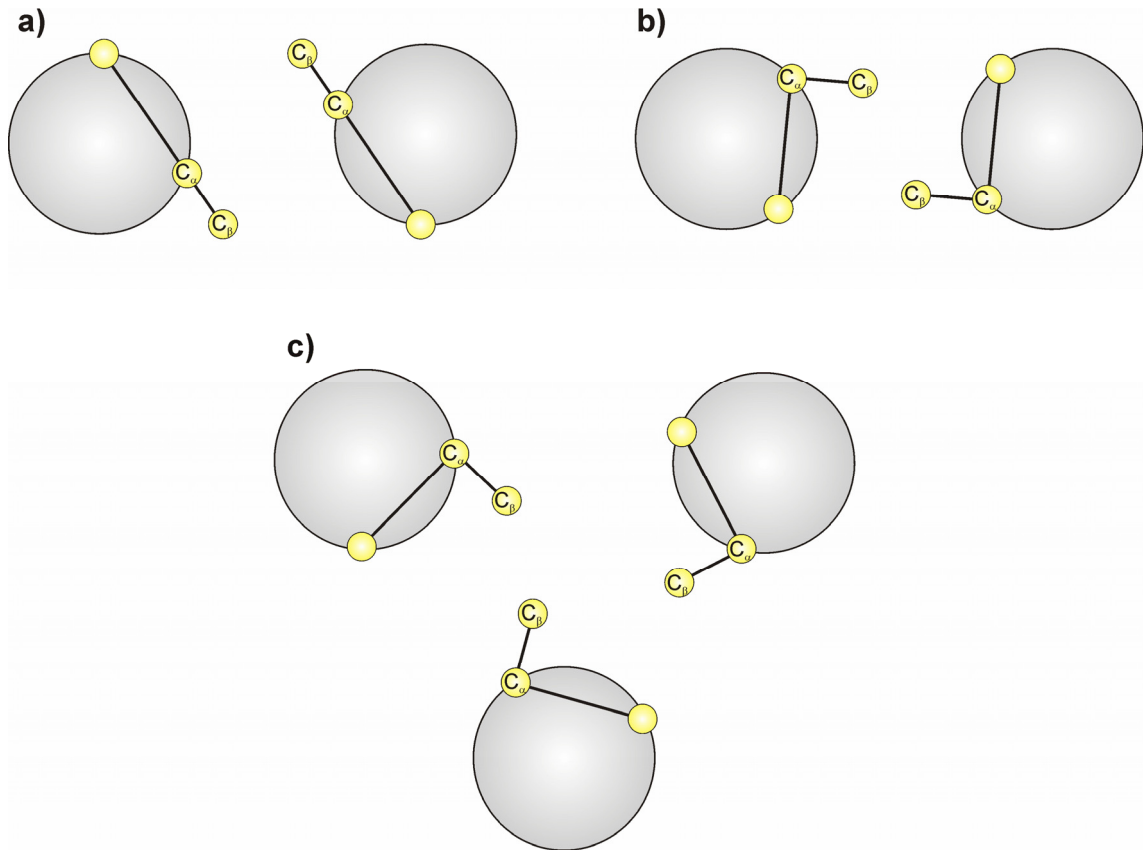


Figure 8.3. Schematic diagrams for different core-packing geometries; a) parallel packing at position a, b) perpendicular packing at position d of a dimeric coiled coil, and c) acute packing at a d-layer of a coiled coil trimer.

8.1.3 Analytical techniques

A battery of analytical techniques was applied in order to characterize the coiled coil-induced aggregation of MUA-functionalized gold nanoparticles. The measurement of the surface Plasmon resonance band by means of UV/Vis spectroscopy is a very simple method to detect aggregation of gold nanoparticles in solution. Its performance and interpretation of data was done together with Dipl.-Chem. Meike Roskamp.¹⁰⁸ Moreover, circular dichroism spectroscopy was applied to determine the generic folding of both peptides themselves as well as to ensure that the α -helical coiled coil folding is

not disturbed upon interaction with the nanoparticles. To determine the oligomerization state of peptide, analytical ultracentrifugation measurements were carried out in cooperation with Dr. Helmut Cölfen and Antje Völkel.¹¹⁴ Gel electrophoresis measurements done by Dipl.-Chem. Meike Roskamp were further used to confirm a binding of peptide to nanoparticle. Transmission electron microscopic measurements were applied to characterize the morphology of the nanoparticle networks as well as to directly visualize the peptide next to the nanoparticles. Additional cryo-TEM measurements were done in collaboration with PD Dr. Christoph Böttcher.¹¹⁵

8.2 Publication

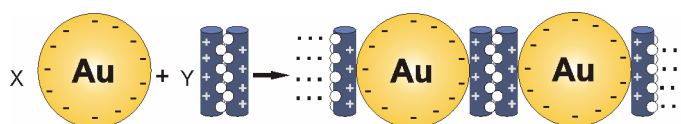
Sara C. Wagner, Meike Roskamp, Helmut Cölfen, Christoph Böttcher, Sabine Schlecht, Beate Kokschi, Switchable electrostatic interactions between gold nanoparticles and coiled coil peptides direct colloid assembly, *Org. Biomol. Chem.* **2009**, 7, 46-51.

This publication was further included in the gallery of hot articles and was honored by being selected for the inside cover page of the January 2009 issue of Organic and Biomolecular Chemistry (RSC).

The original article is available at:

<http://www.rsc.org/ej/OB/2009/b813429d.pdf>

The nanoparticle–peptide interaction described here is based on electrostatic forces and the pH value can act as a trigger to direct the organization of functionalized nanoparticles in a reversible and repeatable manner. The ability of the peptide to interact with the charged gold nanoparticles is directly related to its helical structure and was not found for a random coil peptide with the same net charge. Interestingly, the interaction with nanoparticles seems to induce a fibrillation of the coiled coil peptide.



8.3 Modifications of the peptide design (unpublished results)

Since it turned out that the coiled coil based peptide VW05 can be used to generate a pH dependency of the assembly of nanoparticles, but with the minor drawback that this organization of nanoparticles does not follow a regular trimeric pattern, further modifications in the sequence of VW05 were carried out on either the charge or sterical demand of this peptide with the aim of generating a more ordered structure of nanoparticles. The preserved occupation of positions a and d with leucine allows the same oligomerization state, namely a trimer, as shown for VW05.

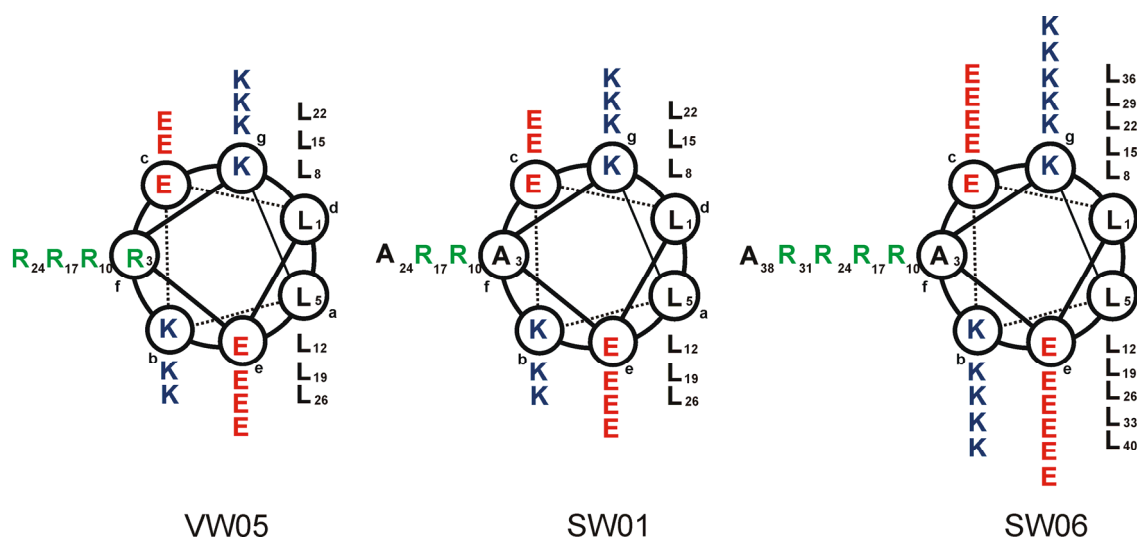


Figure 8.4. Helical wheel presentation of the peptides VW05, SW01, and SW06. All peptides are shown as single helices, but undergo oligomerization due to their amphiphilic character.

Since the aggregation induced by VW05 occurred very rapidly, a decreased charge of coiled coil peptide was expected to weaken the attractive interactions between peptide and nanoparticle and to allow more controlled growth conditions which may favor a more ordered organization of nanoparticle. Therefore, the design of SW01 was derived from VW05 through the substitution of two arginine residues against alanine (Figure 8.4).

In a second peptide design, the overall length of the peptide helix was increased by means of two additional heptads at each end. This modification was considered due to the unfavorable size ratio of peptide to nanoparticle, which still allowed a three-dimensional arrangement of biomolecule around one particle. At the same time, the f positions of the additional heptads contain alanine instead of arginine with the aim of fixing the position of binding domain to the center of peptide helix. Table 8.1

summarizes the calculated net charges of all modifications of peptide VW05 in dependence on the pH. In any case, an attractive interaction with negatively charged gold nanoparticles is possible at pH 9.0.

Table 8.1. pH Dependent net charges of VW05, SW01, and SW06.

pH	Net charge		
	VW05	SW01	SW06
9	3.6	1.6	3.5
9.5	3.0	1.0	2.6
10	1.6	-0.4	0.7
10.5	-0.4	-2.4	-2.4
11	-2.4	-4.0	-5.5
11.5	-3.8	-5.6	-7.4
12	-4.9	-6.4	8.8

In order to determine the binding stoichiometry of peptide to nanoparticle, a fixed nanoparticle concentration of 40 nM was pre-incubated at pH 9.0 with different concentrations of all peptides and for six hours. Then, the peptide-nanoparticle assemblies were removed by centrifugation. The supernatant containing the excess of nanoparticle was then measured by UV/Vis spectroscopy. In theory, above a certain concentration of peptide defining the binding stoichiometry, all nanoparticles are saturated with peptides. In this case, no absorbance is expected to be measured by UV/Vis spectroscopy. Figure 8.5 shows that VW05 as well as SW06 display a binding stoichiometry of about 175 peptides per nanoparticle. The similarities in the binding stoichiometry is very likely a consequence of an almost similar net charge of both peptides at pH 9. As expected, SW01 with a decreased number of arginine residues and lower net charge binds in a higher stoichiometry of 250-500 peptides to the particles.

Binding studies including all peptides revealed that SW01 and SW06 also provoke a red-shift of the surface plasmon resonance band of nanoparticles pointing to a peptide-mediated assembly of nanoparticles. Moreover, the shift of absorption maximum behaves as a function of peptide concentration, but is much more pronounced in the case of the parent peptide VW05. Since VW05 was incubated with a newly prepared charge of MUA functionalized nanoparticles, the values given in Figure 8.6 may slightly deviate from the numbers reported in the previous publication.

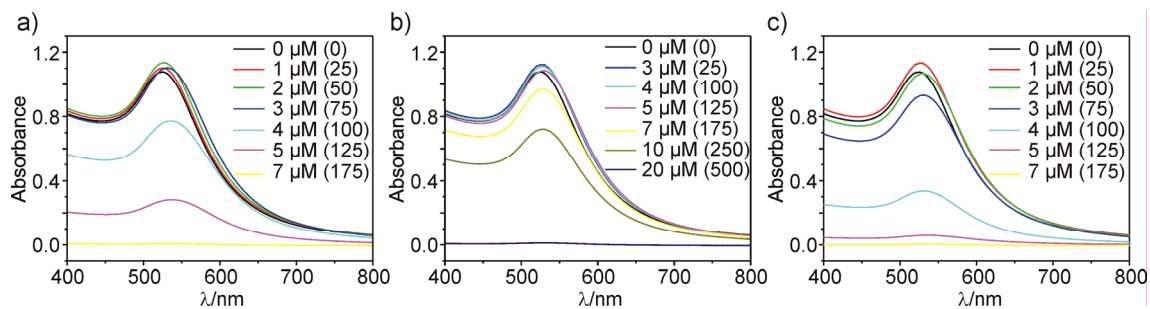


Figure 8.5. UV/Vis spectra of the supernatants of (a) VW05, (b) SW01, and (c) SW06 in the presence of 40 nM Au/MUA nanoparticles and after centrifugation. The numbers in μ M refer to the peptide concentration, the numbers written in brackets correspond to the x-folded excess of peptide to nanoparticle.

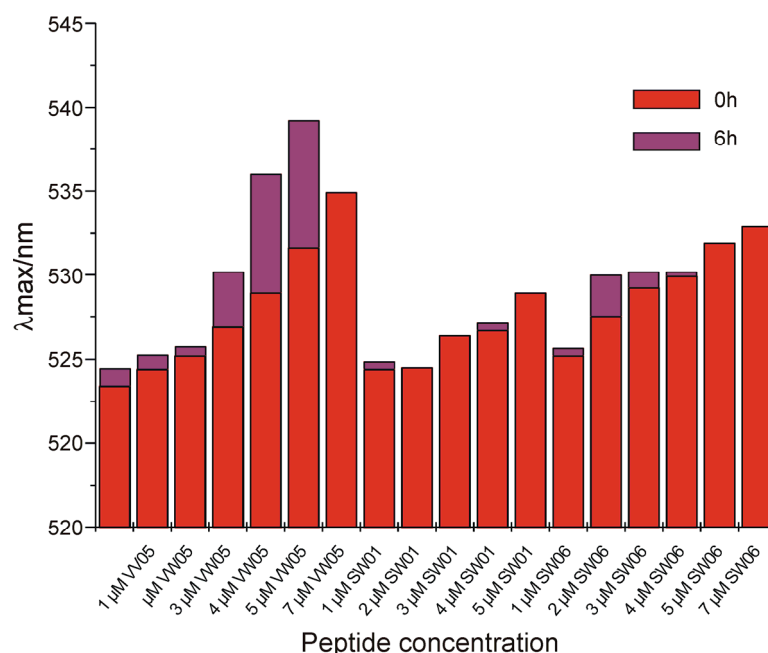


Figure 8.6. Position of absorption maxima of 50 nM Au/MUA nanoparticles at different peptide concentrations of VW05, SW01, and SW06 at pH 9.0.

Finally, TEM measurements were performed to directly monitor the ultrastructure of the nanoparticle assemblies in the presence of SW01 and SW06 (Figure 8.7). In agreement with the lower shifts of absorption maxima, the addition of both peptides did not reveal such large aggregates as found for VW05. Only a densification of nanoparticles but without defined ultrastructure was obtained.

In conclusion, the addition of both new derivatives also enables the assembly of anionic nanoparticles upon electrostatic interactions. Nevertheless, neither the decrease of peptide charge nor the extension of peptide length drove the systems towards more defined and ordered structures.

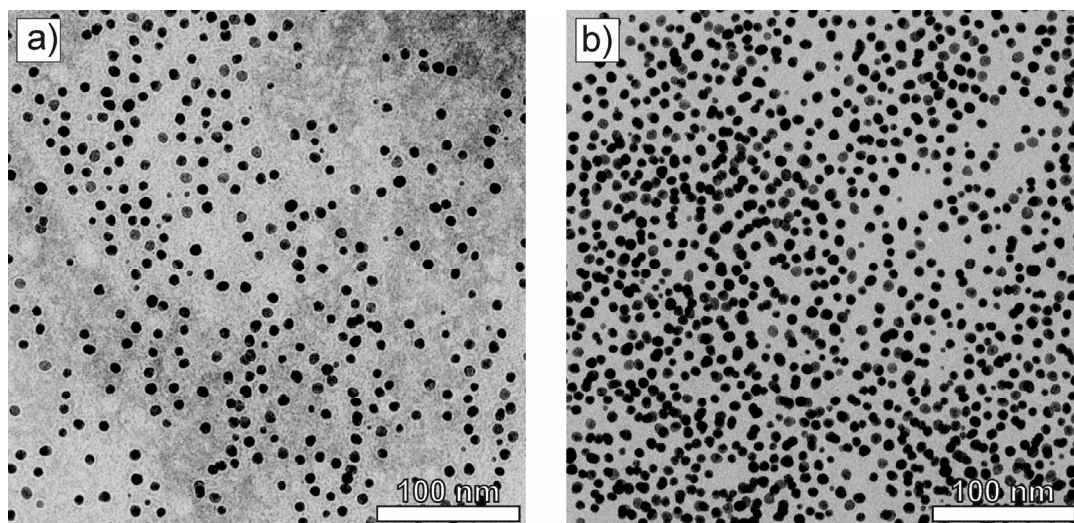


Figure 8.7. TEM micrographs of (a) 10 μM SW01 and (b) 10 μM SW06 in presence of 50 nM of MUA functionalized gold nanoparticles at pH 9.

8.4 Critical discussion of the protein-directed geometry of nanoparticle architectures (unpublished results)

In summary, several design variations were investigated with regard to the induced architecture of nanoparticles. For no peptide reported here, the symmetry of coiled coil structure directly influenced the symmetry of nanoparticle arrangement. Figure 8.8 shows a selected nanoparticle aggregate provoked by the addition of VW05. The aggregate displays almost exclusively densely-packed areas which very likely result from the sample blotting procedure and subsequent drying of the grids. The associated reduction of three to two dimensions makes a resolution of the internal structure of aggregate difficult. Hence, for many assemblies resolved by TEM, an unordered structure was assumed. Nevertheless, as shown by an extract in Figure 8.8, occasional two-dimensional areas could be resolved which display a hexameric rather than trimeric nanoparticle arrangement, a fact that was not considered by our original peptide design.

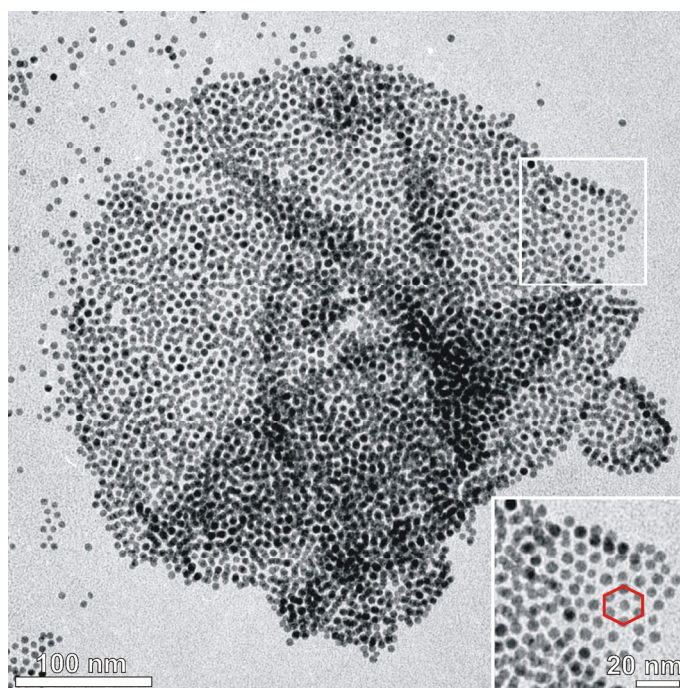

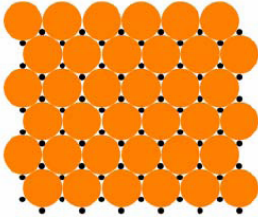
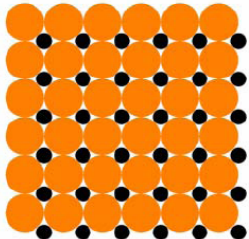
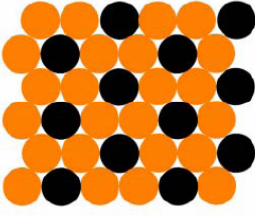


Figure 8.8. TEM micrograph of 10 μM VW05 incubated with 20 nM gold/MUA nanoparticles. The samples were incubated for 24 hours at pH 9. The selected extract shows the hexameric arrangement of gold nanoparticles within a two-dimensional area of the aggregate.

Table 8.2. Simple packing constraint in 2D assembly of binary systems (according to M. Hu et al.).¹⁸

Size ratio r_A/r_B	Stoichiometry A:B	Architecture	Illustration
0 – 0.155	1:1	Linear	
0.155 – 0.414	2:1	Hexagonal	
0.414 – 1.000	1:1	Tetragonal	
> 1.000	1:2	Hexagonal	

From our current side of view, this observation may be understood from the perception of solid state chemistry. For instance, as mentioned in one of the previous chapters, the application of the 20S proteasome protein with a D7 symmetry yielded a tetragonal arrangement of nanoparticles. The authors explained this finding by the steric restriction based on the Pauling rules. One very important aspect of the Pauling rules is that a coordinated polyhedron of anions is formed about each cation, while the coordination number of anions (A) around one cation (B) is determined by the radius ratio. Table 8.2 summarizes different packings of binary systems according to their size ratios. In the case of Hainfeld and co-workers, the calculated size ratio r_A/r_B of gold nanoparticles (A) to protein (B) was estimated to be between 0.32 and 0.60 which agrees with the steric hindrance in tetragonal packing (0.41-1.00). The electrostatic interaction between coiled coil peptide and nanoparticle leads here to a very rapid and hardly controllable assembly process whose final state of aggregate may be also described by means of such general principles for crystal structure formation. The size

ratio of coiled coil trimer to nanoparticle can therefore be calculated as follows. The overall radius (R_{trimer}) of a coiled coil trimer was estimated by means of a publication of P. B. Harbury et al. who resolved the crystal structure of the GCN4-pII trimer (Figure 8.9).¹¹⁶ Using their structural parameters for the supercoil radius R_0 (0.67 nm) and the normal α -helix radius R_1 (0.224 nm), the overall radius R_{trimer} was calculated by the sum of both to be 0.894 nm. Thereby, this value only describes the radius of the skeletal structure of a coiled coil trimer, since the structural parameters reported in Ref. 116 neglect the contribution of side chains. Taking into account that the gold nanoparticles, including their ligand shell, possess an averaged radius of 3.1 nm, the overall size ratio of $R_{\text{trimer}}/R_{\text{np}}$ corresponds to a value of 0.288. According to Table 8.2, this value points to a hexagonal architecture upon crystal arrangement. At the same time, this packing type would be related to a 2:1 binding stoichiometry of peptide to nanoparticle (see Table 8.2). The fact that gel electrophoretic measurements as well as UV/Vis spectroscopy revealed a 200-fold excess of peptide to nanoparticle may result from the contemporaneous nanoparticle-induced assembly of peptide into extended fibers. Consequently, only a reduced amount of peptide in solution would be available for undergoing electrostatic interactions with nanoparticles.

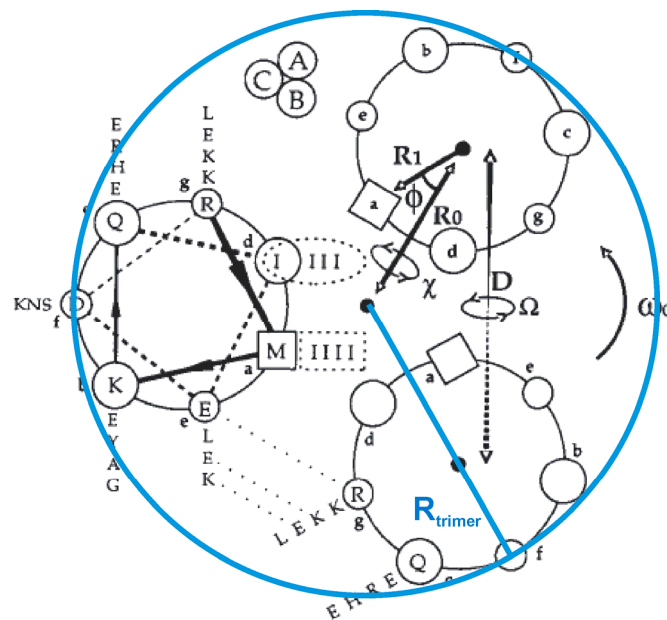


Figure 8.9. Helical wheel projection of the GCN4-pII trimer. View is from the N terminus, and residues in the first two helical turns are boxed or circled. Heptad positions are labelled a-g. The R_0 , ω_0 , α , ϕ , and R_1 variables from a coiled-coil parameterization suggested by Crick^{117,118} and the D and Ω variables defined in ref. 119 are illustrated (according to P. B. Harbury et al.).¹¹⁶

One may also wonder whether in the case of the monomeric VW05-ref, an unfavorable size ratio of peptide to nanoparticle may prevent such a densely packed architecture. In previous studies on a different peptide, but with the same number of residues, cryo-electron microscopic measurements revealed a diameter of about 2 nm for its monomeric state.¹²⁰ Provided that this size may be also applied to the monomeric structure of VW05-ref, a size ratio $R_{\text{monomer}}/R_{\text{np}}$ of 0.323 could be calculated. This would favor a hexameric arrangement of nanoparticles, as well. Regarding the fact, that no assembly of nanoparticles has been observed, the multivalent presentation of charge in a well-defined structure such as the coiled coil folding seems to be still required for an efficient packing of nanoparticles.

9 Results: Coiled coil model peptides to study protein misfolding

9.1 Concept

9.1.1 Peptide design

In neurodegenerative diseases, the native state of protein, which is either unfolded or α -helical, undergoes a folding transition triggered by environmental conditions such as pH, ionic strength, or the presence of metal ions. As a result, a pathogenic β -sheet form of protein is formed which subsequently assembles into amyloidogenic plaques. This folding transition event may be reduced to two distinct folds, the native and the β -sheet rich state, that has to be mimicked under given environmental conditions by the design of suitable model peptides. According to a previous chapter, the α -helical coiled coil folding has attracted a lot of attention for the development of such model peptides in the last decade.

In literature, several approaches have been followed to introduce β -sheet propensity into coiled coil sequences. One widespread approach extends the placement of hydrophobic residues in i , $i+3$, and $i+4$ positions of the coiled coil such that the peptide sequence displays a binary pattern of hydrophobic and hydrophilic residues in an extended conformation. Such binary sequences have been under intensive investigation and were shown to possess a high potential for the formation of β -sheet containing aggregates. Studies of Hartgerink and co-workers demonstrated that the arrangement of only a few hydrophobic residues into a patch in the middle of sequence may be also sufficient to induce β -sheet folding to the whole peptide. Altogether, most of the published coiled coil based model peptides for studying amyloid formation require either elevated temperatures or unnatural modifications to induce the transformation of the coiled coil. To overcome these drawbacks and to get closer to natural conditions, we developed coiled coil based model peptides that simply react on pH changes with an altered conformation.

All here reported peptides possess the ability to emulate a native α -helical fold of protein due to their preserved coiled coil recognition domain. The occupation of a and d positions by leucine and the juxtaposition of lysine and glutamate in positions e and g allow the peptides to form a hydrophobic core as well as interhelical salt bridges upon

oligomerization of α -helices. Likewise, the peptide sequences were equipped with elements that make the peptide folding sensitive to pH changes. Several studies in our group successfully showed that the arrangement of charged residues into extended domains of the α -helix is a suitable tool to introduce pH dependency to the coiled coil stability. For instance, the design shown in Figure 9.1, which is very similar to that of one of the peptide sequences of the following publication, confirms that extended domains of lysine are suitable to destabilize the coiled coil at acidic conditions such as pH 4. A physiological pH going along with a reduced charge of lysine domain recovers the adoption of the α -helical coiled coil folding.

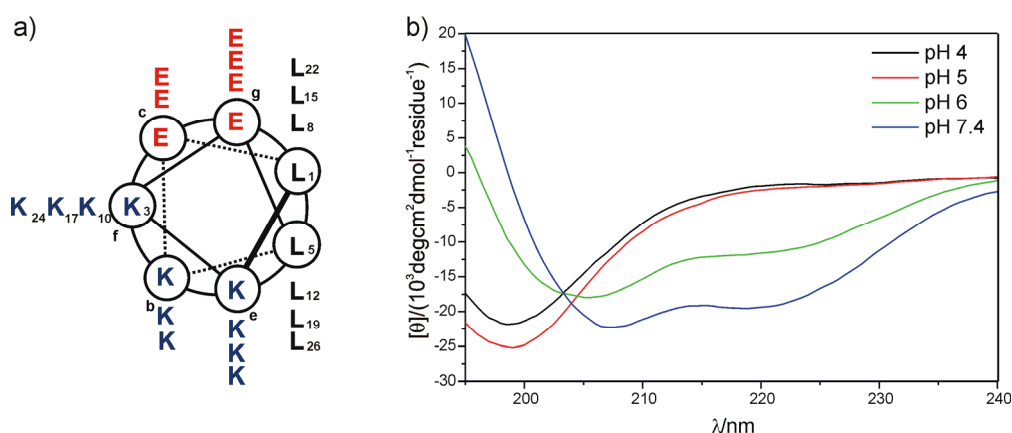


Figure 9.1. a) Helical wheel presentation of a single helix containing an extended lysine domain. b) CD spectra of this peptide taken at 100 μ M and at various pH values. The spectra were recorded by Morhaf Abu Ammar).

Not only electrostatic interactions but also the composition of residues with their intrinsic secondary structure propensities however plays a considerable role in protein folding. Upon decreasing the extent of the lysine domain, a second peptide design shown in Figure 9.2 was derived. Although this second design also enables attractive interactions upon coiled coil formation, this peptide surprisingly occurred unfolded at pH 7.4 whereas the first peptide design still allowed an α -helical folding. Here, the unfolding of peptide was obviously attributed to the introduction of serine, which possesses a lower propensity for α -helical structures than lysine does. The exact conformational parameters of amino acids are given in Table 10.1 in the following chapter.

The design of model peptides of the following publication combines both these tools, the extended charged domains for the pH sensitivity and the intrinsic secondary structure propensities. The latter was used not only to destabilize the coiled coil

structure, but also to enhance the overall β -sheet propensity upon introduction of valine.

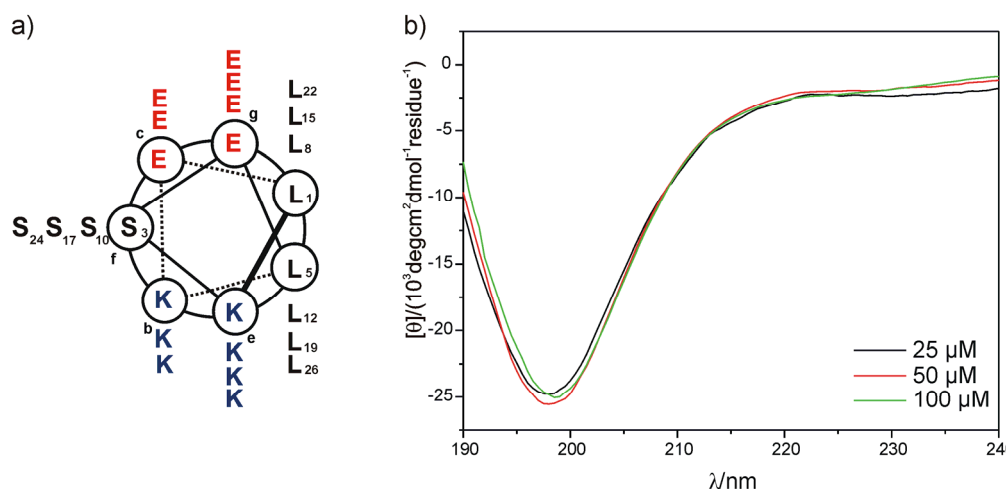


Figure 9.2. a) Helical wheel presentation of a single helix. Compared to the design shown in Figure 9.1, the charged domain of lysine has been reduced. b) CD spectra of this peptide taken at pH 7.4 and at various peptide concentrations.

9.1.2 Analytical techniques

A battery of analytical techniques was applied to characterize the folding behavior of the model peptides invented here. CD spectroscopy was used to study the conformation of peptide depending on the pH, peptide concentration, incubation time, and ionic strength. Furthermore, CD spectroscopy was also used for thermal denaturation experiments in order to gain information about the stability of the different coiled coil structures. Dye binding assays using ThT were performed to obtain more information about the kinetics of fibril formation. All these comprehensive investigations by means of both techniques were shared with M. Sc. Raheleh Rezaei Araghi.¹²¹ The overall morphology of peptidic assemblies was characterized by cryo-transmission electron microscopy in cooperation with Dr. Hans von Berlepsch and PD Dr. Christoph Böttcher.¹¹⁵

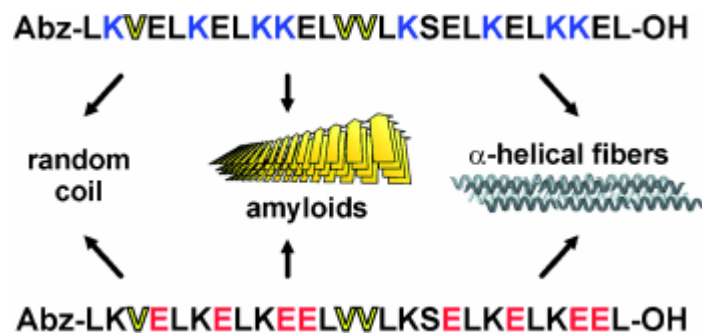
9.2 Publication

Kevin Pagel*, Sara C. Wagner*, Raheleh Rezaei Araghi, Hans von Berlepsch, Christoph Böttcher, Beate Kokschi, Intramolecular charge interactions as a tool to control the coiled-coil-to-amyloid transformation, *Chem. Eur. J.* **2008**, *14*, 11442-11451 (* Joint first authors).

The original article is available at:

<http://www3.interscience.wiley.com/cgi-bin/fulltext/121519576/PDFSTART>

pH switch: Excessively charged domains have been implemented into a coiled-coil-based amyloid model system to create sensitivity towards pH changes. Depending on the applied environmental conditions, different conformations and assembly morphologies, such as random coils, α -helical fibers, or classical amyloids, are formed (see picture).



10 Results: Nanoparticle-induced peptide folding and fibril formation

10.1 Design of nanoparticles

In the studies presented here, we have primarily focused on the physiological pH to study the impact of nanoparticles on protein folding. Because of their high aggregation tendency at $\text{pH} \leq 8$, MUA/Au nanoparticles as used for the coiled coil mediated organization of nanoparticles in chapter 8 cannot be applied for studies at this pH value. Therefore, the design of gold nanoparticles was modified by using MUAsulfate instead of MUA in the ligand shell of nanoparticle. This kind of nanoparticle is stable over a wider range of pH due to the lower pK_a of the ligand molecule, which can be calculated to be 1.84 ± 0.50 using the Advanced Chemistry Development software V8.14 for Solaris. Preliminary studies on the stability of MUAsulfate/Au nanoparticles showed that Tris/HCl buffer (10 mM, pH 7.4) revealed stable particles over an observation of at least one month (data not shown). The synthesis of the nanoparticles was done in the Schlecht research group by Meike Roskamp.

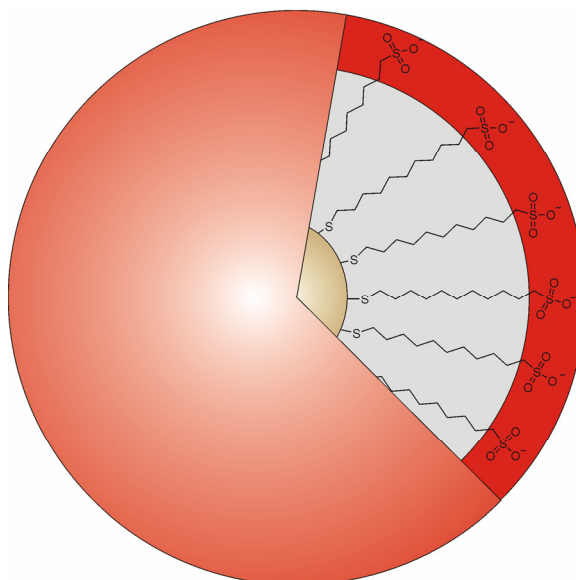


Figure 10.1. Design of MUAsulfate functionalized gold nanoparticles, shown for an idealized state of completely extended ligands.

10.2 Peptide design

As discussed in one of the previous chapters, the impact of nanoparticles on protein misfolding is a topic of current interest. Contradictory effects have been found for the folding behavior of proteins in the presence of nanoparticles. For instance, Linse and colleagues found that uncharged copolymer nanoparticles are capable of inducing the self-assembly of β_2 -microglobulin. However, the same kind of nanoparticle successfully inhibited amyloid formation of the A β peptide. In general, the application of natural proteins involved in neurodegenerative diseases implies a spontaneous protein aggregation which can be hardly controlled. As a result, Linse and co-workers were not able to commit whether the proteins bind in a monomeric or oligomeric form to the nanoparticles, a fact that may have a significant impact on the kinetic pathway of amyloid formation. The application of model peptides is often attended with an improved solubility which allows a defined initial state of folding and facilitates the analytical characterization. Moreover, small substitutions within the peptide sequence may be applied to tune aggregation properties of the peptide by varying the charge, hydrophobicity, and secondary structure propensities.

The design and characterization of coiled coil based amyloid-forming model peptides discussed in the previous chapter and publication provided an essential basis for the following studies. From this series of de novo designed peptides, two peptides were selected for the binding studies to nanoparticles. One of these peptides served as a parent peptide for further modifications. According to their design, both selected peptides are able to adopt a random coil, α -helical or β -sheet structure in dependence on peptide concentration and pH value. Both peptides need a sufficiently high peptide concentration for the adoption of any ordered conformation, but importantly differ in their pH range required for β -sheet formation. At physiological pH, only peptide B is able to form β -sheets above a certain concentration limit; low concentrations lead to unfolding of the peptide. In contrast, the unfolding of peptide A turns into a coiled coil formation upon increasing the peptide concentration at pH 7.4. Besides, peptide A with its higher number of positively charged residues is expected to bind in a higher stoichiometry to the nanoparticle than peptide B does. However, a comparison of the aggregation tendency of both peptides in presence of nanoparticles allows one to estimate which of these features, intrinsic aggregation tendency or binding stoichiometry, is decisive here.

Both peptides were exposed in an unfolded and monomeric form to the nanoparticles to allow a defined initial state of folding. Because the studies showed that the binding stoichiometry plays the major role in this event, additional peptide sequences were

derived from peptide A in order to investigate more deeply the necessity of β -sheet inducing elements. In other words, it was further addressed whether every peptide regardless of its intrinsic structural propensities is capable of undergoing nanoparticle-induced fibril formation in the case of a sufficiently high binding stoichiometry. As mentioned in the previous paper, valine residues were introduced in the peptide sequence in order to increase the overall β -sheet propensity of peptide. Therefore, in the additional studies, these valine residues were systematically replaced by a second amino acid. Conceptually, this amino acid has to fulfil three criteria; it is required to have a lower β -sheet propensity than valine, but at the same time, should not increase the overall helicity. Only an initial state of folding comparable to that of peptide A allows an overall comparison of these results to those obtained for the parent peptide. Apart from that, the new residue should not be charged in order to preserve the binding stoichiometry to the nanoparticle upon electrostatic interactions.

Table 10.1. Assignment of amino acids as formers, breakers, and indifferent for helical and β -sheet regions in proteins based on P_α and P_β values (according to P. Y. Chou and G. D. Fasman).¹²³

Helical Residues ^a	P_α		β -Sheet Residues ^b	P_β	
Glu (-)	1.53	} H_α	Met	1.67	} H_β
Ala	1.45		Val	1.65	
Leu	1.34		Ile	1.60	
His (+)	1.24	} h_α	Cys	1.30	} h_β
Met	1.20		Tyr	1.29	
Gln	1.17		Phe	1.28	
Trp	1.14		Gln	1.23	
Val	1.14		Leu	1.22	
Phe	1.12	} l_α	Thr	1.20	} l_β
Lys (+)	1.07		Trp	1.19	
Ile	1.00		Ala	0.97	
Asp (-)	0.98	} i_α	Arg (+)	0.90	} i_β
Thr	0.82		Gly	0.81	
Ser	0.79		Asp (-)	0.80	
Arg (+)	0.79	} b_α	Lys (+)	0.74	} b_β
Cys	0.77		Ser	0.72	
Asn	0.73		His (+)	0.71	
Tyr	0.61	} B_α	Asn	0.65	} B_β
Pro	0.59		Pro	0.62	
Gly	0.53		Glu (-)	0.26	

^aHelical assignments: H_α , strong α former; h_α , α former; l_α , weak α former; i_α , α indifferent; b_α , a breaker; B_α , strong α breaker. ^b β -sheet assignments: H_β , strong β former; h_β , β former; l_β , weak β former; i_β , β indifferent; b_β , a breaker; B_β , strong β breaker.

Upon statistical analysis of protein crystal structures, P. Y. Chou and G. D. Fasman derived a classification of the 20 naturally-occurring amino acids regarding their α -helical and β -sheet propensities (Table 10.1).^{122,123} The substitutions reported in the

following manuscript were carried out by selecting glycine as suitable amino acid. According to Table 10.1, glycine and valine are assigned with P_{β} values of 0.81 and 1.65, respectively. Moreover, glycine and valine display an α -helix propensity P_{α} of 0.53 and 1.14, respectively.

10.3 Analytical techniques

A battery of analytical techniques was applied to study the impact factor of nanoparticles on the folding and aggregation of peptide. CD spectroscopy was applied to investigate the conformational behavior in the presence of nanoparticles. Electron microscopy was used to elucidate the morphology of peptide assemblies in the presence of nanoparticles. The general binding parameters were determined by means of isothermal titration calorimetry. Moreover, together with Dipl.-Chem. Meike Roskamp, gel electrophoretic measurements were performed to confirm binding stoichiometries calculated by ITC measurements.¹⁰⁸

10.4 Manuscript

Sara C. Wagner, Meike Roskamp, Manjula Pallerla, Raheleh Rezaei Araghi, Sabine Schlecht, Beate Korsch, Nanoparticle induced folding and fibril formation of coiled coil based model peptides, submitted.

Nanoparticle induced folding and fibril formation of coiled coil based model peptides

*Sara C. Wagner, Meike Roskamp, Manjula Pallerla, Raheleh Rezaei Araghi, Sabine Schlecht[§], Beate Kokschr**

[*] Prof. Dr. B. Kokschr, S. C. Wagner, Dr. M. Pallerla, R. Rezaei Araghi
Department of Organic Chemistry
Freie Universität Berlin
Takustr. 3
14195 Berlin (Germany)
E-mail: kokschr@chemie.fu-berlin.de

Prof. Dr. S. Schlecht, M. Roskamp
Department of Inorganic Chemistry
Freie Universität Berlin
Fabeckstr. 34-36
14195 Berlin (Germany)

§ Current address: Department of Inorganic and Analytical Chemistry, Institute of Chemistry, Justus-Liebig University Gießen.

Keywords: Protein folding, fibril formation, nanoparticle, coiled coil, aggregation.

Abstract: Nanomedicine is a rapidly growing field and has the potential to deliver treatments for many illnesses. However, only relatively little is known about the biological risks of nanoparticles. Some studies have shown that nanoparticles can have an impact on the aggregation properties of proteins, including fibril formation. Moreover, these studies also showed that the capacity of nanoscale objects to induce or prevent misfolding of the proteins strongly depends upon the primary structure of the protein. This report sheds light on the role of peptide primary structure in directing nanoparticle-induced misfolding by means of two model peptides. The design of the model peptides is based on the α -helical coiled coil folding motif, but also includes features that enable them to respond to pH changes, allowing pH-dependent β -sheet formation. Previous studies showed that the two peptides differ in the pH range required for β -sheet folding. Time-dependent circular dichroism spectroscopy (CD) and

transmission electron microscopy (TEM) were carried out to characterize peptide folding and aggregate morphology in the presence of negatively charged gold nanoparticles (AuNps). Both peptides were found to undergo nanoparticle-induced fibril formation. The determination of binding parameters by isothermal titration calorimetry (ITC) further revealed that the different propensities of both peptides to form amyloid-like structures in the presence of AuNps is primarily due to binding stoichiometry to the AuNps. Modifications of one of the peptide sequences showed that AuNp-induced β -sheet formation is in fact related to the structural propensity of the primary structure and not a generic feature of peptide sequences with a sufficiently high binding stoichiometry to the nanoparticles.

1. Introduction

The irreversible aggregation of proteins into amyloid deposits is a common feature of many neurodegenerative diseases such as Alzheimer's disease and Parkinson's disease.^[1] Although amyloid-forming proteins do not usually possess high sequence homology, impressive structural similarities, such as an unbranched morphology, diagnostic dye binding, and a characteristic X-ray diffraction pattern, are found for their fibrillar assemblies.^[2] A key feature of these diseases is a conformational transition from the native compact folded form into the pathological β -sheet rich structure, followed by self-assembly into fibrils.^[3] Several factors, such as the pH and ionic strength of the solvent, the presence of metal ions, and a certain composition of lipid membranes are widely accepted to trigger this structural transition. With regard to the general impact of surfaces on the misfolding of proteins, studies using membranes have yielded valuable information. Hence, a variety of lipid membranes have been shown to induce electrostatically driven binding of the amyloid β peptide (A β); this was followed by accelerated aggregation into toxic species at rates significantly higher than in a

membrane-free environment.^[4] Furthermore, these studies showed that the ability of biological membranes to modulate pathological conversion into amyloidogenic aggregates strongly depends upon the properties of the surface.^[5] At the same time, two main molecular effects are thought to be responsible for the increase in toxic form of the protein.^[6] First, the binding of proteins to membranes leads to the so-called surface-crowding effect.^[7] Second, through bringing residues in close proximity which otherwise would be spatially separated the association of proteins to a particular kind of membrane may destabilize the native fold of the protein and thus, above a certain critical surface concentration limit, facilitate the transformation into toxic aggregates. However, the triggers and mechanisms involved in the misfolding of proteins are so far poorly understood.

The surface-induced pathological self-assembly of proteins occurs not only in the presence of biological membranes but is also relevant for other kinds of materials, such as nanoparticle. Compared to membranes, nanoparticles possess an enormous surface-to-volume ratio so that the influence of the surface-crowding effect becomes even more pronounced. Several in vitro studies showed that the interaction between protein and nanoparticle can result in the formation of β -sheet containing deposits.^[8-11] In one of these studies, Linse et al. found that uncharged copolymer nanoparticles are capable of inducing the self-assembly of β_2 -microglobulin, a human protein involved in dialysis-related amyloidosis.^[8] Interestingly, in the case of the amyloid β peptide, it was found that the same kind of nanoparticle can inhibit, and even temporarily reverse, the fibrillation of protein.^[12] These and other studies deal with an interaction between a nanoparticle and a naturally occurring protein with an intrinsically complex structure. Studies by Linse and colleagues also demonstrated that the capacity of the nanoscale objects to induce a disease-like amyloid formation or prevent such aggregation strongly depends upon the primary structure of the protein. Nonetheless, nanoparticles can affect

protein fibrillogenesis. This fact is one reason for growing concerns about the toxicity of nanoparticles^[13], whereas nanomedicine raises high expectations for better healthcare^[14] and has already entered a variety of different fields such as medical diagnostics and drug transport^[15]. We believe that model peptides are a promising tool for a systematic study of the role of primary structure in nanoparticle-induced misfolding. In recent years, the application of model peptides has contributed to the elucidation of the origin and molecular mechanisms of amyloid-related disorders.^[16] This is in part due to their facile synthetic accessibility and, often, the relative ease of analytical characterization of the aggregating peptides because of improved solubility. Moreover, small changes within the short sequence of model peptides can be used to tune the aggregation properties of the peptide by varying the charge, hydrophobicity, and secondary structure propensities.^[17]

We recently published the design of a series of model peptides that, depending on concentration and pH, adopt different conformations and amyloid-like fibril morphologies.^[18] The sequences of these peptides are based on the naturally occurring, well-studied α -helical coiled coil folding motif. In this report, we studied the aggregation behavior of two of these de novo designed model peptides in the presence of nanoparticles at physiological pH. The peptides are expected to bind to the anionic nanoparticles by electrostatic interactions. We focus here on the impact of the peptide's sequence on nanoparticle-induced aggregation; the impact of size and surface composition of the nanoparticle is outside the scope of this study. The type of nanoparticle used here is a 5-nm spherical gold core coated with mercaptoundecane sulphonic acid. We also studied several derivatives of one of both peptides by reducing the number of β -sheet preferring amino acids in order to investigate more deeply to what extent the β -sheet tendency of the peptide itself directs aggregation behaviour in the presence of the nanoparticles.

2. Design of the parent model peptides

The stability of α -helical coiled coil structures relies on the hydrophobic core packing of at least two and up to five amphiphilic α -helices that are wound around one another with a slight left-handed superhelical twist.^[19] As a result, the primary structure is characterized by a periodic repeat of seven residues, the so-called 4–3 heptad repeat, which is commonly denoted from a to g. In both peptides, the capability of coiled coil folding was preserved by leucine in positions a and d as well as lysine and glutamic acid in positions e and g (**Figure 1**). Since positions b, c, and f are solvent-exposed, these positions have been used here to implement additional features which increase the sensitivity of the peptide to react to environmental changes as well as allow the adoption of further non-helical conformations under certain conditions. Here, valine residues have been incorporated to enhance the β -sheet forming tendency of the peptide. Charged residues were arranged into extensively charged domains in order to generate pH-sensitivity.

In previous studies, we showed that these extended charged domains are sufficient to disfavor α -helical folding in a pH dependent manner.^[18] We also demonstrated that, at low peptide concentrations, this destabilization leads to a random coil conformation, whereas higher peptide concentrations may induce a transformation into β -sheet structures with subsequent aggregation into amyloid-like fibrils.

Since we were interested in the impact of charged nanoparticles on the aggregation behaviour of these peptides under physiological conditions, we primarily focus on the pH value of 7.4 in the current study. At this pH, peptide A adopts an unfolded structure at concentrations below 300 μ M. Above this concentration limit and in the absence of any interaction partner, peptide A adopts an α -helical coiled coil structure and does not transform into a β -sheet structure, even at concentrations up to its solubility limit of 1 mM. In contrast, peptide B does not show any tendency to adopt a helical folding at pH

7.4. This peptide requires a concentration above a limit of 150 μM to fold into a β -sheet structure; at lower concentrations, peptide B remains unfolded.

In the following studies, these peptides were applied to the nanoparticles under conditions where the peptides alone are unfolded. Both peptides differ in their calculated net charge, which is +2.0 for peptide A and -2.0 for peptide B.^[20]

Nevertheless, an electrostatic interaction between peptide and nanoparticle is not only determined by the overall net charge of peptide. Recently, we demonstrated that especially the local charge at the facial site of the coiled coil structure allows an electrostatically attractive interaction between peptide and nanoparticle, even when their net charges are not complementary to each other.^[21]

3. Folding behaviour in presence of anionic nanoparticles

Time-dependent CD studies were carried out at pH 7.4 at nanoparticle concentrations ranging from 2.5 nM to 40 nM, covering an excess of peptide to nanoparticle in a range from 20,000 fold to 1,250 fold (**Figures S1 and S2**). For better comparison, the secondary structure composition of both peptides were calculated from all CD spectra using the JFIT CD analysis program^[22] and is shown for different incubation times and nanoparticle concentrations in **Figure 2**. According to the calculations, both peptides are mostly unfolded at a peptide concentration of 50 μM . Upon addition of nanoparticles and at a very short incubation time of five minutes, an increasing amount of α -helical structure is observed. The nanoparticle-induced helicity is very likely a consequence of the placement of lysine residues in *i*, *i*+3 and *i*+4 positions, since also studies of other groups showed that such an arrangement of charged residues can result in a surface-assisted stabilization of α -helical structure.^[23] Moreover, the correlation between nanoparticle concentration and the amount of α -helicity differs for both peptides, the result of different binding parameters (Figure S1 and S2, insets). However,

the electrostatic nature of the interaction between peptide and nanoparticle is demonstrated by additional CD measurements upon variation of the ionic strength and pH of the buffer (**Figure S3**).

At longer incubation times, the induced α -helical structure does not have to be stable, but undergoes a conformational change to β -sheet structure, depending on the nanoparticle concentration. At nanoparticle concentrations of 2.5 to 10 nM, this β -sheet formation occurs within 24 hours for peptide A; higher particle concentrations seem to retard this process. At the highest nanoparticle concentration of 40 nM, the trend for β -sheet formation is absent even for an incubation of over three weeks. However, determination of the kinetics of fibril formation by means of a Thioflavin T binding assay cannot be applied due to the strong absorption properties of gold nanoparticles. The general tendency of β -sheet formation appears to be much weaker for peptide B since a nanoparticle-induced β -sheet formation seems to require longer incubation times and is occurring for a smaller range of nanoparticle concentrations. An obvious development of β -sheet structures requires an incubation time of two weeks at 10 nM of gold nanoparticles and at least four weeks at 2.5 and 5 nM of nanoparticles. In contrast to peptide A, 20 and 30 nM of nanoparticles reveal a stable mostly helical conformation without any transformation. Similar to peptide A, higher nanoparticle concentrations appear not to be linked to more β -sheet formation.

4. Morphological studies on nanoparticle-induced fibril formation

In general, TEM allows the visualization of sufficiently large peptidic structures upon the addition of negative staining reagent, even when these structures represent only a minor part of the peptide. Here, TEM was applied to all samples contained in Figure 2,

including those without any β -sheet structure in order to study the influence of nanoparticle concentration on the morphology of the amyloid-like fibrils.

In the case of peptide A, low nanoparticle concentrations of 2.5 and 5 nM reveal relatively stiff fibers consisting of laterally assembled protofilaments 2-3 nm in width (**Figure 3a**). The general arrangement of both 26 amino acid-containing peptides into these β -sheet rich protofilaments includes very likely a hairpin- or sandwich-like internal organization. At nanoparticle concentrations above 5 nM, a more flexible arrangement of protofilaments by occasionally twisted fibers can be detected as a coexisting morphology (Figure 3b). For all fibers of peptide A, a length of several hundreds of nanometers was determined.

At low nanoparticle concentrations, less than or equal to 5 nM, peptide B forms ribbons that very clearly consist of 9 or more laterally assembled protofilaments (Figure 3e).

Furthermore, these ribbons can be partially twisted which leads to more tubular structures with an overlapping and crossbred arrangement of protofilaments. The length of these fibers is in the range of several hundreds of nanometers. When increasing the nanoparticle concentration above 5 nM, the amount of tubular structures increases significantly and is almost exclusively present at nanoparticle concentrations of 40 nM (Figure 3c). The width of these tubes varies between 30 and 100 nm. In all TEM images taken from peptide B, the diameter of protofilaments was determined to be 3.6 ± 0.2 nm by calculating the Fourier-Transform of an extract of the electron micrograph (Figure 3d). This calculation is only possible for peptide B because of the highly periodic arrangement of protofilaments as well as the regularity of their diameter.

Impressive structural differences between both peptides became obvious upon variation of the nanoparticle concentration. These differences very likely result from different growth conditions, as was also found by other groups.^[24] A longer lag time may allow the formation of higher ordered ultrastructures. In all samples studied by electron

microscopy, the fibrils are not necessarily connected to the nanoparticles. The fact that, occasionally, nanoparticles are arranged along the outside of the fibers is rather a consequence of the blotting procedure applied to prepare the samples for TEM measurements.

5. Determination of thermodynamic binding parameters

ITC was used to determine the thermodynamic parameters for complexation of the anionic gold nanoparticles with both model peptides (**Figure S4, Table 1**). By fitting the data with a one-set of binding sites mode, a stoichiometry of 1202 ± 32 and 238 ± 63 of peptide molecules to nanoparticle was obtained for peptide A and peptide B, respectively. This finding is very probably a consequence of the higher number of lysine residues within the sequence of peptide A. Differences in the binding stoichiometries of both peptides were confirmed by gel electrophoresis measurements, as shown in the supporting information. In theory, a 6-nm particle possesses a surface area of $1.2 \times 10^{-16} \text{ m}^2$. Provided that the peptide's helix binds with its facial lysine-rich side to the nanoparticle, a 26 amino acid peptide displays a cross-sectional area of approximately $1.9 \times 10^{-18} \text{ m}^2$.^[25] As a consequence, up to 63 peptide molecules would fit into the first layer of a 6-nm particle. With regard to the stoichiometry, the existence of multiple layers of peptide around one nanoparticle can be assumed.

The ITC measurements also revealed a weaker binding affinity in the case of peptide B. With regard to the molar binding energy, no obvious differences could be determined. In both cases, the arrangement of peptides around the nanoparticle is an entropically-disfavoured process owing to the nanoparticle-induced α -helical folding.

6. Variation of β -sheet propensity

In order to further validate the impact of the peptide's primary structure on the nanoparticle-induced secondary structure formation and transition, we generated variants of peptide A with decreased β -sheet propensity. We selected peptide A as the parent peptide for these modifications because of its high binding stoichiometry. As mentioned in the design chapter, three valine residues were initially incorporated into the sequence of both model peptides to enhance the overall β -sheet propensity of the system. In the following, we replaced valine by an uncharged residue to intend a stoichiometry in the same range as for peptide A upon electrostatic binding to nanoparticles. The new residue was chosen to have a lower propensity for β -sheet structures but, at the same time, does not increase the overall stability of α -helical structures in order to allow an initial folding state comparable to peptide A. For that reason, valine was systematically substituted by glycine either singly or multiply within one peptide sequence (**Table 2**). Although glycine displays a very low propensity for β -sheet structures^[26], this amino acid may be found within β -turns because of its conformational flexibility.^[27] In preliminary studies, a glycine-induced β -sheet folding of all derivatives was ruled out (**Figure S5**).

The general binding parameters to the gold nanoparticles were determined by ITC for all glycine-modified peptides (**Figure S6, Table 3**). Surprisingly, all monosubstituted sequences of peptide A display a higher binding stoichiometry compared to the parent peptide. This finding might be a consequence of the higher conformational flexibility of the glycine variants which might destabilize the formation of a fully extended α -helix at the nanoparticle surface allowing for the binding of more peptide molecules. This assumption is also in good agreement with the calculated ΔS values which are much

smaller than those of peptide A. However, the substitution of two valine residues by glycine yields binding parameters which are similar to those of peptide A.

For all glycine containing peptides, time-dependent CD measurements were carried out at 50 μ M of peptide and at nanoparticle concentrations ranging from 2.5 up to 40 nM in order to compare their folding behaviour to peptide A. Upon addition of nanoparticles, an induction of α -helical conformation was detected for all glycine variants (**Figure S7**). The dependency of the helical content on the nanoparticle concentration resembles peptide A in its overall features (**Figure S8**). However, the glycine variants differ in the incubation times required for the folding transition into the β -sheet structure while, as resulting from different binding parameters, the required nanoparticle concentrations may be different for every peptide. All of the monosubstituted peptides undergo a folding transition within 24 hours or longer, depending on the nanoparticle concentration. In comparison, the disubstituted peptides do not transfer into β -sheets before an incubation time of one (13G14G) or two weeks (3G13G, 3G14G) (**Figure S9**). However, the peptide containing three glycine residues completely remains α -helical even after an observation period of two months (Figure S9 shows an incubation of four weeks). Amyloid-like structures were detected for the glycine derived peptides at selected nanoparticle concentrations by TEM (representative images are depicted in Figure S10 for all mutants except for the trisubstituted one and selected nanoparticle concentrations).

7. Discussion

We have applied two coiled coil derived model peptides to the study of electrostatic interactions with charged gold nanoparticles. Due to their different net charges, the peptides display different binding stoichiometries to the nanoparticles. Because of the particular placement of lysine residues within the primary structure, the peptides adopt a

surface-induced α -helical folding upon binding to the nanoparticles. Calculated from their different binding stoichiometries, the helical structures are very likely arranged in many layers around one nanoparticle. This finding may result from the high number of charged ligand molecules in the particle shell, namely 1411 ± 135 of thiols as determined by EDX analysis in one of our previous publications.^[28] However, it turns out that the α -helical conformation undergoes a folding transition into β -sheet rich structures with subsequent aggregation into amyloid-like structures. Since both peptides alone transform from random coil into β -sheet under certain pH conditions¹⁸, the nanoparticle-induced α -helical conformation is probably not a prerequisite for fibril formation. Furthermore, the dependency of incubation time required for the folding transition on the nanoparticle concentration points to two other important factors which direct this process (a schematic view is given in **Figure 5**):

- (1) The surface-crowding effect seems to play a very important role since amyloid formation occurs concentration-dependently and its kinetics is determined by the appearance and concentration of a critical nucleus. In principle, the surface crowding of peptide around one nanoparticle is limited by the binding stoichiometry. An increase of nanoparticle concentration enhances the amount of formed nuclei which catalytically triggers the quantitative transformation into β -sheets. In other words, a higher nanoparticle concentration should result in a faster folding transition. Within a range of nanoparticle concentrations from 2.5 to 10 nM, these marginal differences were only detected for peptide B because of its slower β -sheet formation compared to peptide A.
- (2) The extension of nuclei into fibers requires a sufficiently high concentration of monomeric peptide in solution. Importantly, nuclei are not a fixed unit; once formed, they can either progress to fibrils or disintegrate if not extended in time.^[29] If nearly all peptide molecules are involved in the binding to the nanoparticles, as it is the case at 50

μM of peptide A and 40 nM of nanoparticles, the extension of nuclei into fibers is dramatically reduced or prevented. For that reason, there seems to be a turning point where the further increase in the nanoparticle concentration does not longer accelerate the β -sheet formation. At nanoparticle concentrations of 20 to 40 nM, only a very slow or no transition is detectable for peptides A and B, respectively.

In general, our 26 amino acid peptides can be prepared at a concentration not higher than 1 mM because of limited solubility. Thereby, in the absence of any interaction partner, only peptide B is capable of adopting a β -sheet structure at peptide concentrations above the limit of 200 μM and at pH 7.4, although both peptides contain β -sheet inducing elements. With regard to the results presented here, it appears that nanoparticle-induced fibril formation is primarily a consequence of the binding stoichiometry of peptide to nanoparticle, and that the intrinsic aggregation tendency of peptide plays only an incidental role.

In the literature, it has been stated that the ability of polypeptide chains to form amyloid structures is not restricted to the specific proteins associated with recognized clinical disorders.^[30] It seems that amyloid formation is a generic feature of polypeptide chains in a regime of high protein concentration. Therefore, we further addressed the question whether the here applied system consisting of a 26 amino acids containing peptide and a 6-nm large nanoparticle still requires β -sheet inducing elements within the peptide's primary structure in order to form into β -sheet rich fibrils. In order to reduce the β -sheet propensity, seven variants of peptide A were generated by a systematic replacement of valine against glycine. In comparison with peptide A, all monosubstituted variants as well as variant 3G13G displayed changed binding parameters in the presence of gold nanoparticles. However, in the case of all mono- and disubstituted glycine derivatives,

all peptides underwent a nanoparticle-induced α -helical folding which then transformed into β -sheet containing structures, but at different incubation times.

Although it turned out that substitutions in the sequence of peptide A are quite difficult and may alter the binding parameters to the nanoparticles, we believe that especially the folding behaviour of the variants 3G14G, 13G14G and 3G13G14 is comparable to peptide A because of almost similar binding features. In particular, the results obtained for peptide 3G13G14G confirm that the ability to undergo a nanoparticle-induced β -sheet folding with subsequent aggregation into amyloids is not a generic feature of peptide sequences with sufficiently high binding capacities but rather a consequence of β -sheet directing structural features.

8. Conclusion

The here presented results demonstrate that model peptides can undergo a nanoparticle-induced folding transition into β -sheets followed by a subsequent aggregation process into fibrils. Moreover, our results show that the nanoparticle-induced aggregation process is primarily determined by the stoichiometry of peptide to nanoparticle, which dramatically reduces the critical concentration of the peptide solution required for the fibril formation process. At the same time, the peptide's primary structure has to provide β -sheet-inducing features; otherwise, no aggregation into amyloid-like structures is observed. Taken together, these facts lead to the expectation that the potential to misfold in the presence of nanoparticles is not only limited to proteins of the known neurodegenerative diseases, but may generally concern other proteins or peptides containing β -sheet inducing elements.

Although the small size of the functionalized gold nanoparticles employed here represents an extreme situation of surface-to-volume ratio, our results demonstrate a generalizable trend of peptides to undergo nanoparticle-induced aggregation and

provide an informative basis about the biological risks of nanoparticle applications in terms of amyloid formation. Apart from that, our model system provides information about the mechanism of fibril formation in the presence of surfaces, an area which still remains challenging. By means of such peptides, we envisage future evaluation systems that will enable estimation of the biological effects of nanoparticles and support their safe medicinal applications.

Acknowledgements

The authors gratefully thank Dr. C. Böttcher and Dr. H. v. Berlepsch for helpful discussion of the TEM images. This work was financially supported by the Fonds der Chemischen Industrie (research fellowship of S. C. W.) and the Deutsche Forschungsgemeinschaft (SFB 765). Special thanks go to Allison Berger for proof-reading of the manuscript.

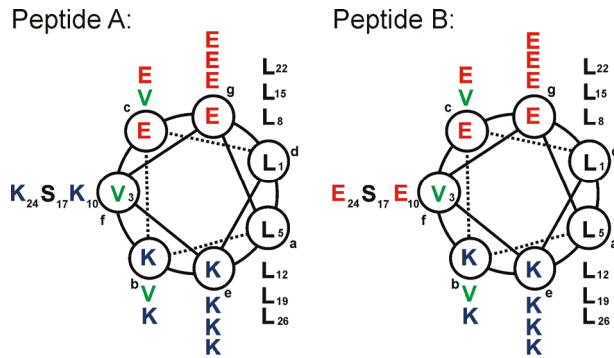
References.

- [1] a) J. W. Kelly, *Curr. Opin. Struct. Biol.* **1996**, *6*, 11-17; b) M. Stefanie., C. M. Dobson, *J. Mol. Med.* **2003**, *81*, 678-699.
- [2] O. S. Makin, L. C. Serpell, *FEBS J.* **2005**, *272*, 5950-5961.
- [3] a) C. Soto, *Mol. Med. Today* **1999**, *5*, 343-350; b) L. C. Serpell, *Biochem. Biophys. Acta* **2000**, *1502*, 16-30; c) P. Hammerström, R. L. Wiseman, E. T. Powers, J. W. Kelly, *Science* **2003**, *299*, 713-716; d) J. Hardy, D. J. Selkoe, *Science* **2002**, *297*, 353-356; e) J. P. Taylor, J. Hardy, K. H. Fischbeck, *Science* **2002**, *296*, 1991-1995; f) C. Soto, *Nat. Rev. Neurosci.* **2003**, *4*, 49-60; g) S. W. Liebman, *Proc. Natl. Acad. Sci. U.S.A.* **2002**, *99*, 9098-9100.
- [4] H. Zhao, E. K. J. Tuominen, P. K. J. Kinnunen, *Biochemistry* **2004**, *43*, 10302-10307.
- [5] M. Bokvist, F. Lindström, A. Watts, G. Gröbner, *J. Mol. Biol.* **2004**, *335*, 1039-1049.

- [6] C. Aisenbrey, T. Borowik, R. Byström, M. Bokvist, F. Lindström, H. Misiak, M.-A. Sani, G. Gröbner, *Eur. Biophys. J.* **2008**, *37*, 247-255.
- [7] a) A. P. Minton, *Biophys. J.* **1999**, *76*, 176-187; b) M. Bokvist, G. Gröbner, *J. Am. Chem. Soc.* **2007**, *129*, 14848-14849.
- [8] S. Linse, C. Cabaleiro-Lago, W.-F. Xue, I. Lynch, S. Lindman, E. Thulin, S. E. Radford, K. A. Dawson, *Proc. Natl. Acad. Sci. U.S.A.* **2007**, *104*, 8691-8696.
- [9] S. Rocha, A. F. Thünemann, M. C. Pereira, M. Coelho, H. Möhwald, G. Breszesinski, *Biophys. Chem.* **2008**, *137*, 35-42.
- [10] D. Zhang, O. Neumann, H. Wang, V. M. Yuwono, A. Barhoumi, M. Perham, J. D. Hartgerink, P. Wittung-Stafshede, N. J. Halas, *Nano Lett.* **2009**, *9*, 666-671.
- [11] W.-H. Wu, X. Sun, Y.-P. Yu, J. Hu, L. Zhao, Q. Liu, Y.-F. Zhao, Y.-M. Li, *Biochem. Biophys. Res. Commun.* **2008**, *373*, 315-318.
- [12] C. Cabaleiro-Lago, F. Quinlan-Pluck, I. Lynch, S. Lindman, A. M. Minogue, E. Thulin, D. M. Walsh, K. A. Dawson, S. Linse, *J. Am. Chem. Soc.* **2008**, *130*, 15437-15443.
- [13] a) J. De la Fuente, C. C. Berry, *Bioconjugate Chem.* **2005**, *16*, 1176-1180; b) V. L. Colvin, K. M. Kulinowski, *Proc. Natl. Acad. Sci. U.S.A.* **2007**, *104*, 8679-8680.
- [14] E. Katz, I. Willner, *Angew. Chem. Int. Ed.* **2004**, *43*, 6042-6108.
- [15] K. Riehemann, S. W. Schneider, T. A. Luger, B. Godin, M. Ferrari, H. Fuchs, *Angew. Chem. Int. Ed.* **2009**, *48*, 872-897.
- [16] a) K. Pagel, B. Kokschi, *Curr. Opin. Struct. Biol.* **2008**, *12*, 730-739; b) Y. Takahashi, A. Ueno, H. Mihara, *ChemBioChem* **2002**, *3*, 637-642.
- [17] a) F. Chiti, M. Stefanie, N. Taddei, G. Ramponi, C. M. Dobson, *Nature* **2003**, *424*, 805-808; b) M. López de la Paz, K. Goldie, J. Zurdo, E. Lacroix, C. M. Dobson, A. Hoenger, L. Serrano, *Proc. Natl. Acad. Sci. U.S.A.* **2002**, *99*, 16052-16057.

- [18] a) K. Pagel, S. C. Wagner, K. Samedov, H. v. Berlepsch, C. Böttcher, B. Kokschi, *J. Am. Chem. Soc.* **2006**, *128*, 2196-2197; b) K. Pagel, S. C. Wagner, R. Rezaei Araghi, H. v. Berlepsch, C. Böttcher, B. Kokschi, *Chem. Eur. J.* **2008**, *14*, 11442-11451.
- [19] a) Y. B. Yu, *Adv. Drug Delivery Rev.* **2002**, *54*, 1113-1129; b) J. M. Mason, K. M. Arndt, *ChemBioChem* **2004**, *5*, 170-176; c) D. N. Woolfson, *Adv. Protein Chem.* **2005**, *70*, 79-112.
- [20] For both peptides, the net charge has been calculated using the EMBL WWW Gateway to Isoelectric Point Service (<http://www.embl-heidelberg.de/cgi/pi-wrapper.pl>).
- [21] S. C. Wagner, M. Roskamp, H. Cölfen, C. Böttcher, S. Schlecht, B. Kokschi, *Org. Biomol. Chem.* **2009**, *7*, 46-51.
- [22] E. L. Altschuler, N. V. Hud, B. Mazrimas, B. Rupp, *J. Pept. Res.* **1997**, *50*, 73-75.
- [23] a) A. Verma, H. Nakade, J. M. Simard, V. M. Rotello, *J. Am. Chem. Soc.* **2004**, *126*, 10806-10807; b) Y. Fillon, A. Verma, P. Ghosh, D. Ernenwein, V. M. Rotello, *J. Am. Chem. Soc.* **2007**, *129*, 6676-6677; c) M. Lundqvist, P. Nygren, B.-H. Jonsson, K. Broo, *Angew. Chem. Int. Ed.* **2006**, *45*, 8169-8173; d) L. A. Capriotti, T. P. Beebe, J. P. Schneider, *J. Am. Chem. Soc.* **2007**, *129*, 5281-5287.
- [24] N. M. Kad, S. L. Myers, D. P. Smith, D. A. Smith, S. E. Radford, N. H. Thomson, *J. Mol. Biol.* **2003**, *330*, 785-797.
- [25] The cross sectional area of a 26-amino acids containing helix was calculated by means of the data determined for the crystal structure of an isoleucine-zipper trimer (P. B. Harbury, P. S. Kim, T. Alber, *Nature* **1994**, *371*, 80-83). The diameter of a single α -helix was determined to be of approximately 0.5 nm while neglecting the volume of side chains, while an axial shift of 1.48 Å per residue was measured.

- [26] P. Y. Chou and G. D. Fasman classified the propensity of all naturally occurring amino acids to adopt a certain folding by the so-called conformational parameters $P\alpha$ for helical and $P\beta$ for β -sheet structures (*Biochemistry* **1974**, *13*, 222-245). According to their calculations, valine and glycine are assigned by a value of 1.14 and 0.53 for $P\alpha$ and 1.65 and 0.81 for $P\beta$, respectively.
- [27] a) J. Hennetin, B. Jullian, A. C. Steven, A. V. Kajava, *J. Mol. Biol.* **2006**, *358*, 1094-1105; b) S. K. Brahmachari, R. S. Bhatnagar, V. S. Ananthanarayanan, *Biopolymers* **1982**, *21*, 1107-1125.
- [28] J. Dervedde, S. Enders, H.-U. Reissig, M. Roskamp, S. Schlecht, *Chem. Comm.* **2009**, 932-934.
- [29] R. Kodali, R. Wetzel, *Curr. Opin. Struct. Biol.* **2007**, *17*, 48-57.
- [30] C. M. Dobson, *Nature* **2003**, *426*, 884-890.



Peptide A:
 $\text{H}_2\text{N-Abz-LKVELKELKKEELVVKSELKELKKEEL-CO}_2\text{H}$

Peptide B:
 $\text{H}_2\text{N-Abz-LKVELKELKEELVVKSELKELKEEL-CO}_2\text{H}$

Figure 1. Helical wheel representation and sequences of peptides A and B. Blue, red: Accumulation of equally charged residues (blue: positive, red: negative) that destabilize helical folding at pH 7.4 and in absence of any interaction partner. Green: Solvent-exposed valine residues that serve for the β -sheet tendency of the peptides.

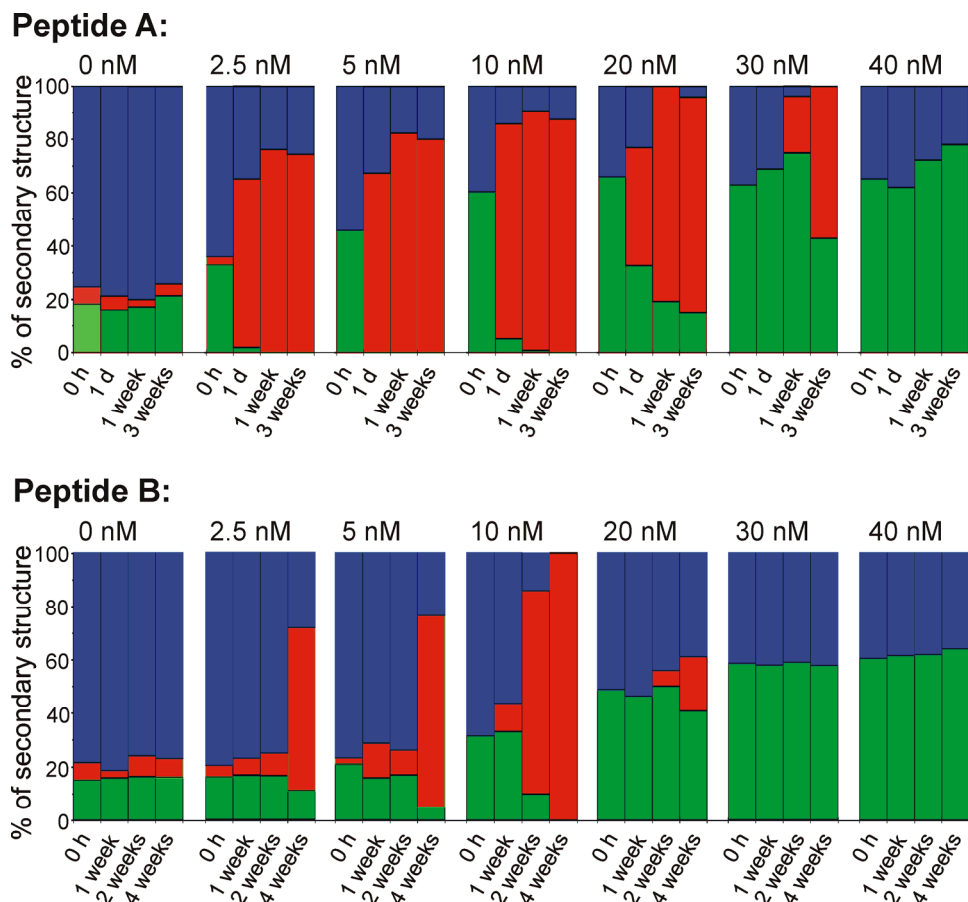


Figure 2. Populations of secondary structures of peptide A and B in presence of different nanoparticle concentrations, ranging from 0 to 40 nM (green: α -helix; red: β -sheet; blue: random coil). All samples refer to a fixed peptide concentration of 50 μM and are shown for different incubation times. For secondary structure analysis, the program JFIT was applied to the CD spectra of Figure S1 and S2.

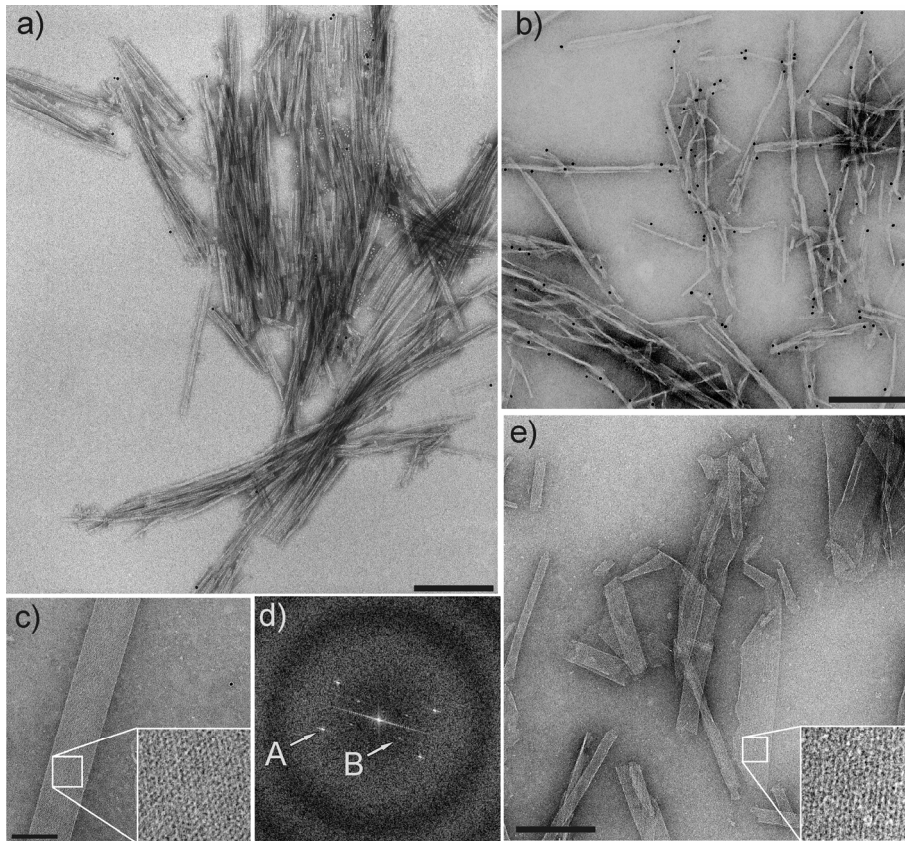


Figure 3. TEM images of 50 μM peptide A (a, b) and 50 μM peptide B (c, e) in presence of 5 nM (a, e) and 40 nM (b, c) gold nanoparticles. The samples were incubated for three weeks. (d) Fourier transform of an extract of (c) showing two different signals at a distance of 7.1 (B) and 3.6 (A) nm. Scale bars: 200 nm (a, b, e) and 100 nm (c).

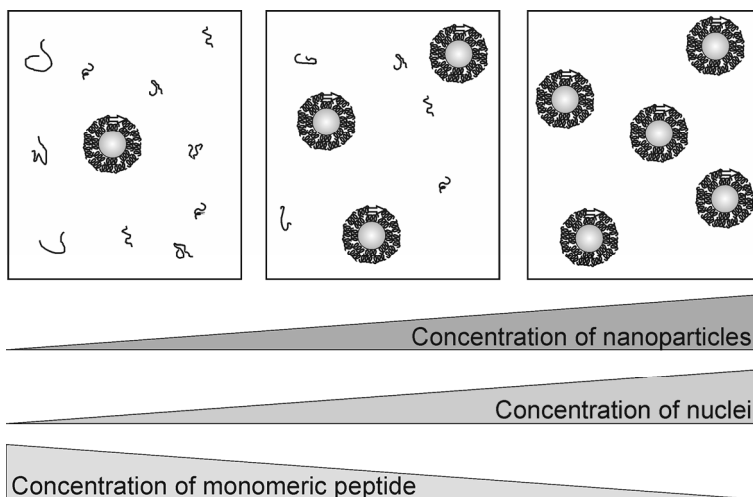


Figure 4. Schematic cartoon describing the correlation between the kinetics of the nanoparticle induced fibril formation and the nanoparticle concentration. The nucleus is depicted by an arrow in the protein shell surrounding one particle.

Table 1. Thermodynamic parameters for complexation of anionic gold nanoparticles with peptides.

	N	K [10 ⁵ /M]	ΔH [kcal/mol]	ΔS [cal/deg*mol]
Peptide A	1202 ± 32	2.2 ± 0.2	-21.2 ± 0.8	-45.6
Peptide B	238 ± 63	1.2 ± 0.3	-29.9 ± 9.2	-75.6

Table 2. Sequences of peptide A and its glycine modifications.

Peptide A	H ₂ N-Abz-LKVELKELKKELVVLKSELKELKKEL-CO ₂ H
Peptide A3G	H ₂ N-Abz-LK G ELKELKKELVVLKSELKELKKEL-CO ₂ H
Peptide A13G	H ₂ N-Abz-LKVELKELKKEL G VLKSELKELKKEL-CO ₂ H
Peptide A14G	H ₂ N-Abz-LKVELKELKKELV G LKSELKELKKEL-CO ₂ H
Peptide A3G13G	H ₂ N-Abz-LK G ELKELKKEL G VLKSELKELKKEL-CO ₂ H
Peptide A3G14G	H ₂ N-Abz-LK G ELKELKKELV G LKSELKELKKEL-CO ₂ H
Peptide A13G14G	H ₂ N-Abz-LKVELKELKKEL G G LKSELKELKKEL-CO ₂ H
Peptide A3G13G14G	H ₂ N-Abz-LK G ELKELKKEL G G LKSELKELKKEL-CO ₂ H

Table 3. Parameter values obtained by fitting the binding isotherms of peptide A and its glycine-modified sequences to a one-set of binding mode.

	N	K [10 ⁵ /M]	ΔH [kcal/mol]	ΔS [cal/deg*mol]
Peptide A3G	3188 ± 16	9.8 ± 0.5	-8.4 ± 0.1	-0.3
Peptide A13G	1621 ± 21	6.9 ± 0.4	-13.4 ± 0.2	-17.4
Peptide A14G	2150 ± 26	4.5 ± 0.2	-10.6 ± 0.2	-9.1
Peptide A3G13G	1476 ± 24	4.2 ± 0.2	-13.7 ± 0.3	-19.3
Peptide A3G14G	1241 ± 39	3.2 ± 0.2	-18.7 ± 0.8	-36.6
Peptide A13G14G	1130 ± 37	2.9 ± 0.2	-17.9 ± 0.8	-34.0
Peptide A3G13G14G	994 ± 50	2.4 ± 0.2	-26.6 ± 1.5	-61.1

Nanoparticle induced folding and fibril formation of coiled coil based model peptides

*Sara C. Wagner, Meike Roskamp, Manjula Pallerla, Raheleh Rezaei Araghi, Sabine Schlecht[§], Beate Koksch**

Supporting informations. Materials and Methods.

Peptide Synthesis and and purification. The peptides were synthesized on an automated Syro XP synthesizer (MultiSynTech GmbH, Witten, Germany) using a standard fluorenyl-methoxycarbonyl (Fmoc) chemistry protocol with Fmoc-Leu-OWang resin (0.65 mmolg⁻¹). For concentration determination, the peptides were N-terminally labelled with anthranilic acid (Abz) that has an absorption maximum at 320 nm. The peptides were cleaved from the resin with 95% (w/v) trifluoroacetic acid, 4% (w/v) triisopropylsilane and 1% (w/v) water. The crude peptides were purified by reversed phase HPLC by using a Knauer Smartline manager 5000 system (Knauer GmbH, Berlin, Germany) equipped with a C8(2) (10 µm) Phenomenex® LunaTM column (Phenomenex Inc., Torrance, CA, USA). The Peptides were eluted with a linear gradient of water/acetonitrile/0.1% trifluoroacetic acid and identified by ESI-ToF MS. All MS analysis were performed by using an Agilent 6210 ESI-ToF LC-MS spectrometer (Agilent Technologies Inc., Santa Clara, CA, USA) with direct infusion from a Harvard Apparatus 11 Plus syringe pump (Harvard Apparatus, Holliston, MA, USA). Peptide purity was determined by analytical HPLC by using a Merck LaChrom Elite system (Merck kGaA, Darmstadt, Germany) equipped with a C8(2) (10 µm) Phenomenex® LUNATM column (Phenomenex Inc., Torrance, CA, USA). The applied gradients were similar to those of preparative HPLC.

Sample preparation. The pure peptides were dissolved in freshly prepared and filtered Tris/HCl buffer (10 mM, pH 7.4). The peptide concentration was determined by measuring the absorbance at $\lambda=320$ nm by using a Varian Cary 50 photometer (Varian Medical Systems, Palo Alto, CA, USA) and PMMA cuvettes (1.5 mL, Plastibrand®, VWR, International GmbH, Darmstad, Germany). As a reference, a calibration curve using Abz-Glycine (Bachem GmbH, Weil am Rhein, Germany) in the appropriated buffer at different concentrations was recorded. Fibrils in presence of nanoparticles were formed by incubation at a fixed temperature of 25°C under stationary conditions.

Au/MUA nanoparticle synthesis. Au nanoparticles were synthesized according to a procedure published by Stucky et al. (J. Am. Chem. Soc. 2006, 128, 6550-6551). 0.435 g of tert-butylamin-borane complex was added to a solution of 0.247 g AuPPh₃Cl (0.5 mmol, 1 eq) and 0.25 mL dodecanethiole (1.0 mmol, 2 eq) in 40 mL benzene. The mixture was stirred at 55 °C for 1 hour before cooling to room temperature. Then 40 mL of ethanol were added and the precipitant separated by centrifugation. The black solid powder was washed with an excess of ethanol, dried under vacuum, and resolved in 25 mL of chloroform. 30.6 mg mercaptoundecane sulphonic acid (0.1 mmol) were solved in a solution of 8 mL triple-distilled water and 50 μ L tetramethylammonium hydroxide (TMAH, 25 wt-% in methanol). 3 mL of a 0.33 μ M solution of dodecanethiole-protected gold nanoparticles was added and the mixture stirred at room temperature for 6 hours, which led to a complete phase transfer of the colloids from the organic into the water phase. The organic phase was removed and in order to remove the ligand's excess the colloid solution was dialysed against 300 mL triple-distilled water three times. The further transfer of the colloids into 10 mM Tris/HCl buffer (pH 7.4) was done by dialysis for three times.

By TEM measurements, the average diameter of gold core of nanoparticles can be estimated to be 5.3 ± 0.5 nm by counting at least 300 particles. By taking into consideration the size of this ligand shell, an overall diameter of approximately 6 nm can be calculated for one nanoparticle.

CD Spectroscopy. CD spectra were recorded on a J-810 spectrophotometer (Jasco GmbH, Gross-Umstadt, Germany) using a quartz cuvette of 1-mm path length at 20 °C. The spectra were taken as the average of 3 scans by collecting data from 240 to 190 nm at 0.5 nm intervals, a 2 nm bandwidth, and 2s response time. All CD spectra were corrected by the buffer spectra and converted into mean residue ellipticity $[\theta]$ according to the following equation

$$[\theta] = \frac{\theta_{obs}}{10000 \cdot l \cdot c \cdot n}$$

using the Origin Software (version 7.0, Microcal, USA).

Transmission electron microscopy. 6 μ L aliquots of the corresponding solution were placed for 60 s on glow-discharged (60 s plasma treatment at 8 W in a BALTEC MED 020) carbon-coated collodium support films covering 400-mesh copper grids (BALTEC, Lichtenstein). After blotting and negative staining with phosphotungstic acid (PTA, 1%) the grids were left to air-dry. TEM images were recorded with a Philips CM12 transmission electron microscope (FEI company, Oregon, USA) at 100 kV accelerating voltage and at primary magnification 58000x on Kodak SO-163 negative film by using a defocus of -900 nm.

Image J (version 1.38x, Wayne Rasband, USA) was used for the determination of the diameter of peptide fibers and the size of the gold core of nanoparticles. The standard deviation of the average diameter was calculated using the Origin Software (version 7.0,

Microcal, USA). Moreover, Image J was also used to calculate the Fourier-Transformation of the electron microscopy images. By means of the Fourier-Transformation, the diameter of protofilaments was calculated by using the following equation:

$$d[m] = \frac{x \cdot res}{r(FFT) \cdot M},$$

where x is the overall size of the square sector out of the TEM image in pixel (here selected to be 1024 pi), res is the resolution obtained by the scanning process of the TEM negative (2.54 cm divided by 1200 pi), M is the magnification and r(FFT) is the length [pi] measured in the Fourier-Transformation image. The measured and calculated distances in Figure X correspond to 52 pi (7.147 nm) and 103 pi (3.6 nm).

Agarose gel electrophoresis. Gel electrophoresis was performed at room temperature with a Gel XL Ultra V-2 Electrophoresis System (Labnet International, Windsor, Great Britain) in a 1 % agarose gel in Tris/HCl buffer (0.05 M, pH 7.4). The output voltage was held constant at 100 V. Electrophoresis was stopped when the bands began to broaden (after approximately 10 – 15 minutes).

Isothermal titration calorimetry. ITC measurements were carried out at 30°C on a VP-ITC MicroCal instrument (MicroCal, LLC, Northampton, MA). The solutions of gold nanoparticles and peptides were prepared in 10 mM Tris/HCl buffer at pH 7.4, and both solutions were degassed for 15 min before each titration. For peptide A and its glycine derivatives, 8 µL of the peptide solution (100-200 µM; exact peptide concentration was determined by UV/Vis spectroscopy) was injected 30 times into a nanoparticle solution (5 nM) over a period of 16 s with an adequate interval of 200 s between injections to allow complete equilibration.

For peptide B, the titration was carried out by injecting 12 μL of 130 μM peptide B into a 17 nM gold nanoparticle solution over a period of 22 s with a temporal separation of 300 s.

For all measurements, a background correction was done to account for heat of dilution by subtracting the data of the peptide injected into buffer from the data points obtained by titrating peptide into the nanoparticle solution.

Supporting informations. Additional figures.

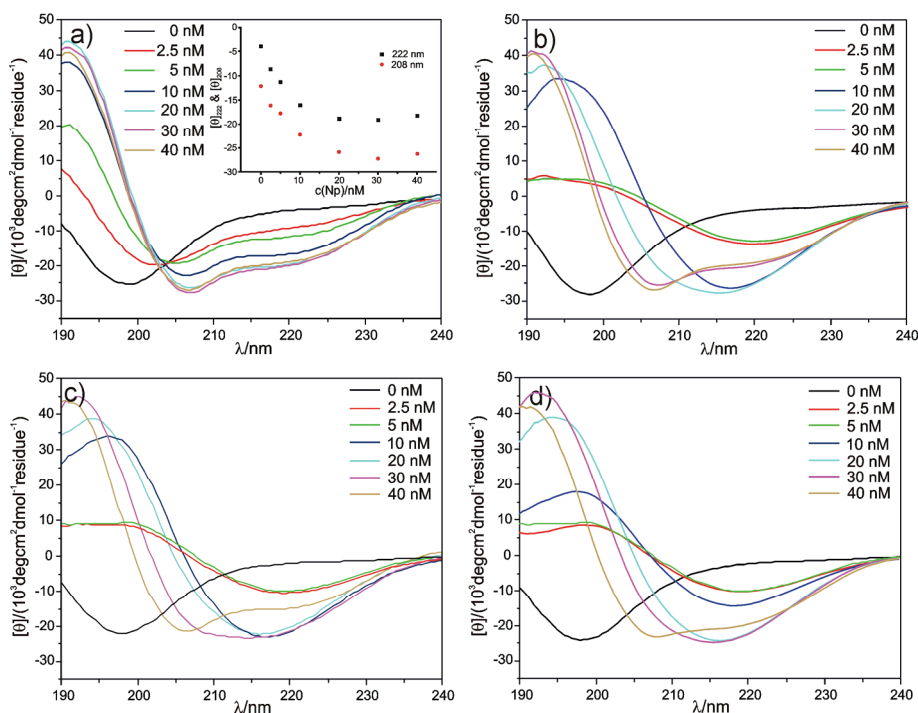


Figure S1. CD spectra of 50 μM peptide A at pH 7.4 in presence of different nanoparticle concentrations. The spectra are shown for an incubation time of (a) five minutes, (b) one day, (c) one week, and (d) three weeks. Inset: Molar ellipticity at 208 and 222 nm plotted against nanoparticle concentration.

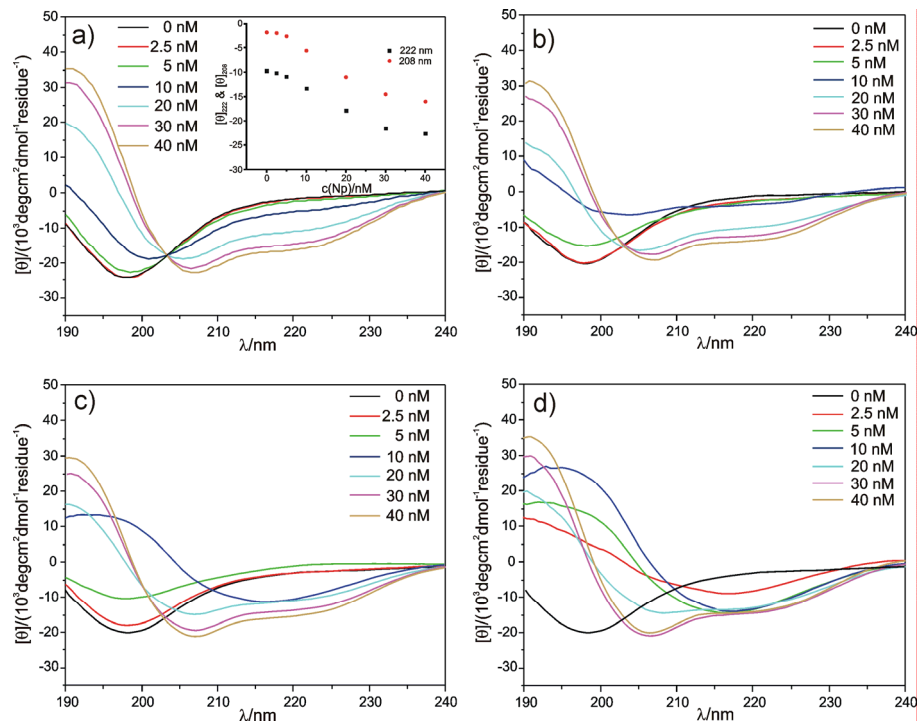


Figure S2. CD spectra of 50 μM peptide B at pH 7.4 in presence of different nanoparticle concentrations. The spectra are shown for an incubation time of (a) five minutes, (b) one week, (c) two weeks, and (d) four weeks. Inset: Molar ellipticity at 208 and 222 nm plotted against nanoparticle concentration.

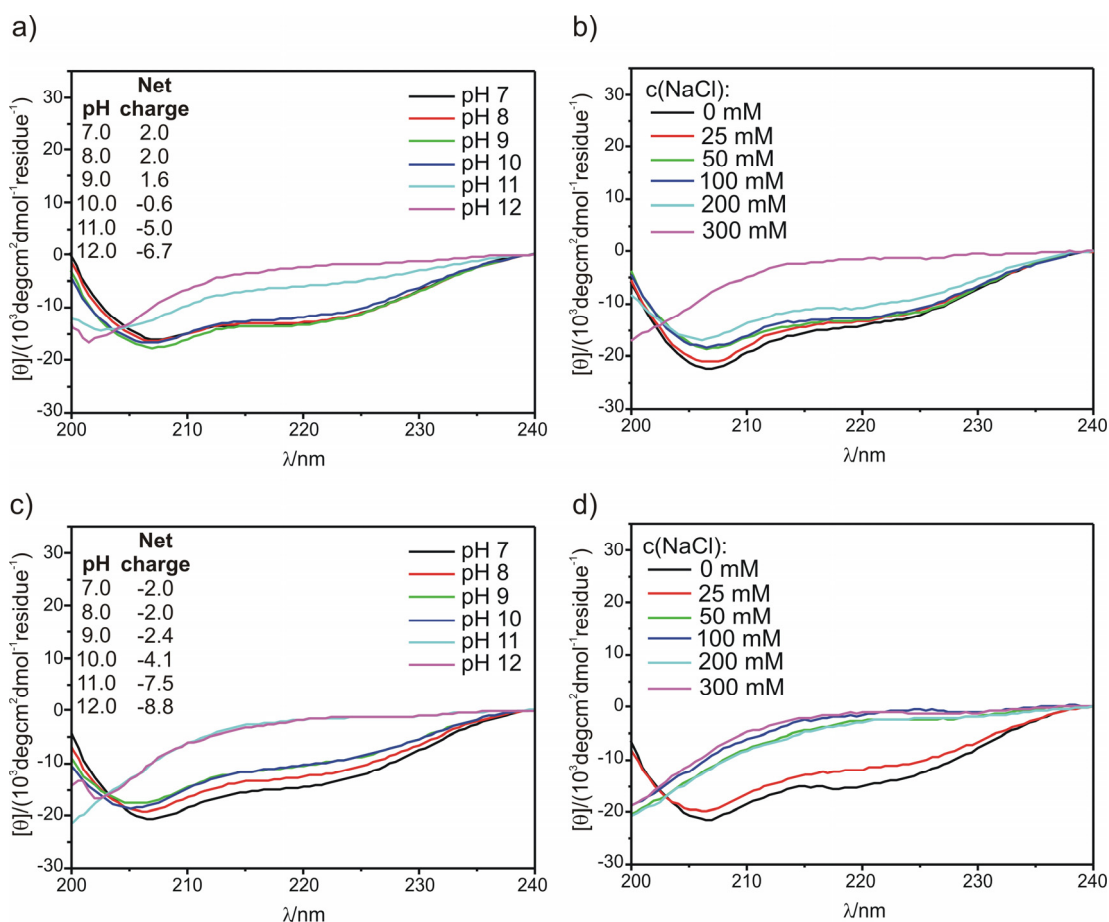


Figure S3. pH Dependent CD spectra of 50 μM (a) peptide A and (c) peptide B in presence of 40 nM gold nanoparticles (inset: pH dependency of the calculated peptide's net charge); CD spectra of 20 μM (b) peptide A and (d) peptide B in presence of 20 nM gold nanoparticles at pH 7.4 and different concentrations of NaCl.

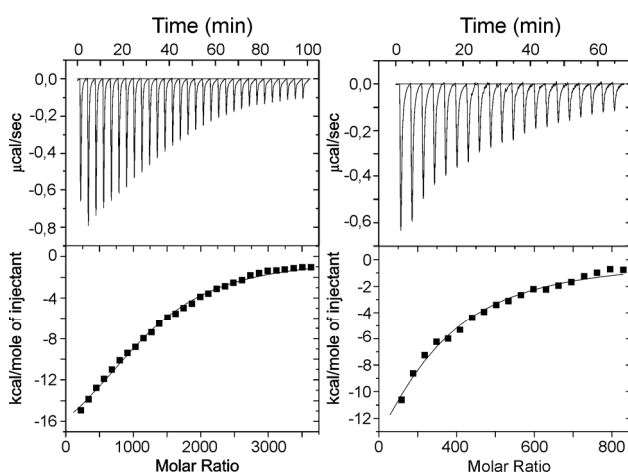


Figure S4. Isothermal titration calorimetry data at 30°C from titration of peptide A (left) and peptide B (right) into a solution of gold nanoparticle. For peptide A, the peptide's and the nanoparticle's concentration corresponded 250 μM and 15 nM, respectively. In case of peptide B, 25 nM of colloids were titrated with 200 μM of peptide. The top panel shows the raw data which is integrated as the kcal of heat

released/mol of injectant. The black line shows the fitted curve assuming a one-set of binding sites mode.

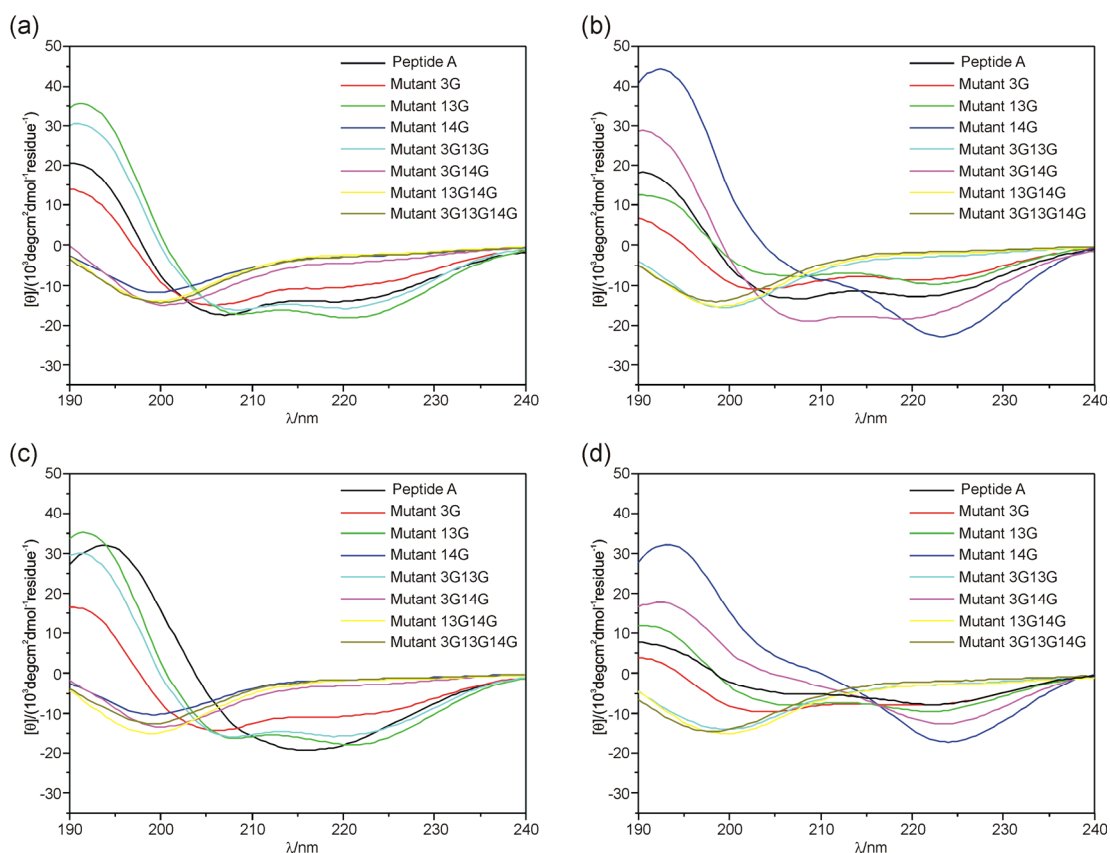


Figure S5. CD spectra of 600 μM of peptide A and its glycine derivatives shown for an incubation time of 30 minutes (a, b) and two weeks (c, d). The samples were studied not only at pH 7.4 (b, d) but also at pH 4.0 (a, c) in order to cover conditions where β -sheet formation of peptide A occurs.

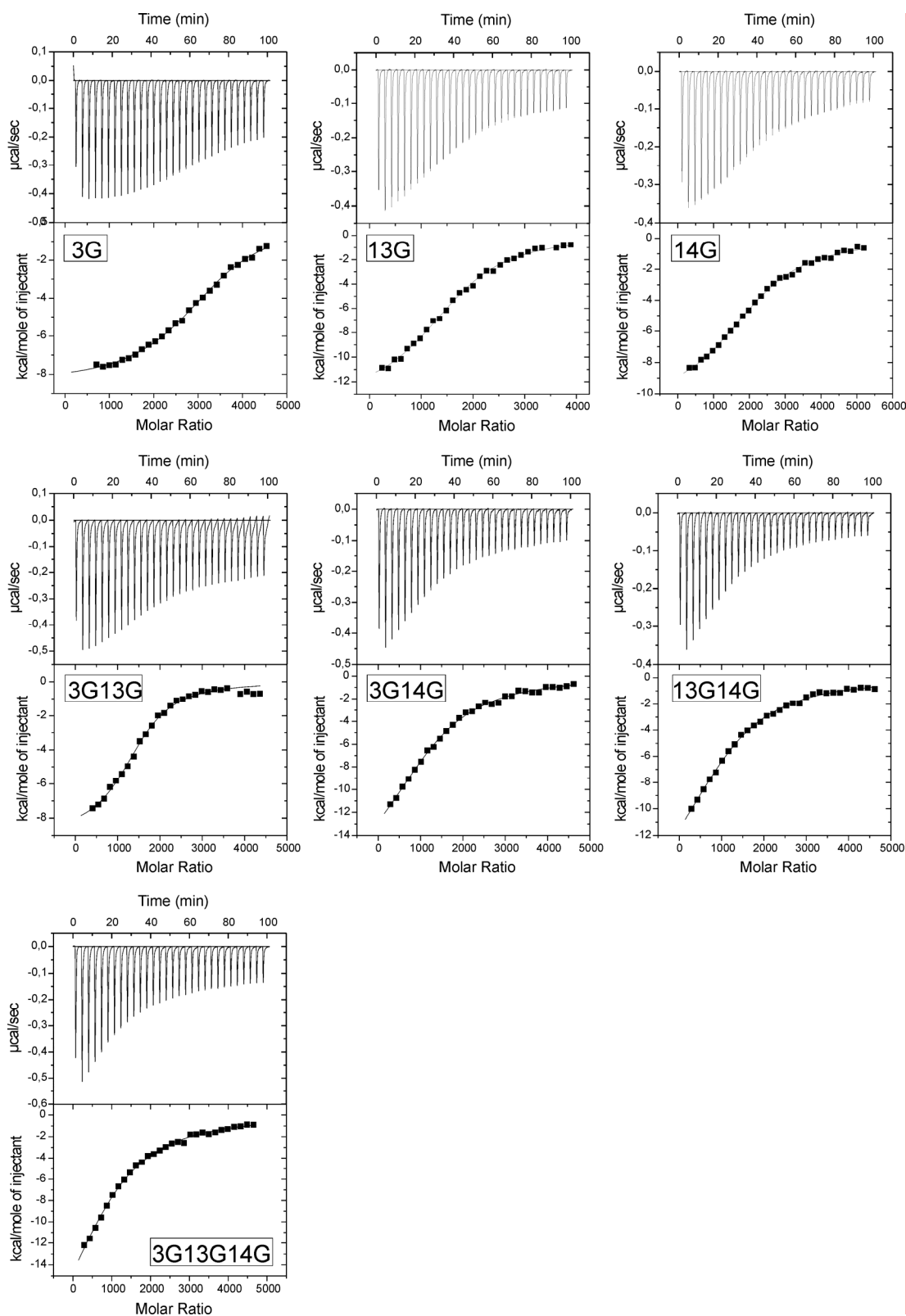


Figure S6. ITC enthalpograms when 5 nM gold nanoparticles were titrated with the glycine derivatives of peptide A (concentration ranging from 100-150 μ M). The exact peptide concentration was determined by UV/Vis spectroscopy before starting the titration.

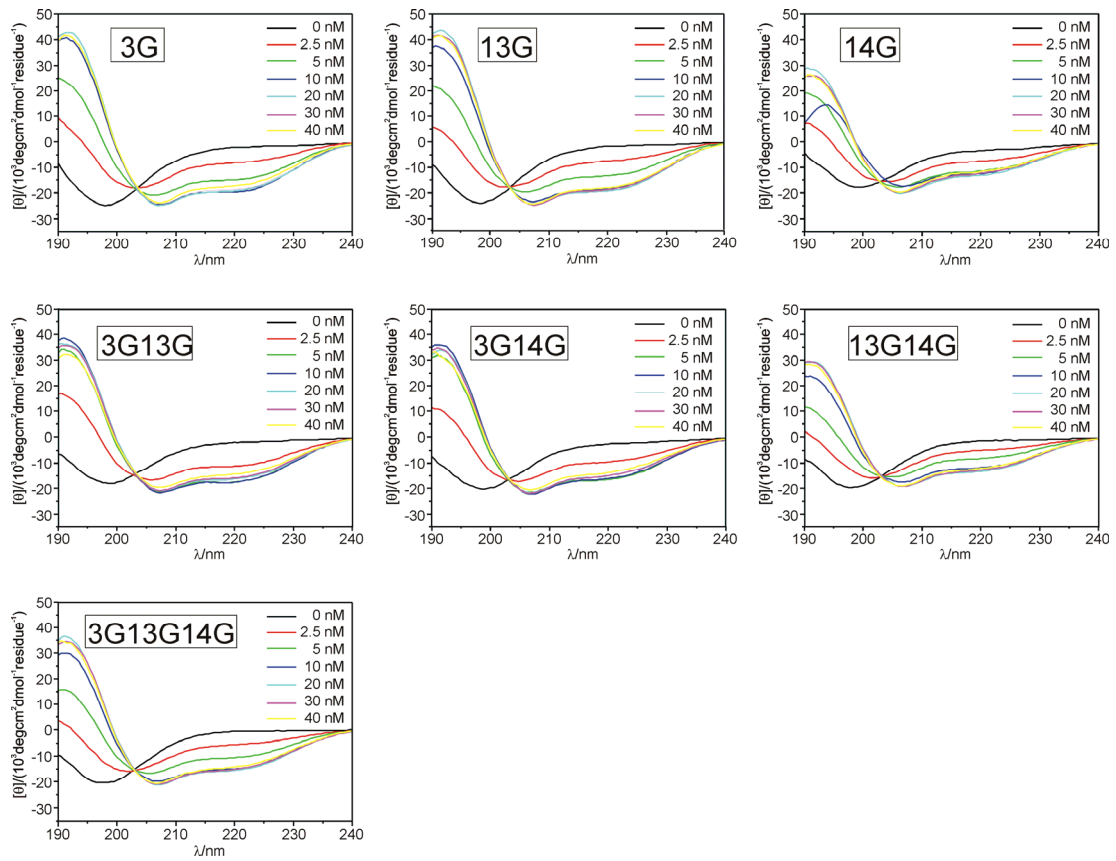


Figure S7. CD spectra of 50 μM of glycine derivatives of peptide A at pH 7.4 and in presence of different nanoparticle concentrations. The samples were incubated for 5 minutes.

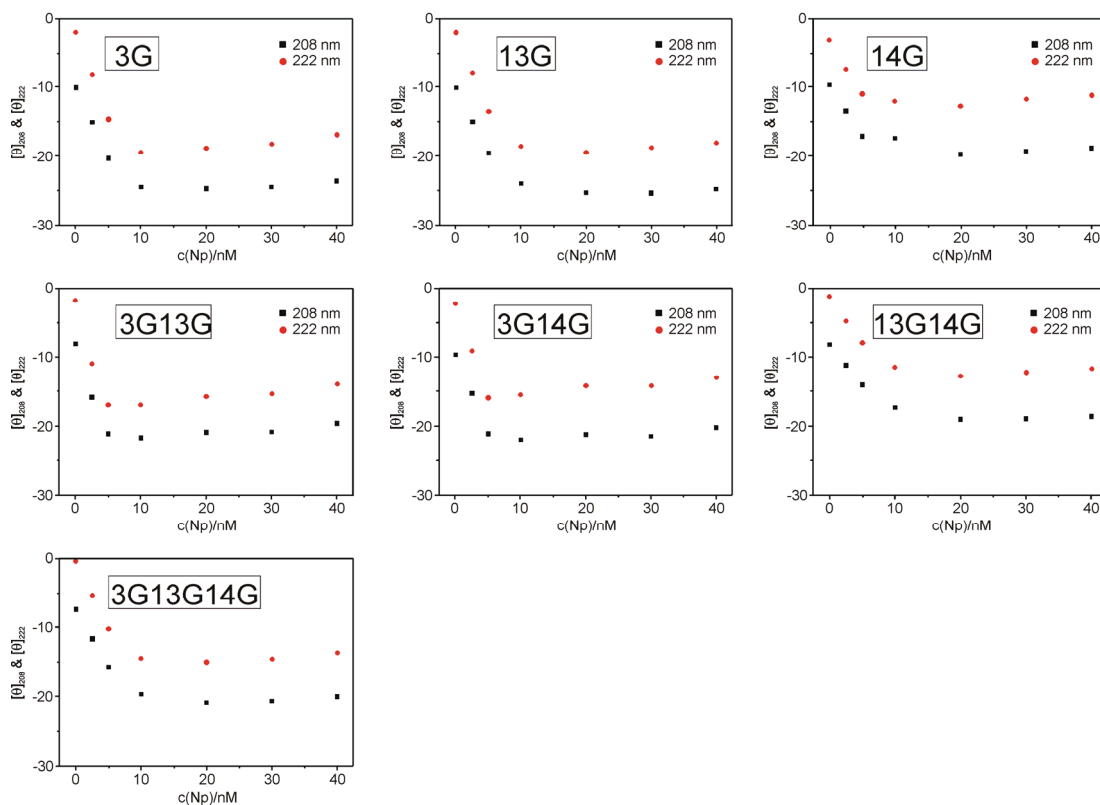


Figure S8. Plot of molar ellipticity at 208 and 222 nm of glycine modified derivatives of peptide A against nanoparticle concentration. The corresponding intensity values were taken from the CD spectra shown in Figure S7.

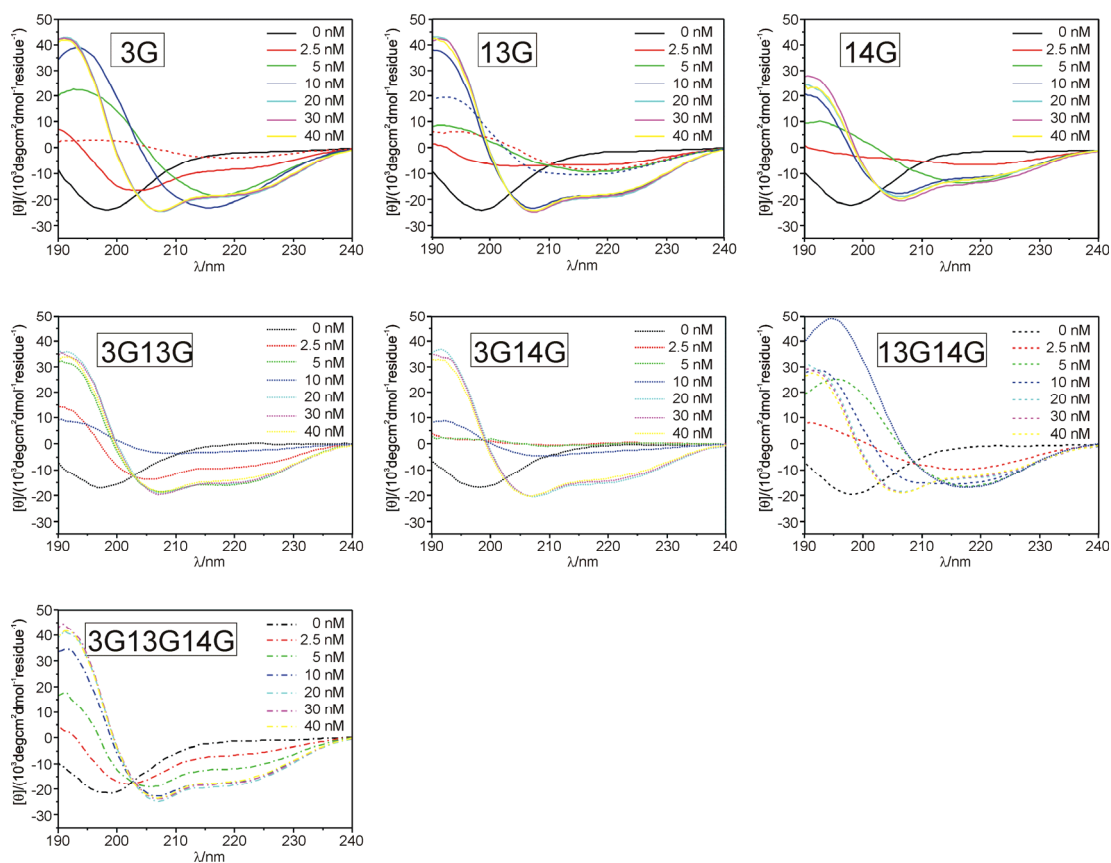


Figure S9. CD spectra of 50 μM of glycine derivatives of peptide A at pH 7.4 and in presence of different nanoparticle concentrations. The presented spectra correspond to an incubation time of 24 hours (solid line), one week (dashed line), two weeks (dotted line) and four weeks (dashed and dotted line shown for 3G13G14).

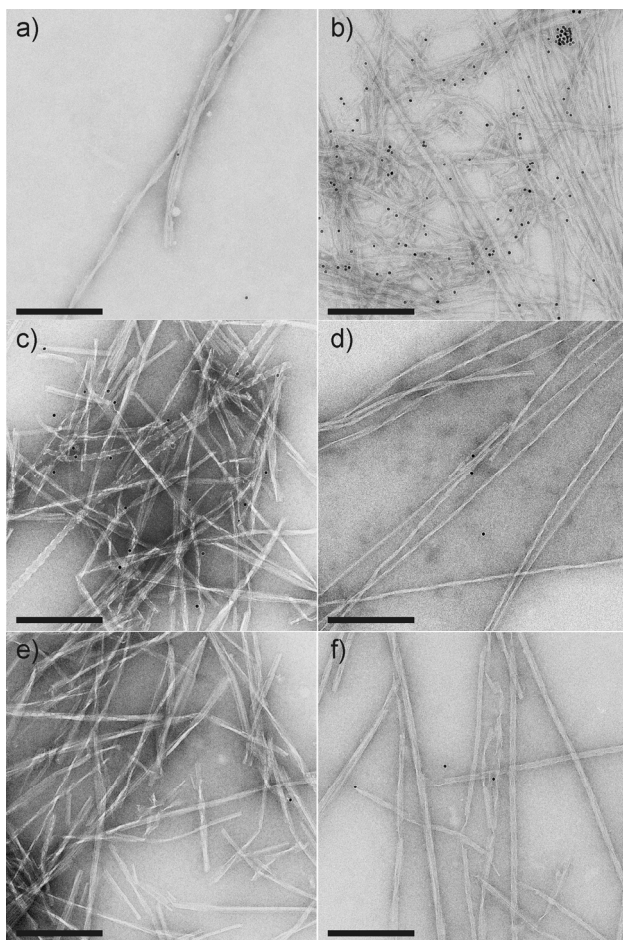


Figure S10. TEM micrographs taken from samples of 50 μM (a) mutant 3G and 30 nM nanoparticles, (b) mutant 13G and 2.5 nM nanoparticles, (c) mutant 14G and 5 nM nanoparticles, (d) mutant 3G13G and 5 nM nanoparticles, (e) mutant 3G14G and 5 nM nanoparticles, and (f) mutant 13G14G and 5 nM nanoparticles. Scale bars: 200 nm.

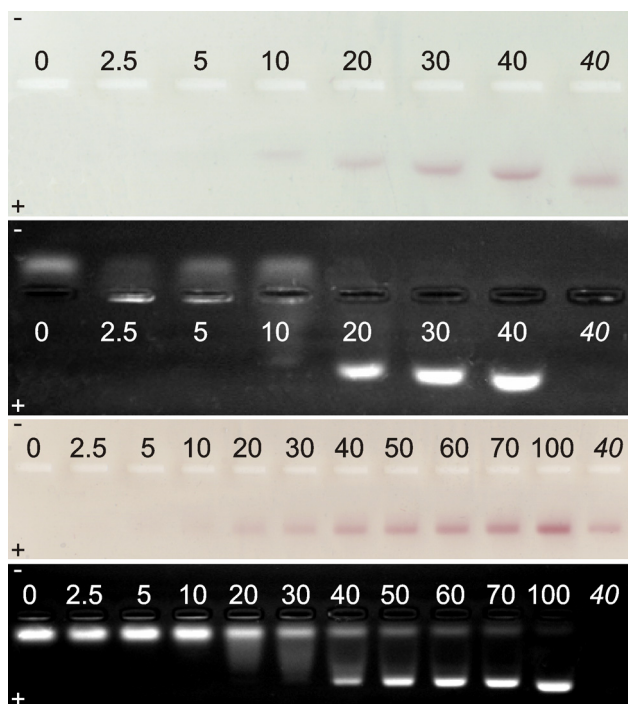
Determination of binding stoichiometry by gel electrophoresis

Figure S11. Agarose gels of 50 μM peptide A (a, b) and 50 μM peptide B (c, d) at pH 7.4 at different nanoparticle concentrations. The gels were visualized by (a, c) visible light and (b, d) fluorescence emission following excitation at 314 nm. The numbers refer to the nanoparticle concentration in nM; italic numbers refer to reference samples containing nanoparticles without peptide.

Gel electrophoresis was further conducted to confirm a binding and the stoichiometry of peptides to nanoparticle found by ITC measurements. While the position of nanoparticles can be easily determined by visible light, the visualization of peptide is reached by fluorescence emission following excitation at 314 nm, corresponding to the absorption wavelength of the peptide's UV-label. Peptide A alone shows a well-defined low-mobility band that points to a positive net charge and seems not to be significantly changed at very low concentrations of nanoparticles (Figure S11). Upon increasing the concentration of gold nanoparticles from 10 to 20 nM, an impressive change of direction of peptide A becomes obvious that indicates an excess of nanoparticle to peptide and corresponds to a range of 5000 to 2500 peptides per nanoparticle. Since the accuracy of this method depends on the absorption of both components and underlies a

certain detection limit that is approximately 30 μM in case of the UV-label of peptide, this method yields only a very rough stoichiometry and was carried out to support differences in binding stoichiometries found for both peptides by ITC. Since ITC measurements yield a saturation of one nanoparticle with 1202 ± 38 peptides, it is possible that still an amount of unbound peptide is present at a nanoparticle concentration of 20 nM but cannot be detected because of its low absorbance. In contrast, peptide B shows a separation of nanoparticle-bound peptide from the excess at higher nanoparticle concentrations compared to peptide A. Only at a nanoparticle concentration of 100 nM, an almost complete binding of peptide to nanoparticle seems to be obvious which presents a stoichiometry of 500 peptides per nanoparticle. ITC measurements yield a stoichiometry of 238 ± 63 peptides per nanoparticle. For that reason, this discrepancy can be explained by the accuracy of this method as mentioned above for peptide A.

10.5 Further modifications in VW19 (unpublished results)

In the above-mentioned publication, one aim was to show that β -sheet inducing elements are required in the peptide sequence to enable a nanoparticle-induced fibril formation. Therefore, three valine residues were systematically replaced in the peptide sequence with glycine in order to decrease the overall β -sheet propensity of peptide. Due to its lacking a side chain, glycine may thereby change the intrinsic features of the peptide chain by allowing a high conformational flexibility. With regard to the results mentioned in the manuscript, introduction of glycine had a strong impact on the binding properties such as the binding stoichiometry. Depending on the grade of substitution, the glycine derivatives displayed higher binding stoichiometries than the parent peptide, although the net charge of peptide was not changed upon the substitution and the general binding of peptide to nanoparticle is expected to be based on electrostatic interactions. Apparently, the higher conformational flexibility of the altered peptide chain allows a higher number of peptide molecules to arrange around one nanoparticle. Regarding the changed binding parameters upon the substitution with glycine, the question remained whether a more applicable residue can be found. Additional investigations were carried out using alanine instead of glycine. According to a classification of the 20 naturally occurring amino acids published by P. Y. Chou and G. D. Fasman, alanine and valine are designated with a conformational parameter $P\beta$ of 0.97 and 1.65 (Table 10.1). At the same time, alanine goes along with a higher conformational parameter for helical folding compared to valine, since alanine and valine are assigned with $P\alpha$ values of 1.45 and 1.14, respectively.

In literature, alanine-scanning mutagenesis, a method of systematic alanine substitution, has been extensively used for the identification of functional epitopes in proteins.¹²⁴ The rationale behind alanine-scanning is that all interactions of a side chain except for the $C\beta$ are eliminated.¹²⁵ The contribution of the deleted groups relative to the methyl moiety of alanine is assessed from the difference between the properties of the wild-type relative to the alanine mutant.

Table 10.2. Derivatives of VW19 obtained by substitutions of valine residues against alanine.

VW19	H ₂ N-LKVELKELKKELVVLKSELKELKKEL-CO ₂ H
VW19 A13	H ₂ N-LKVELKELKKELAVLKSELKELKKEL-CO ₂ H
VW19 A14	H ₂ N-LKVELKELKKELVALKSELKELKKEL-CO ₂ H
VW19 A13A14	H ₂ N-LKVELKELKKELAALKSELKELKKEL-CO ₂ H

According to Table 10.2, three alanine variants were investigated. Monosubstitutions were carried out at positions 13 and 14, since especially the center of peptide sequence should determine the overall folding of peptide. An introduction of alanine at position 3 was expected to have a smaller impact on the overall folding compared to the other monosubstitutions and therefore, was not included in the preliminary studies discussed here. Furthermore, the disubstituted VW19 variant with two adjacent alanine residues was included in the investigations. According to statistical studies of Chou and Fasman, the arrangement of at least four strong helix formers, as present in the motif LAAL, may act as a nucleus for the overall α -helical folding of peptide.¹²³ As revealed by CD spectroscopic measurements, the alanine substitutions selected here are sufficient to increase the overall α -helicity of peptide in comparison with the parent peptide (Figure 10.2). As expected, the disubstituted derivative displayed a higher amount of helicity compared to the other peptides. In light of these results, the introduction of alanine obviously changed the initial state of folding by introducing α -helicity and oligomerization upon the coiled coil formation and, thus, did not turn out to be a suitable alternative to the application of glycine in order to study the impact of β -sheet inducing elements.

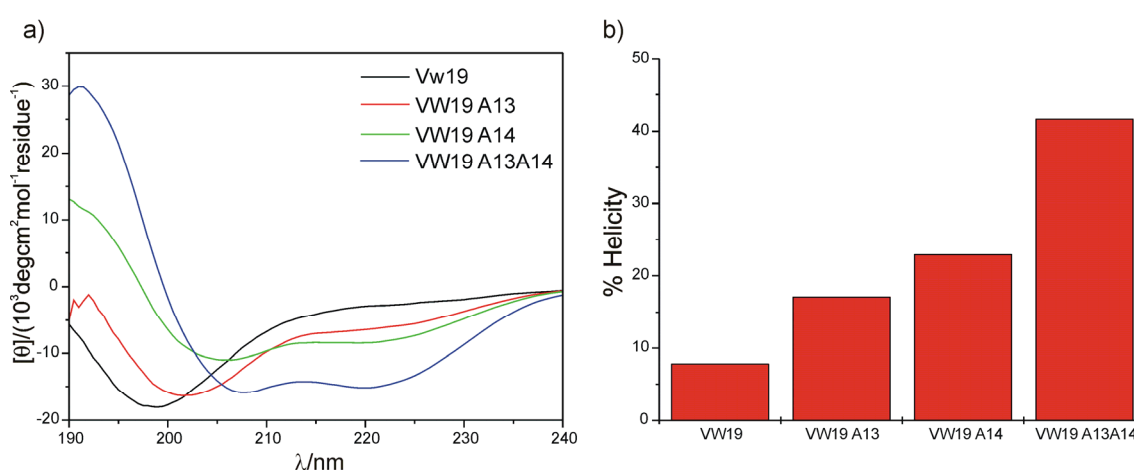


Figure 10.2. a) CD spectra of the parent peptide VW19 and its alanine derivatives. The spectra are shown for a peptide concentration of 50 μM at pH 7.4 and an incubation time of 30 minutes. b) % of α -helicity of VW19 and its alanine derivatives calculated from the CD spectra according to a method of Chen et al.¹²⁶

11 Summary and Conclusions

The combination of coiled coil peptides and functionalized gold nanoparticles chosen here was used to gain information on different aspects of the interaction between protein and nanoparticle.

The first objective was to investigate the impact of coiled coil peptides on the organization of nanoparticles. It was found that 26 amino acid peptides are efficient tools to mediate aggregation of nanoparticles. Furthermore, the system of peptide and nanoparticle reported here is based on electrostatic interactions. As shown in studies on VW05, this particular kind of interaction enables the nanoparticle assembly to be controlled simply by means of pH conditions referring to the peptide's net charge. In the case of VW05, a pH of 12 seems to prevent an electrostatically attractive interaction; here, no peptide-induced aggregation occurred. Remarkably, cyclic changes of pH were applied to direct the nanoparticle assembly in a reversible and repeatable manner. Nevertheless, the coiled coil folding motif, which is trimeric, does not dictate the intrinsic geometry of the nanoparticle arrangement. According to TEM measurements, the addition of the coiled coil peptide VW05 resulted in the formation of three-dimensional, densely packed nanoparticle architectures, in which no well-defined geometrical order could be clearly resolved. Occasionally, two dimensional areas could be detected within the aggregates that showed a hexameric rather than trimeric structure. This hexameric arrangement may be explained by the underlying principles of crystal formation, where the size ratio between anion and cation determines the overall packing geometries. Further modifications on the design of VW05 by either reducing the charge of peptide or extending the length of peptide were not sufficient to prevent the predominant formation of such three-dimensional structures.

Altogether, the results obtained here contribute essentially to the general knowledge on developing de novo design of peptides for bionanostructures. In agreement with examples in the literature, the direct transmission of the geometry of protein folding motif to the nanoparticle architectures has proven to be quite challenging and was not achieved in this study. Moreover, the peptide-mediated nanoparticle assembly also turned out to be very rapid and difficult to control. Further studies by Dipl.-Chem. Meike Roskamp upon variation of the growing conditions with reduced peptide concentrations, pH titrations, or temperature changes did not change the overall morphology of nanoparticle structures in the presence of VW05.¹²⁷ Cryo-TEM measurements also demonstrated that VW05 itself partially undergoes an aggregation upon binding to the particle; a side effect that, in addition to the lacking order, makes this system unsuitable for traditional applications in materials science. The system

presented here seems to provide better access to pH responsive bionanomaterials with, for instance, possible detection applications.

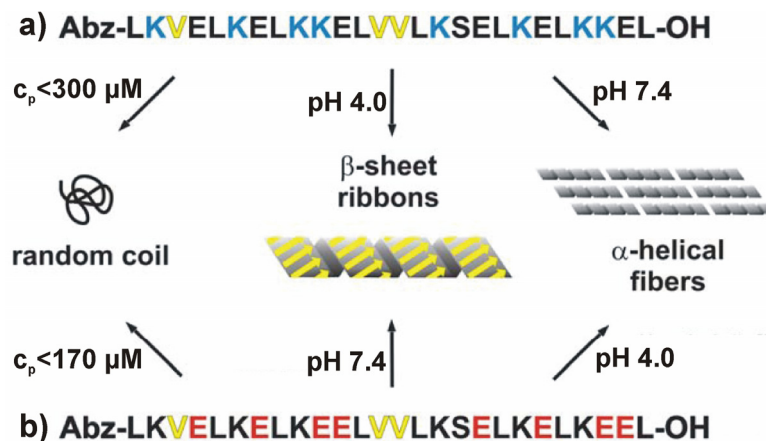


Figure 11.1. Scheme summarizing the pH and concentration dependent folding behaviour of a) peptide A and b) peptide B. Only peptide concentrations above a certain limit enable an adoption of defined conformation such as α -helical or β -sheet structures. Otherwise, the peptides occur unfolded regardless of pH.

While the results in the first part showed that coiled coil peptides were able to induce nanoparticle assembly, the second part of this thesis took the aggregation of VW05 as a starting point and concentrated more deeply on the impact of particle on the assembly state of peptide. More precisely, the formation of β -sheet structures with subsequent aggregation into fibrillar structures was studied. In preliminary studies, coiled coil based model peptides were therefore invented that are able to mimic the protein misfolding occurring in neurodegenerative diseases depending on the pH conditions. A schematic overview of these different folding preferences is given in Figure 11.1. These peptides were then applied to electrostatic binding to charged gold nanoparticles at pH 7.4. A critical evaluation of their different aggregation tendencies in the presence of nanoparticles revealed that the binding stoichiometry apparently plays a major role in triggering the surface-assisted self-assembly of peptide. Namely, a strong nanoparticle-assisted aggregation tendency was found for a coiled coil peptide with a very high binding stoichiometry that alone does not show any β -sheet tendency at physiological pH. Obviously, the binding to the nanoparticle generates an extraordinarily high local peptide concentration that may transcend the general peptide concentration in solution to a much larger degree. As a consequence, the general amyloid formation tendency of the peptide alone is weaker than with nanoparticles, since peptide solutions can be only prepared for concentrations up to their solubility

limit. The fact that amyloid formation is not restricted to the specific proteins associated with clinical disorders, but seems to be a generic feature of polypeptide chains in a regime of high peptide concentration has already been stated and proven in literature.¹²⁸ Nevertheless, studies performed in this thesis have disclosed that the binding capacity of the nanoparticles employed here is not sufficient to force any peptide regardless of its secondary structure features into amyloid-like structures. Substitutions of β -sheet preferring valine residues in one of the two peptide sequences against glycine confirmed that β -sheet inducing elements are still required. Unexpectedly, in some cases, these substitutions altered the binding parameters to the nanoparticle. Not each glycine derivative with its aggregation behavior is directly comparable to the parent peptide, which gives reason for further substitution studies in future.

With regard to safe medical applications, a profound knowledge about the biological effects of nanoparticles is of paramount interest. Current studies in literature are only addressing the impact of nanoparticles on protein misfolding in case-by-case studies. Even the same kind of nanoparticle may yield diverse effects for different proteins. As found by Linse and co-workers, copolymer nanoparticles are able to trigger aggregation of the β_2 -microglobulin protein¹²⁹ whereas, in the case of the A β peptide, an inhibition of amyloid formation was found.¹³⁰ These and other results indicate that especially the primary structure and its intrinsic features have a decisive effect upon protein folding in the presence of nanoparticle. The study described here is the first approach to apply model peptides to this issue and allows the conclusion of more general principles on such things as the influence of conformation preferences and binding stoichiometry, here determined by the net charge of peptide. These results are the first step towards the development of model peptide based future evaluation systems to systematically estimate the biological risks of nanoparticles.

12 Outlook

The results obtained in the first part of this thesis demonstrated the potential of coiled coil peptides for the pH tunable assembly of anionic gold nanoparticles. At the same time, the system of peptide and nanoparticle reported here has several drawbacks, such as its lacking an ordered symmetry, a rapid and hardly controllable aggregation, and the unwanted nanoparticle-assisted assembly of the peptide itself. The latter is caused by the extremely high surface-to-volume ratio of nanoparticle whose size was chosen here to be about 6 nm. A reduction of the size of nanoparticle should therefore constrain or even prevent this phenomenon. However, the repetition of the binding assays with smaller nanoparticles would not only be interesting from this side of view. As mentioned in the previous chapter, electrostatic interactions resulted rapidly in the formation of assemblies whose internal structure appeared to follow the packing rules of crystal formation rather than to have been determined by the intrinsic symmetry of the coiled coil structure. As shown in Table 8.2, an overall diameter of gold nanoparticle between 1.8 and 4.3 nm should provoke a tetragonal arrangement of particles in two dimensions in the case of coiled coil trimers. Results obtained by nanoparticles in this size range would shed more light on the principles underlying the structuring of nanoparticles with peptides.

In future studies, a covalent attachment of nanoparticle to peptide should be also envisaged. For instance, a modification of the solvent exposed face of each peptide strand with nanoparticles allows the nanoparticles to be arranged by the oligomerization state of α -helices. In addition, this covalent approach may be also used to regularly arrange nanoparticles on the surface of peptide fibers provided that the involved peptide displays a strong fibril formation propensity.

In the second part of this thesis, a system of coiled coil peptide and nanoparticle was successfully developed to mimic nanoparticle-assisted amyloid formation as found for naturally occurring proteins associated with neurodegenerative diseases. Regarding the above-mentioned substitution studies, the introduction of glycine instead of valine caused altered binding parameters in some cases. Moreover, additional substitutions with alanine turned out to be even less suitable than glycine for the reduction of β -sheet propensity due to a changed initial conformation of peptide. Altogether, the substitutions applied here have led to more general principles on nanoparticle-induced misfolding and to a way to further modifications subtly tuning the β -sheet propensity of peptide. Nevertheless, in the future, the system of model peptide and

nanoparticle presented here may be used to gain more information about the impact of nanoparticles on protein folding and aggregation. The number of peptide layers around one particle may be experimentally determined by combining Small-Angle X-ray (SAXS) scattering and dynamic light scattering (DLS) measurements. SAXS could be used to determine size of the gold core of nanoparticles.¹³¹ DLS measurements would yield information about the hydrodynamic radius of the particle with and without the additional peptidic shell. These results would then illustrate the extent to which local enrichment of peptide assists the nucleation step in the amyloid formation process. Additional studies with a stepwise reduction of the nanoparticle charge would further demonstrate the general influence of the binding stoichiometry. In this work, it has been shown that the binding stoichiometry directs the protein folding in presence of nanoparticle using only two model peptides and seven derivatives of one of both peptides. Importantly, other kinds of interactions such as van-der-Waals forces between peptide and nanoparticle, should be also investigated in the future studies. This would be achieved by the employment of, for instance, copolymer nanoparticles. Based on this knowledge, the coiled coil based testing system developed here may then be extended to a variety of nanoparticles with potential applications in medicine.

13 Literature

1. R. P. Feynman in *Minituarization* (Ed.: H. D. Gilbert), Reinhold, New York, 1961, pp. 282-296.
2. C. M. Niemeyer, *Angew. Chem. Int. Ed.* **2001**, *40*, 4128-4158.
3. A. N. Shipway, E. Katz, I. Willner, *ChemPhysChem* **2000**, *1*, 18-52.
4. I. Brigger, C. Dubernet, P. Couvreur, *Adv. Drug Delivery Rev.* **2002**, *54*, 631-651.
5. D. L. Feldheim, C. A. Foss Jr. in *Metal Nanoparticles: Synthesis, Characterization, and Application*, Marcel Dekker, New York, 2002.
6. N. Zheng, J. Fan, G. D. Stucky, *J. Am. Chem. Soc.* **2006**, *128*, 6550-6551.
7. C. M. Niemeyer, *Angew. Chem. Int. Ed.* **2003**, *42*, 5796-5800.
8. C. M. Niemeyer, *Angew. Chem. Int. Ed.* **2001**, *40*, 4128-4158.
9. T. J. Harris, G. v. Maltzahn, A. M. Derfus, E. Ruoslahti, S. N. Bhatia, *Angew. Chem. Int. Ed.* **2006**, *45*, 3161-3165.
10. G. v. Maltzahn, T. J. Harris, J.-H. Park, D.-H. Min, A. J. Schmidt, M. J. Sailor, S. N. Bhatia, *J. Am. Chem. Soc.* **2007**, *129*, 6064-6065.
11. W. Shenton, S. A. Davis, S. Mann, *Adv. Mater.* **1999**, *11*, 449-452.
12. S. R. Whaley, D. S. English, E. L. Hu, P. F. Barbara, A. M. Belcher, *Nature* **2000**, *405*, 665-666.
13. E. Katz, I. Willner, *Angew. Chem. Int. Ed.* **2004**, *43*, 6042-6108.
14. S. Cobbe, S. Connolly, D. Ryan, L. Nagle, R. Eritja, D. Fitzmaurice, *J. Phys. Chem. B.* **2003**, *107*, 470-477.
15. S. Connolly, D. Fitzmaurice, *Adv. Mater.* **1999**, *11*, 1202-1205.
16. W. Shanton, S. A. Davis, S. Mann, *Adv. Mater.* **1999**, *11*, 449-452.
17. S. Kim, J. W. Park, D. Kim, D. Kim, I.-H. Lee, S. Jon, *Angew. Chem. Int. Ed.* **2009**, *48*, 4138-4141.
18. M. Hu, L. Qian, R. P. Brinas, E. S. Lyman, J. F. Hainfeld, *Angew. Chem. Int. Ed.* **2007**, *46*, 5111-5114.
19. S. Si, T. K. Mandal, *Langmuir* **2007**, *23*, 190-195.
20. S. Si, A. Kotal, T. K. Mandal, *J. Phys. Chem. C* **2007**, *111*, 1248-1255.
21. E. D. Matayoshi, G. T. Wang, G. A. Krafft, J. Erickson, *Science* **1990**, *247*, 954-958.
22. G. B. Irvine, M. Ennis, C. H. Williams, *Anal. Biochem.* **1990**, *185*, 304-307.
23. M. Zhao, L. Josephson, Y. Tang, R. Weissleder, *Angew. Chem. Int. Ed.* **2003**, *42*, 1375-1378.

24. C. Guarise, L. Pasquato, V. De Filippis, P. Scrimin, *Proc. Natl. Acad. Sci.* **2006**, *103*, 3978-3982.
25. A. Laromaine, L. Koh, M. Murugesan, R. V. Ulijn, M. M. Steven. *J. Am. Chem. Soc.* **2007**, *129*, 4156-4157.
26. G. v. Maltzahn, D.-H. Min, Y. Zhang, J.-H. Park, T. J. Harris, M. Sailor, S. N. Bhatia, *Adv. Mater.* **2007**, *19*, 3579-3583.
27. J. Liu, Q. Zheng, Y. Deng, C.-S. Cheng, N. R. Kallenbach, M. Lu, *Proc. Natl. Acad. Sci. U. S. A.* **2006**, *103*, 15457-15462.
28. J. M. Mason, K. M. Arndt, *ChemBioChem* **2004**, *5*, 170-176.
29. M. M. Gromiha, D. A. D. Parry, *Biophys. Chem.* **2004**, *111*, 95-103.
30. L. Baltzer, H. Nilsson, J. Nilsson, *Chem. Rev.* **2001**, *101*, 3153-3163.
31. J. G. Adamson, N. E. Zhou, R. S. Hodges, *Curr. Opin. Biotechnol.* **1993**, *4*, 428-437.
32. J. M. Slocik, F. Tam, N. J. Halas, R. R. Naik, *Nano Lett.* **2007**, *7*, 1054-1058.
33. M. G. Ryadnov, B. Ceyhan, C. M. Niemeyer, D. N. Woolfson, *J. Am. Chem. Soc.* **2003**, *125*, 9388-9394.
34. M. M. Stevens, N. T. Flynn, C. Wang, D. A. Tirell, R. Langer, *Adv. Mater.* **2004**, *16*, 915-918.
35. K. Enander, D. Aili, L. Baltzer, I. Lundström, B. Liedberg, *Langmuir* **2005**, *21*, 2480-2487.
36. D. Aili, K. Enander, J. Rydberg, I. Lundström, L. Baltzer, B. Liedberg, *J. Am. Chem. Soc.* **2006**, *128*, 2194-2195.
37. D. Aili, K. Enander, J. Rydberg, I. Nesterenko, F. Björefors, L. Baltzer, B. Liedberg, *J. Am. Chem. Soc.* **2008**, *130*, 5780-5788.
38. C. M. Dobson, A. Sali, M. Karplus, *Angew. Chem. Int. Ed.* **1998**, *37*, 868-893.
39. C. M. Dobson, *Nature* **2003**, *426*, 884-890.
40. B. Hardesty, G. Kramer, *Prog. Nucleic Acid Res. Mol. Biol.* **2001**, *66*, 41-66.
41. F. U. Hartl, M. Hayer-Hartl, *Science* **2002**, *295*, 1852-1858.
42. A. Horwich, *J. Clin. Invest.* **2002**, *110*, 1221-1232.
43. S. Y. Tan, M. B. Pepys, *Histopathology* **1994**, *25*, 403-414.
44. J. W. Kelly, *Curr. Opin. Struct. Biol.* **1998**, *8*, 101-106.
45. P. Divry, M. Florkin, *C. R. Soc. Biol.* **1927**, *97*, 1808-1810.
46. A. S. Cohen, E. Calkins, *Nature* **1968**, *183*, 1202-1203.
47. C. M. Dobson, *Trends Biochem. Sci.* **1999**, *24*, 329-332.
48. F. Chiti, M. Stefani, N. Taddei, G. Ramponi, C. M. Dobson, *Nature* **2003**, *424*, 805-808.
49. J.-C. Rochet, P. T. Lansbury, *Curr. Opin. Struct. Biol.* **2000**, *10*, 60-68.

50. R. Kodali, R. Wetzel, *Curr. Opin. Struct. Biol.* **2007**, *17*, 48-57.
51. W. S. Gosal, I. J. Morten, E. W. Hewitt, D. A. Smith, N. H. Thomson, S. E. Radford, *J. Mol. Biol.* **2005**, *351*, 850-864.
52. M. W. West, W. Wang, J. Patterson, J. D. Mancias, J. B. Beasley, M. H. Hecht, *Proc. Natl. Acad. Sci. U.S.A.* **1999**, *96*, 11211-11216.
53. M. T. Pastor, A. Esteras-Chopo, M. L. de la Paz, *Curr. Opin. Struct. Biol.* **2005**, *15*, 57-63.
54. X. I. Ambreggio, B. Kuhlmann, *Curr. Opin. Struct. Biol.* **2006**, *16*, 525-530.
55. N. V. Dokholyan, *Curr. Opin. Struct. Biol.* **2006**, *16*, 79-85.
56. K. Pagel, B. Koksich, *Curr. Opin. Chem. Biol.* **2008**, *12*, 730-739.
57. H. Xiong, B. L. Buckwalter, H. M. Shieh, M. H. Hecht, *Proc. Natl. Acad. Sci.* **1995**, *92*, 6349-6353.
58. M. W. West, W. Wang, J. Patterson, J. D. Mancias, J. R. Beasley, M. H. Hecht, *Proc. Natl. Acad. Sci. U.S.A.* **1999**, *96*, 11211-11216.
59. M. Mutter, R. Gassmann, U. Buttke, K.-H. Altmann, *Angew. Chem. Int. Ed.* **1991**, *30*, 1514-1516.
60. G. P. Dado, S. H. Gellman, *J. Am. Chem. Soc.* **1993**, *115*, 12609-12610.
61. H. L. Schenck, G. P. Dado, S. H. Gellman, *J. Am. Chem. Soc.* **1996**, *118*, 12487-12494.
62. R. A. Kammerer, D. Kostrewa, J. Zurdo, A. Detken, C. Garcia-Echeverria, J. D. Green, S. A. Müller, B. H. Meier, F. K. Winkler, C. M. Dobson, M. O. Steinmetz, *Proc. Natl. Acad. Sci. U.S.A.* **2004**, *101*, 4435-4440.
63. M. O. Steinmetz, C. Garcia-Echeverria, R. A. Kammerer, *Int. J. Pept. Res. Ther.* **2005**, *11*, 43-52.
64. R. A. Kammerer, M. O. Steinmetz, *J. Struct. Biol.* **2006**, *155*, 146-153.
65. H. Dong, J. D. Hartgerink, *Biomacromolecules* **2007**, *8*, 617-623.
66. B. Ciani, E. G. Hutchinson, R. B. Sessions, D. N. Woolfson, *J. Biol. Chem.* **2002**, *277*, 10150-10155.
67. Y. Takahashi, A. Ueno, H. Mihara, *Chem. Eur. J.* **1998**, *4*, 2475-2484.
68. Y. Takahashi, A. Ueno, H. Mihara, *ChemBioChem* **2001**, *1*, 75-79.
69. Y. Takahashi, A. Ueno, H. Mihara, *ChemBioChem* **2002**, *3*, 637-642.
70. T. Cedervall, I. Lynch, S. Lindman, T. Berggard, E. Thulin, H. Nilsson, K. A. Dawson, S. Linse, *Proc. Natl. Acad. Sci. U.S.A.* **2007**, *104*, 2050-2055.
71. D. Chopra, M. Gulati, V. Saluja, P. Pathak, P. Bansal, *Recent Patents CNS Drug Discov.* **2008**, *3*, 216-225.
72. L. A. Munishkina, E. M. Cooper, A. L. Uversky, V. N. Fink, *J. Mol. Recognit.* **2004**, *17*, 456-464.

73. L. Shang, Y. Wang, J. Jiang, S. Dong, *Langmuir* **2007**, *23*, 2714-2721.
74. X. Wu, G. Narshimhan, *Biochim. Biophys. Acta* **2008**, *1784*, 1694-1701.
75. A. Verma, H. Nakade, J. M. Simard, V. M. Rotello, *J. Am. Chem. Soc.* **2004**, *126*, 10806-10807.
76. P. S. Ghosh, A. Verma, V. M. Rotello, *Chem. Commun.* **2007**, 2796-2798.
77. P. S. Ghosh, G. Han, B. Erdogan, O. Rosado, V. M. Rotello, *J. Pept. Sci.* **2008**, *14*, 134-138.
78. Y. Fillon, A. Verma, P. Ghosh, D. Ernenwein, V. M. Rotello, J. Chmielewski, *J. Am. Chem. Soc.* **2007**, *129*, 6676-6677.
79. L. A. Capriotti, T. P. Beebe, J. P. Schneider, *J. Am. Chem. Soc.* **2007**, *129*, 5281-5287.
80. M. Lundqvist, P. Nygren, B.-H. Jonsson, K. Broo, *Angew. Chem. Int. Ed.* **2006**, *45*, 8169-8173.
81. H. Zhao, E. K. J. Tuominen, P. K. J. Kinnunen, *Biochemistry* **2004**, *43*, 10302-10307.
82. W.-H. Wu, X. Sun, Y.-P. Yu, J. Hu, L. Zhao, Q. Liu, Y.-F. Zhao, Y.-M. Li, *Biochem. Biophys. Res. Commun.* **2008**, *373*, 315-318.
83. S. Rocha, A. F. Thünemann, M. C. Pereira, M. Coelho, H. Möhwald, G. Brezesinski, *Biophys. Chem.* **2008**, *137*, 35-42.
84. D. Zhang, O. Neumann, H. Wang, V. M. Yuwono, A. Barhoumi, M. Perham, J. D. Hartgerink, P. Wittung-Stafshede, N. J. Halas, *Nano Lett.* **2009**, *9*, 666-671.
85. S. Linse, C. Cabaleiro-Lago, W.-F. Xue, I. Lynch, S. Lindman, E. Thulin, S. E. Radford, K. A. Dawson, *Proc. Natl. Acad. Sci. U.S.A.* **2007**, *104*, 8691-8696.
86. C. Cabaleiro-Lago, F. Quinlan-Pluck, I. Lynch, S. Lindman, A. M. Minogue, E. Thulin, D. M. Walsh, K. A. Dawson, S. Linse, *J. Am. Chem. Soc.* **2008**, *130*, 15437-15443.
87. L. Fei, S. Perrett, *Int. J. Mol. Sci.* **2009**, *10*, 645-655.
88. A. N. Shipway, E. Katz, I. Willner, *ChemPhysChem* **2000**, *1*, 18-52.
89. K. L. Kelly, E. Coronado, L. L. Zhao, G. C. Schatz, *J. Phys. Chem. B* **2003**, *107*, 668-677.
90. Q. Huo, *Coll. Surf. B Biointerf.* **2007**, *58*, 3-7.
91. D. G. Fernig, *Anal. Chem.* **2007**, *79*, 4215-4221.
92. G. D. Fasman in *Circular dichroism and the conformational analysis of biomolecules*, Plenum Press: New York, 1996.
93. N. Greenfield, G. D. Fasman, *Biochemistry* **1969**, *8*, 4108-4116.
94. W. C. Johnson, *Proteins* **1990**, *7*, 205-214.
95. L. Reimer in *Transmission Electron Microscopy: Physics of Image Formation and Microanalysis*, Springer-Verlag, Berlin, 1989.

96. F. Lottspeich, H. Zorbas in *Bioanalytik*, Spektrum Akademischer Verlag Heidelberg, Berlin, 1998.
97. J. R. Harris, D. Bhella, M. Adrian, *Microscopy and Analysis* **2006**, 17-21
98. H. Naiki, K. Higuchi, M. Hosokawa, T. Takeda, *Anal. Biochem.* **1989**, *177*, 244-249.
99. H. LeVine, *Methods Enzymol.* **1999**, *309*, 274-284.
100. M. R. H. Krebs, E. H. C. Bromley, A. M. Donald, *J. Struct. Biol.* **2005**, *149*, 30-37.
101. R. Khurana, C. Coleman, C. Ionescu-Zanetti, S. A. Carter, V. Krishna, R. K. Grover, R. Roy, S. Singh, *J. Struct. Biol.* **2005**, *151*, 229-238.
102. W. B. Turnbull, A. H. Daranasm, *J. Am. Chem. Soc.* **2003**, *125*, 14859-14866.
103. T. Wiseman, S. Williston, J. F. Brandts, L.-N. Lin, *Anal. Biochem.* **1989**, *179*, 131-137.
104. M. J. Blandamer in *Biocalorimetry: Applications of Calorimetry in the Biological Sciences*, Wiley, Chichester, UK, 1998.
105. Z. Sun, W. Ni, Z. Yang, X. Kou, L. Li, J. Wang, *Small* **2008**, *4*, 1287-1292.
106. D.-J. Yao, Y.-R. Yang, C.-C. Tai, W.-H. Hsiao, Y.-C. Ling, *J. Micromech. Microeng.* **2007**, *17*, 1435-1441.
107. J. Simard, C. Briggs, A. K. Boal, V. M. Rotello, *Chem. Comm.* **2000**, 1943-1944.
108. Current address of Meike Roskamp: Department of Inorganic Chemistry, Institute of Chemistry and Biochemistry, Fabeckstr. 34-36, 14195 Berlin, Germany.
109. T. Vagt, O. Zschörnig, D. Huster, B. Koksich, *ChemBioChem* **2006**, *7*, 1361-1371.
110. R. M. C. Dawson, D. C. Elliot, W. H. Elliot, and K. M. Jones in *Data for Biochemical Research*, 3rd edition, Oxford Science Publications, 1986, pp. 1-31.
111. D. N. Woolfson, *Adv. Prot. Sci.* **2005**, *70*, 79-112.
112. J. F. Conway, D. A. D. Parry, *Int. J. Biol. Macromol.* **1991**, *13*, 14-16.
113. D. N. Woolfson, T. Alber, *Prot. Sci.* **1995**, *4*, 1596-1607.
114. Current address of Dr. Helmut Cölfen and Antje Völkel: Max-Planck-Institute of Colloids and Interfaces, 14424 Potsdam, Germany
115. Current address of Dr. Christoph Böttcher and Dr. Hans von Berlepsch: Research Center for Electron Microscopy, Freie Universität Berlin, Fabeckstr. 36a, 14195 Berlin, Germany
116. P. B. Harbury, P. S. Kim, T. Alber, *Nature* **1994**, *371*, 80-83.
117. P. B. Harbury, T. Zhang, P. S. Kim, T. Alber, *Science* **1993**, *262*, 1401-1407.
118. F. H. C. Crick, *Acta crystallogr.* **1953**, *6*, 685-689.
119. C. Cothia, M. Levitt, D. Richardson, *J. Mol. Biol.* **1981**, *145*, 215-250.
120. K. Pagel, S. C. Wagner, K. Samedov, H. von Berlepsch, C. Böttcher, B. Koksich, *J. Am. Chem. Soc.* **2006**, *128*, 2196-2197.

-
121. Current address of Raheleh Rezaei Araghi: Department of Organic Chemistry, Institute of Chemistry and Biochemistry, Freie Universität Berlin, Takustr. 3, 14195 Berlin, Germany.
122. P. Y. Chou, G. D. Fasman, *Biochemistry* **1974**, *13*, 211-222.
123. P. Y. Chou, G. D. Fasman, *Biochemistry* **1974**, *13*, 222-245.
124. K. L. Morrison, G. A. Weiss, *Curr. Opin. Chem. Biol.* **2001**, *5*, 302-307.
125. B. C. Cunningham, J. A. Wells, *Science* **1989**, *244*, 1081-1085.
126. Y. H. Chen, J. T. Yang, K. H. Chan, *Biochemistry* **1974**, *13*, 3350-3359.
127. Personal communication.
128. C. M. Dobson, *Nature* **2003**, *426*, 884-890.
129. S. Linse, C. Cabaleiro-Lago, W.-F. Xue, I. Lynch, S. Lindman, E. Thulin, S. E. Radford, K. A. Dawson, *Proc. Natl. Acad. Sci. U.S.A.* **2007**, *104*, 8691-8696.
130. C. Cabaleiro-Lago, F. Quinlan-Pluck, I. Lynch, S. Lindman, A. M. Minogue, E. Thulin, D. M. Walsh, K. A. Dawson, *J. Am. Chem. Soc.* **2008**, *130*, 15437-15443.
131. B. Chu, T. Liu, *J. Nanopart. Res.* **2000**, *2*, 29-41.